**ISTANBUL TECHNICAL UNIVERSITY ★ GRADUATE SCHOOL OF SCIENCE ENGINEERING AND TECHNOLOGY**

# MODELING OF THE LATERAL LOAD RESISTANCE OF MASONRY INFILLED FRAMES WITH INNOVATIVE STEEL TIES

**M.Sc. THESIS**

**MirSalar Kamari**

**Department of Civil Engineering**

**Structural Engineering Program**

**Thesis Advisor: Asst. Prof. Oğuz Güneş**

**AUGUST 2016**

**ISTANBUL TECHNICAL UNIVERSITY ★ GRADUATE SCHOOL OF SCIENCE ENGINEERING AND TECHNOLOGY**

# MODELING OF THE LATERAL LOAD RESISTANCE OF MASONRY INFILLED FRAMES WITH INNOVATIVE STEEL TIES

**M.Sc. THESIS**

**MirSalar Kamari**

**(50113026)**

**Department of Civil Engineering**

**Structural Engineering Program**

**Thesis Advisor: Asst. Prof. Oğuz Güneş**

**AUGUST 2016**

**İSTANBUL TEKNİK ÜNİVERSİTESİ ★ FEN BİLİMLERİ ENSTİTÜSÜ**

# YENİLİKÇİ ÇELİK BAĞLAR İÇEREN YIĞMA DOLGU DUVARLI BETONARME ÇERÇEVELERİN YATAY YÜK DİRENCİNİN MODELLENMESİ

**YÜKSEK LİSANS TEZİ**

**MirSalar Kamari**

**(501131026)**

**İnşaat Mühendisliği Anabilim Dalı**

**Yapı Mühendisliği Programı**

**Tez Danışmanı: Yrd.Doç.Dr. Oğuz Güneş**

**AĞUSTOS 2016**

MirSalar Kamari, a M.Sc. student of ITU Graduate School of Science Engineering and Technology student ID 501131026 successfully defended the thesis entitled "Modeling of the Lateral Load Resistance of Masonry Infilled Frames with Innovative Steel Ties", which he prepared after fulfilling the requirements specified in the associated legislations, before the jury whose signatures are below.

| | | |
|---|---|---|
| **Thesis Advisor :** | **Asst. Prof. Oğuz Güneş**<br>Istanbul Technical University | ..... |
| **Jury Members :** | **Prof. Dr. Kadir Güler**<br>Istanbul Technical University | ..... |
| | **Assoc. Prof. Dr. Cem Yalçın**<br>Bogazici University | ..... |

**Date of Submission : 2 May 2016**
**Date of Defense : 17 Aug 2016**

***To my mother***

# FOREWORD

I had honor to be supervised by Professor Oğuz Güneş, who helped me through all and every steps of my thesis. His supervision empowered me to master very practical, useful, and powerful skills that will be with me, for rest of my life. His deep insight, and sympathy, made him my greatest role model in my life. I acknowledge and deeply appreciate his intense supervision in my thesis. I will never forget all of his advices and his effective corporation through development of my thesis. I hope, I could be able to give all his kindness back to him, and spread and utilize the knowledge I learnt from him in my life.

I acknowledge and appreciate the period of time that "Scientific and Technological Research Council of Turkey" (Turkish: *Türkiye Bilimsel ve Teknolojik Araştırma Kurumu,* TÜBİTAK) supported our effort to deliver my thesis.

The Istanbul Technical University's prestigious academic environment made me expand my vision and horizon about science. I will never forget all I learnt from ITU.

AUGUST 2016 MirSalar Kamari

## TABLE OF CONTENTS

**Page**

## LIST OF TABLES

# LIST OF FIGURES

**MODELING OF THE LATERAL LOAD RESISTANCE OF MASONRY INFILLED FRAMES WITH INNOVATIVE STEEL TIES**


SUMMARY

This research aimed at modeling a cyclic load-deformation hysteresis relationship, captured from experimental results of a reinforced concrete (RC) frame with and without an infill masonry wall. In-plane behavior of masonry walls plays a major role in the overall cyclic loading response of an RC frame and the lateral load resistance, which are important design aspects. The out-of-plane behavior of a masonry wall is the most frequently encountered failure mode under seismic loads. In order to increase the out-of-plane stability of the infill wall, innovative steel ties were installed in the masonry wall and their contribution of the masonry infill was studied. To simulate the RC frame behavior for different tie configurations, respective behavior of RC frames under cyclic loading were studied, and two main simulation strategies were conducted.

First, nonlinear spring models were utilized to model the nonlinear behavior of joints regions in the RC bare frames under incremental cyclic loading. To simulate the effect of infill walls with or without steel ties, a diagonal pin jointed nonlinear spring was added to the RC frame to account for the corresponding rigidity of the wall. This modeling strategy relies on analysis of the specimen section, mainly its geometry and material properties, and does not correlate the experimental results to the analysis outputs.

Second strategy was to calibrate a nonlinear plastic spring based on experimental results to simulate its hysteresis behavior under lateral cyclic loading. Understanding the linear or nonlinear relationship between load and deformation in structural materials or structural frames is important for an accurate simulation. Therefore, modeling load-deformation relationship based on experimental results could be a viable approach to predict load-deformation behavior of a similar frame under a loading pattern. To reduce the experimental data size recorded with measuring devices or Linear Variable Differential Transformers (LVDTs), regular and irregular data resampling technics were implemented. Hysteresis models to simulate the cyclic response of an RC frame were reviewed, then simulation strategies were implemented to obtain a best fit to the experimental results. The difference between analytical and the experimental results was then studied. A Genetic Algorithm (GA) was used to fit the simulated results to experimental results through minimization of

the disagreement between simulated and experimental results. Genetic Algorithm seeks he best parameters to describe the experimental results. This method could be used to train models to predict the capacity and performance of frames, under different loading patterns. The appendix includes the simulated hysteresis results and demonstrates how the simulated model can fit the experimental results in close agreement.

Three hysteresis models have been used to represent the experimental results. 1-Kenematic hysteresis model, 2-Takeda hysteresis model 3-Pivot hysteresis model. Since Kinematic and Takeda models rely on their backbone to represent the cyclic data, the backbone was extracted from experimental cyclic results and was assigned to these models. However, Pivot model has five more degradation parameters that was obtained through optimization while minimize the deviation between simulated and experimental results. While fitting simulated results to experimental results, Pivot hysteresis model, in comparison with Kinematic and Takeda model, well presented the experimental results.

At the end of the thesis we modeled cyclic lateral excitation of the bare frame and infill frame with Pivot hysteresis model. The backbone load-deformation curve of such hysteresis model was calculated from analytical finite element modeling. Then, the cyclic parameters of the hysteresis model were obtained and assigned to the model using the second strategy. By analytically obtaining the backbone load deformation curve, material and geometry characteristics of the specimen is considered. It can also be assumed that Pivot hysteresis model parameters are not significantly varied while geometry and material characteristics of the frame are changed. Therefore, Pivot hysteresis parameters that have been captured from cyclic excitation behavior of a frame can be assigned for almost any frame that has approximately the similar geometry and material characteristics to that frame.

In this research application of MATLAB has been used as the programming platform and SAP2000 is utilized as the finite element structural solver. To facilitate obtaining the analytical results, an Application Programming Interface (API) has been implemented to utilized the functionality of SAP2000 from MATLAB. This allowed us to take advantage of the state-of-the-art functionalities of SAP2000 from MATLAB as oppose of developing such solver from the ground up. In addition, in this research GA toolbox has been utilized as a convenient GA platform.

The novelty of this research is the implementation of new strategies to model and predict the performance of frames or materials under any cyclic pattern by use of experimental results.

# YENİLİKÇİ ÇELİK BAĞLAR İÇEREN YIĞMA DOLGU DUVARLI BETONARME ÇERÇEVELERİN YATAY YÜK DİRENCİNİN MODELLENMESİ


## ÖZET

Betonarme ve çelik çerçeve sistemlerde dolgu duvarların yatay yük etkisi dikkate alınmamasına ragmen bu çerçeve sistemlerinde dolgu duvarı yapısının varlığı, çerçeveye uygulanan büyük yatay uyarılarda temel kayma gerilmesinin artmasına sebep olmaktadır. Bu tezde yapılan araştırmada ise, betonarme çerçevelerdeki yığma dolgu duvarların davranışları incelenmiştir ve yığma dolgu duvarlardaki baskın hasar modu olan yatay aşırı yüklemelerin düzlem dışı yüklere mağruz kaldığında ortaya çıktığı gözlemlenmiştir. Bu sebeple, düzlem dışı yüklemelerin stabilize olması için yığma dolgu duvarların bağ kiriş elemanlarıyla güçlendirilmesi gerekmektedir.

Sunulan bu tez çalışmasında, dolgu duvarlı ve dolgusuz betonarme çerçeveler üzerinde yapılan deneylerden elde edilen sonuçlarla çevrimsel yük – deformasyon biçimi arasındaki ilişkinin modellenmesi amaçlanmıştır. Dolgu duvarın düzlem dışı stabilitesini arttırmak amacı ile dolgu duvara çelik gergiler uygulanmıştır. Betonarme çerçeveyi farklı dolgu güçlendirme durumlarında simüle etmek için betonarme çerçevenin çevrimsel yüklemesi üzerine çalışılmış ve 2 ana simülasyon stratejisi uygulanmıştır. Bu simülasyon sistemlerinin birincisi, analitik sonuçlara dayanan analitik simülasyondur, ikincisi ise daha önce uygulanmış olan deneysel çalışmalara ve tahmine dayanan, deneysel simülasyondur. Bu çalışma için, 4 adet sistem ele alınmıştır. Bunlar, dolgu duvarlı çerçeve, çıplak betonarme çerçeve, dolgu duvarlı betonarme çerçeve ve iki farklı çeşit donatıyla güçlendirilmiş betonarme çerçevedir. Yapılan çalışmalar boyunca betonarme çerçevenin boyutları ve donatı yerleşimi sabit tutulmuştur.

İlk olarak, aşırı yük uygulanan betonarme çerçevede, boş betonarme çerçevedeki doğrusal olmayan plastik mafsal davranışını taklit etmesi amacı ile doğrusal olmayan yay modelinden faydalanıldı. Dolgu duvarın etkisini simüle etmek için doğrusal olmayan çapraz bir mafsal eklenmiştir. Bu modelleme stratejisi numunenin analitik özeliklerine dayandığı için farklı deney sonuçları arasında ilişki kurulmasını zorlaştırmaktadır.

İkinci yöntem, lineer olmayan yükleme altında davranış biçimini simüle etmek için deney sonuçlarına göre bir lineer olmayan plastik yay kalibre etmektir.yükleme ve deformasyon arasındaki lineer ve lineer olmayan ilişkiyi amlamak en iyi simülasyondur. Bu nedenle herhangi bir çerçevenin herhangi bir yükleme altındaki yük – deformasyon davranışını tahmin etmek için yük – deformasyon ilişkisini deney sonuçlarına göre modellemek çokj iyi bir yaklaşım olabilir. Deneysel veri boyutunu azaltmak için ölçüm cihazları yada LVDT kullanılabilir. Histeresis modeller gözden geçirildi ve ardından deneysel ve analitik simülasyon yöntemleri uygulandı. Deneysel ve analitik sonuçların farklılıkları üzerine çalışıldı. Gelişmiş teknoloji ürünü olan Genetic Algorithm (GA) ile simüle edilen sonuçlar ile deneysel sonuçlar arasındaki uyuşmazlıklar minimize edildi. GA deney sonuçlarını izah etmek için en iyi parametreleri bulacaktır. Bu method eğitim için hazırlanan modellerin herhangi bir deformasyon durumuna maruz kaldıkları zamandaki kapasitelerini ve performanslarını tahmin etmek için kullanılabilir. Bu tezin ek bölümünde simüle edilmiş histeresis sonuçları göstermek amaçlanmıştır ve bu bölüm simüle edilen modelin deneysel sonuçları özgün bir yolla nasıl ispatlayacağını göstermektedir.

Yapılan bu çalışmada, 3 histerezis modeli belirlenmiştir. Bunlar; Kinematik, Takeda ve Pivot histerezis modelleridir. Kinematik ve Takeda histerezis modelleri döngüsel verilere bağlı olmasına rağmen, kullanılan veriler döngüsel verilerden ayıklanarak kullanılmıştır. Buna karşılık, Pivot histerezis modelinde simüle edilmiş ve deneysel çalışmalarla elde edilen veriler arasındaki sapmaları minimize edip optimum değeri elde etmeye çalışılırken 5 adet degridasyon parameter elde edilmiştir. Buna ek olarak, simülize sonuçları, deneysel sonuçlara yerleştirmeye çalışılırken Pivot histerezis modelin, Takeda ve Kinematik histerezis modeline kıyasla daha iyi sonuçlar verdiği gözlemlenmiştir.

Tez çalışmasının sonucunda, çıplak ve dolgu çereçevelerin döngüsel yanal uyarıları Pivot histerezis modeli ile modellenmiştir. Yük-deformasyon eğrisinin modellemesi, analitik sonlu elemanlar modeli ile hesaplanmıştır. Buna ek olarak, histerezis modeline ait döngüsel veriler ikinci stratejik model kullanılarak belirlenmiştir. Yük-deformasyon eğrisinin temelini analitik olarak belirlerken, numunelerin malzeme ve geometrik özellikleri ele alınmıştır. Başka bir deyişle, bu sayede Pivot histerezis modelindeki parametreler, çerçevelerin geometrik ve malzeme özelliklerinin değişmesiyle değişmemektedir. Bunun sonucunda, çerçevelerin döngüsel uyarıdan aldıkları Pivot histerezis parametreleri, yaklaşık olarak aynı geometrik ve malzeme özelliklerine sahip çerçeveler için aynı olarak labul edilebilmektedir.

Bu tez çalışmasında, platformları programlamak için MATLAB programı, sonlu eleman çözümü için ise SAP 2000 programından faydalanılmıştır. Uygulama

programlama arayüzü saysesinde MATLAB programından elde edilen analitik sonuçların SAP 2000 programında işlenmesine olanak sağlanmıştır. Bu yöntem sayesinde yeni bir program geliştirmek yerine, MATLAB programından alınan veriler, SAP 2000 programında işlenmiştir. Buna ek olarak, Genetik Algoritma araç çubuğu, elverişli Genetik Algoritma platform olacak şekilde geliştirilmiştir.

Bu araştırma ile çerçevelerin ve malzemelerin modellenmesi ve performanslarının tahmin edilmesi hususunda deneysel sonuçlara dayanan yeni yöntemler uygulanmıştır. Bu yaklaşım deneysel sonuçlara dayanarak eğitim modellerinde yük deformasyon ilişkinin simüle etmek ve henüz tecrübe edilmemiş problemleri tahmin etmekte kullanılabilecek olsa da, bu çalışmada farklı koşullar altındaki betonarme çerçevenin yük – deformasyon performasını simüle etmek için kullanılmıştır. Çalışmalar sonucunda, karar tablolarında 2 simülasyon sonuçları arasında hesaplanan ihmal edilebilir zaman değerleri olmasına rağmen, Takeda model deney sonuçları için en uygun model olarak belirlenmiştir.

# 1. INTRODUCTION

The masonry infill wall alters the in-plane behavior of its frame, which is always neglected during the design phase. Existence of an infill wall in RC or steel frame could increase its base shear strength even in severe lateral excitations. This research is dedicated to study the effect of masonry infill walls in reinforced concrete frames. The state of the art research reveals that the out-of-plane behavior in masonry infills is the most dominant failure mode in lateral excessive loadings. Therefore, in order to stabilize the out-of-plane behavior of masonry infill wall, it is reinforced with tie elements. So called tie reinforcement elements, can play a major role in increasing the out-of-plane behavior of masonry infill. Two novel tie element configuration has been implemented to reinforce the infill wall. Four sets of experiment have been carried out to study the effect of infill, including reinforced concrete (RC) bare frame, infill RC frame, and two more reinforced RC infills, each with different configuration of the infill reinforcements. The dimension of the RC frame and the reinforcement configuration among all the specimens are the same. The material properties used to build the model, for the experiment are tried to be the same among all four sets of experiment, though there is a little inevitable variation between specimens, which are explained in chapter 3.

## 1.1. Purpose of Thesis

This research is conducted to survey three main goals. First, to model the performance of an RC bare frame versus an RC frame with infill walls. Second, to assess the performance efficiency of infill wall reinforcement, with two novel reinforcement configurations. Third, to represent a novel method to predict the load-deformation performance of any RC frame (with or without infills) due to severe lateral excitations by using the experimental results.

In this regard, four sets of RC frame have been built to study the increase in strength of RC frame due to existence of infills. Base shear versus the lateral displacement for

all of four specimens have been recorded. In other words, for any level of applied displacement the level of base shear has been recorded. The increasing displacement magnitude has been applied to the specimen in a cyclic pattern, therefore, the hysteresis base shear displacement behavior of each specimen is recorded and studied explicitly. The cyclic loading pattern to be applied on the specimens is the same among all them. Therefore, the increase of the rigidity due to existence of infill walls (with or without reinforcement) could be compared against with that of the bare frame case.

### 1.2 Implementation Strategies

Simulation models that is used in any research, represent or describe a specific phenomenon or an experiment. The strategies to simulate the real world data is laid on two main methodologies. First, the simulated data is calculated by the analytical characteristics of its subcomponents. This simulation strategy is called modeling based on analytical results. Well-simulated analytical models might represent the experimental results perfectly, though, these models are hard to implement and costly to analyze. Second, simulation strategy is modeling based on prior experimental results to predict and carry out non-experimented cases. The experimental based modeling well-predicts the demanded results, though, this method may require numerous experimental results as an input, to carry out predictions with an acceptable accuracy.

In this particular research both methods are implemented, discussed, and reviewed. A quick roadmap of this research is explained as the following:

#### 1.2.1 Models based on analytical results

In order to model the specimen based on material properties and geometry characteristics, two levels of detail might be considered to simulate the specimen, namely Finite Element (FE in short) micro and FE macro models. Since micro FE models describe the problem in laborious details, the output results corresponding to these methods are much closer the reality, and the experimental data. On the other hand, micro FE models are hard to implement, and expensive to compute. There is a huge number of studies to simulate the performance of reinforced concrete frames on

excessive lateral loading. The implementation of them using micro FE models has yielded quiet satisfactory and close-to-reality results. Though, computational costs and laborious implementation technics makes them quite useless. Thus, there is always need to simulate the problem in terms of models that are easy to understand, and yet, easy to implement. In this regard, macro FE models have been used to introduce behavior of reinforced concrete frames. It has been assumed that every frame member has rigidity equal to infinity. Plastic joints are placed where they are likely to occur on RC member due to excessive lateral loading, and then, they are modeled with nonlinear springs. The properties of these springs are captured from the material properties, and geometry characteristics. To simulate such springs' nonlinear characteristics, the stress strain relationships of each and every material involved in the specimen are obtained from experiment and then for the sake of simplicity they are idealized with a multi straight line curve. With obtained idealized stress-strain curve for used materials, and with knowing the configuration of lateral and longitudinal reinforcement steels, moment curvature relationship for all columns are calculated. The length of plastic joints of columns is studied and, plastic joints are placed on the top of the columns. To specify the length of the plastic length, non-linear elastic springs are modeled with the same length at the top of columns. Macro model strategy to carry out the load displacement relationship of an RC bare frame is mentioned in Chapter 4 in explicit details. The implemented model is then compared against the experimental results.

To pursue the macro model implementation strategy, modeling the rigidity of infill wall can be taken into account by adding a pin jointed strut member connecting the corner of the frames. In chapter 2 literature associated with the infill has been reviewed and a proper pin jointer infill model has been implemented in chapter 4 and the results are compared with the experimental data in this chapter 4.

### 1.2.2 Models based on experimental results

To study the inelastic response of the column or joint or hinges based on experimental results, calibration of hinges can be carried out to introduce a hysteresis behavior based on a cyclic excitation. These models generally depend on the experimental data to calibrate and find the best parameters to introduce the model. Some of the studies using this particular research can be mentioned as the following:

- Sets of polynomial expressions were introduced by [1] to represent the hysteresis behavior of bean column connections and stiffness degradation.
- A series of exterior beam-column joints experiments were conducted and a triangular joint model were proposed by [2] to match the carried out results and find the best parameters.
- The concept of the effective length was introduced by [3] in which the curvature at the beam-column interface were multiplied to carry out the fixed end rotation.

Since these models are based on the experimental data to introduce a hysteresis behavior, they work best for the observed or experienced case and they not applicable for the cases in which the physical and mechanical characteristics are changed. The lacking of physical and mechanical contribution of material properties and geometry characteristic of such models made them to remain unpopular since then. However, with the advent of Artificial Neural Network (ANN) or Deep Learning (DL) methodologies, in which the outputs are carried out based on the input parameters and series of empirical results. In this particular research, the hysteresis response, namely load-deformation behavior of an RC is modeled through existing popular and mostly used hysteresis rules. A semi-automated algorithm is proposed to first, shorten, reduce, and smooth the load deformation data to eliminate the steady record of gages, second, to choose best hysteresis model based on its fitness with the experimental load-deformation results based a decision making process, and third, to yield and echo the parameters of selected hysteresis model to introduce a huge load–deformation cyclic dataset in term of a handful number of parameters. After conduction of series of experiments with different physical and mechanical contribution of material and geometry properties, these shortened parameters can be used to train an ANN platform to perform a precise prediction of inputs that were not piloted. In chapter 4 shortening the dataset as well as fitting it to a proper hysteresis model have been explained in explicit details.

# 2. LITERATURE REVIEW

In this chapter the literature associated with concrete stress-strength relationship is surveyed to carry out the characteristic of the plastic joints. The moment curvature of the rectangular column sections is calculated using the stress-strength concrete relationship.

The second part of the literature review is allocated survey the literature associated with the masonry infill wall rigidity in the reinforced concrete.

## 2.1 Moment Curvature Relationship of the Reinforced Cross-Section

To carry out the moment-curvature relationship for a particular reinforced cross-section, in the most of the models or software packages, the following assumptions have been considered:

1-The tension carrying capacity of the concrete in its the stress-strain curve is neglected.

2-The stress-strain curve relationship of a steel and concrete is available.

3-Plane sections remain plane and the same condition after bending.

With the above assumption considered and with the stress-strain relationships available for the concrete and the steel material, the Moment-Curvature relationship can be calculated by finding the equivalent forces to carry out the equilibrium which is summarized as follows:

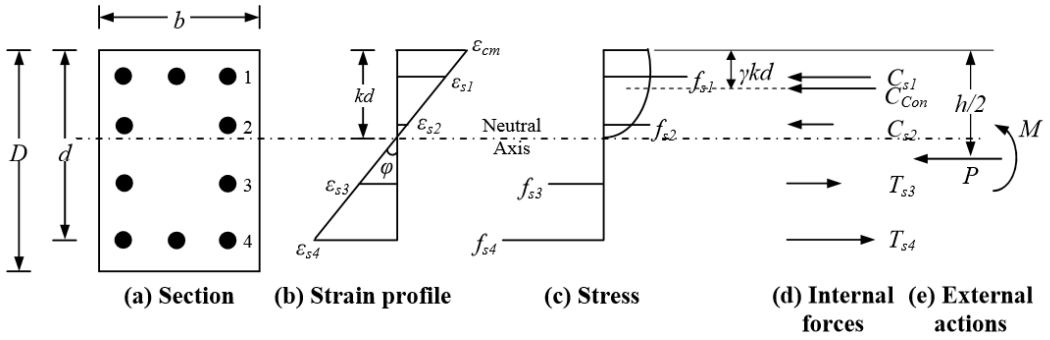


**Figure 2.1 :** Concrete and steel forces action on a typical RC section in bending

$$Area\ under\ stress\ stress\ curve\ of\ concrete = \int_0^{\varepsilon_{cu}} f_c d\varepsilon_c = \alpha f'_c \varepsilon_{cm} \quad (2.1)$$

where,

$$\therefore \alpha = \frac{\int_0^{\varepsilon_{cu}} f_c d\varepsilon_c}{f'_c \varepsilon_{cm}} \quad (2.2)$$

First moment of area about origin of area under stress-strain curve can be carried out as:

$$\int_0^{\varepsilon_{cu}} f_c \varepsilon_c d\varepsilon_c = 1 - \gamma\ \varepsilon_{cm} \int_0^{\varepsilon_{cu}} f_c d\varepsilon_c \quad (2.3)$$

$$\therefore \gamma = 1 - \frac{\int_0^{\varepsilon_{cu}} f_c \varepsilon_c d\varepsilon_c}{\varepsilon_{cm} \int_0^{\varepsilon_{cu}} f_c d\varepsilon_c} \quad (2.5)$$

$$C_{con} = \alpha f'_c bkd \quad (2.4)$$

$C_{con}$ is the compression force of concrete acting at a distance of $\gamma kd$ from the extreme compression fiber.

The force equilibrium equations can be written as:

$$P = \alpha f'_c bkd + \sum_{i=1}^{n} f_{si} A_{si} \tag{2.6}$$

, and moment can be calculated as the following:

$$M = \alpha f'_c bkd \left(\frac{D}{2} - \gamma kd\right) + \sum_{i=1}^{n} f_{si} A_{si} \left(\frac{D}{2} - d_i\right) \tag{2.7}$$

where,

$n$ = Number of reinforcement bars

$f_{si}$ = Stress in the ith bar

$A_{si}$ = Area of ith bar

$D$ = Total depth of section

$d$ = Effective depth of the section

$d_i$ = depth of ith bar from extreme compression fiber

The curvature can be written as:

$$\phi = \frac{\varepsilon_{cm}}{kd} \tag{2.8}$$

With the above formulas, the Moment-Curvature relationship for a given reinforced cross-section and axial loading level can be simply carried out by increasing the strain at the concrete's extreme compression fiber level, namely, $\varepsilon_{cm}$ to check if the equilibrium (2.4) is satisfied. Then, the moment is can be calculated from the equation (2.5), and corresponding curvature is carried out form equation (2.8).

## 2.2 Literature Review on the Stress-strain Models of Reinforced Concrete

A great number of researches has been conducted to model the stress-strain curve of the concrete under a uniaxial compression. The aim of these researches is to introduce a stress block, which its area is equal to the area under stress-strain curve of the concrete. The proposed equivalent stress block, in most of the researches, are introduced in terms of the depth and compression specific strength of the concrete, $f'_c$. Since the transverse reinforcement plays a major role in compression capacity of the concrete, there are two study cases dividing the compression capacity determination of the concrete to unconfined and confined groups. Confinement in a reinforced concrete increases its ductility. While loading a reinforced concrete to its axial load limit, with the internal cracking grow, the transverse reinforcement is stressed avoiding the whole specimen to crush. Confinement in the concrete reinforcement could depend on various parameters from which the following are the most important ones:

1- Transverse ratio and the concrete core ratio effect the confinement. High transverse steel content will burden higher transverse confining pressure.
2- Yield strength of confining steel, since it can then bear more stress level and confining pressure.
3- The ratio of spacing of transverse reinforcement and the size of transverse steel content. Both of the mentioned parameters will lead to more effective confinement stress burdening.
4- The size of longitudinal reinforcement. The longitudinal reinforcement does also have a contribution in confinement.
5- Last but not least the strength of the concrete. Concrete with a higher strength level will obviously fix the confinement in any RC member.

Because the current research deals most with the confined reinforced concrete with rectangular hoops, in the following sections some of the popular models of confined concrete's stress-strain curve are enlisted.

### 2.2.1 Chen et al stress-strain model

Chan proposed a trilinear model to approximate the stress-strain curve of the concrete which contain of two part. First part introduces the unconfined status of the

concrete (part (OAB), second defines the transverse reinforcement contribution on the concrete confinement (part BC). [4]

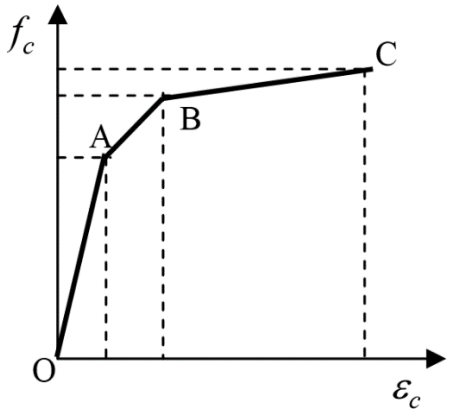


**Figure 2.2 :** Chan proposed stress-strain curve for concrete

### 2.2.2 Baker et al stress-strain model

Baker et al proposed a proposed a parabola to define stress-strain curve of the concrete from the origin to maximum stress level followed by a horizontal line which its length to the maximum strain contribute the effect of the transverse reinforcement. The maximum stress depends on strain gradient across the section. [5]

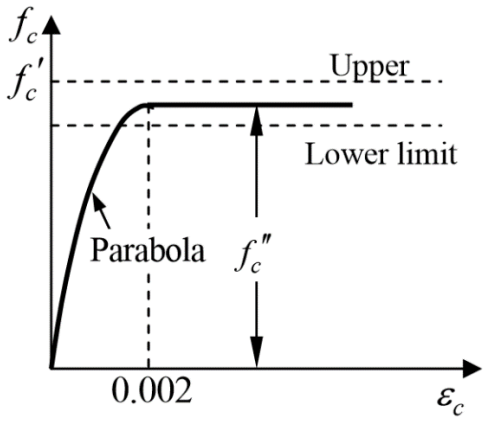


**Figure 2.3 :** Baker et al proposed stress-strain curve of concrete

### 2.2.3 Roy and Sozen stress-strain model

Roy and Sozen introduced the stress-strain relationship for the concrete in form of a bilinear. In this his work, which was conducted on the axially loaded prisms, the first

line defines the linearly connected origin to the maximum stress level and the second one connects it to the maximum strain level whose stress is the half of the maximum stress level. [6]

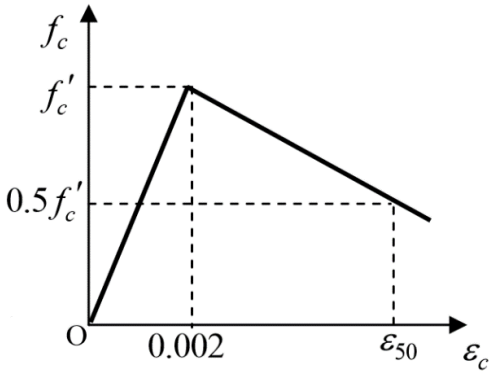


**Figure 2.4 :** Roy et al proposed stress-strain curve of concrete

### 2.2.4 Soliman and Yu stress-strain model

Soliman and Yu suggested the stress-strain curve of the concrete to be in three parts, a parabola, a horizontal line at the maximum stress level and a descending line connecting maximum stress level to the maximum strain level. The key point of their curve depend on the transverse reinforcement ratio, namely steel content and their spacing and confined area. Figure below shows Soliman and Yu model.[7]

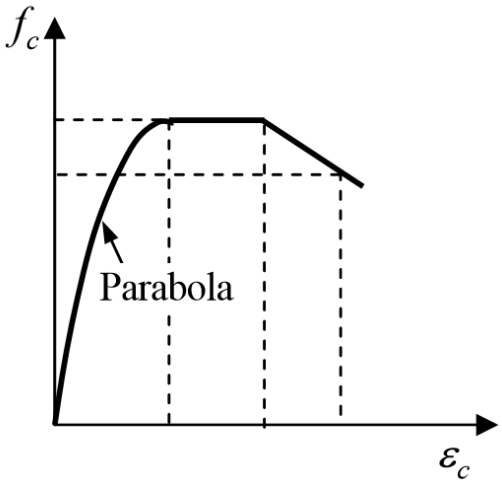


**Figure 2.5 :** Soliman et al proposed stress-strain curve of concrete

### 2.2.5 Sargin et al stress-strain model

Sargin et al proposed a novel model to carry out the stress strain of the concrete based on an equation. It yields a continues curve, and it relates transverse reinforcement ratio, its yield strength and strain gradient across the section and concrete strength. Figure below schematically shows this model [8].

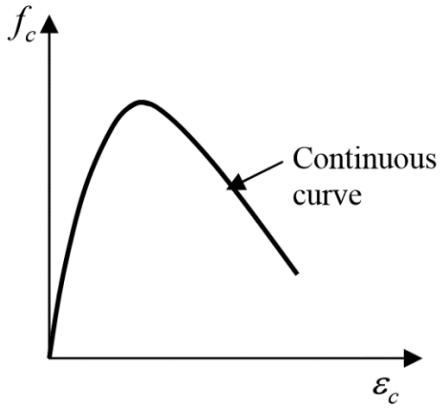


**Figure 2.6 :** Sargin et al proposed stress-strain curve of concrete

The contribution of transverse reinforcement and confinement in all of above models are not intensively taken into account, thus the need for novel methodologies to consider the effect of transverse reinforcement is needed to carry out better stress strain models.

### 2.2.6 Kent and Park stress-strain model

Kent et al in 1971 proposed a novel methodology to carry out the stress-strain relationship of the concrete confined by rectangular hoops, relating the cross sectional area of the stirrup reinforcement, width and depth of the core of the confinement, and spacing of the hoops. This model consists of two sections, first the ascending part of the stress-strain relationship is introduced thanks to a second degree parabola, which is the same for confined and unconfined conditions. The second and descending part, the effect of confinement has been taken into account with a linear equation connecting the maximum stress level to the maximum strain level. [9]

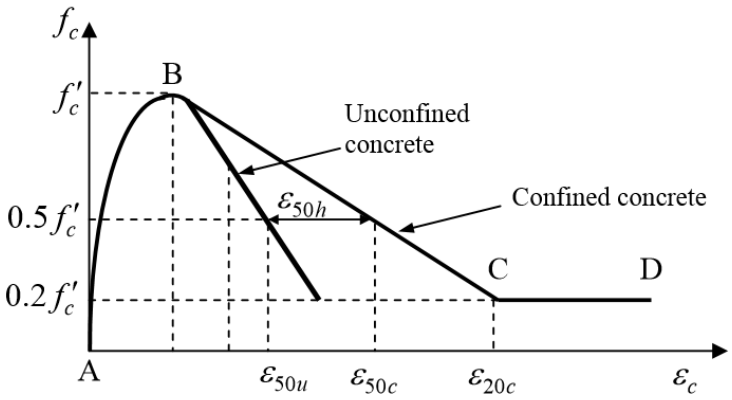


**Figure 2.7 :** Kent et al proposed stress-strain curve of concrete

To calculate the region AB of their model the following equation has been used:

$0 < \varepsilon_c < 0.002$

$$f_c = f'_c \left[\frac{2\varepsilon_c}{0.002} - \left(\frac{\varepsilon_c}{0.002}\right)^2\right] \tag{2.9}$$

It is assumed that the maximum stress level $f'_c$, reaches at the 0.002 strain level.

To carry out the region BC of the stress-strain curve the following formula is used:

$0.002 \leq \varepsilon_c \leq \varepsilon_{20,c}$

$$f_c = f'_c \left[1 - Z(\varepsilon_c - 0.002)\right] \tag{2.10}$$

where:

$$Z = \frac{0.5}{\varepsilon_{50u} + \varepsilon_{50h} - 0.002} \tag{2.11}$$

, which defines the slope of the assumed linear descending branch.

$$\varepsilon_{50u} = \frac{3 + 0.002f'_c}{f'_c - 1000} \tag{2.12}$$

, which defines the value of the strain at stress level of $0.5f'_c$ for unconfined case. The half of the maximum stress level for confined case is denoted as $\varepsilon_{50c}$. The additional ductility gained by transverse reinforcement is shown with $\varepsilon_{50h}$, and is defined as follows:

$$\varepsilon_{50h} = \frac{3}{4}\,\rho_s\,\frac{\overline{b"}}{S_h} \tag{2.13}$$

$f'_c$ = Concrete cylinder strength in psi.

$\rho_s$ = Ratio of volume of transverse reinforcement to volume of concrete core measured to outside of hoops.

$$\rho_s = \frac{2\,(b" + d")\,A_s}{b"\,d"\,S_h} \tag{2.14}$$

$A_s$ = Cross-sectional area of the stirrup reinforcement

$b"$ = Width of confined core measured to outside of hoops

d" = Depth of confined core measured to outside of hoops

$S_h$ = Spacing of hoops

The above parameters are schematically shown in the figure below:

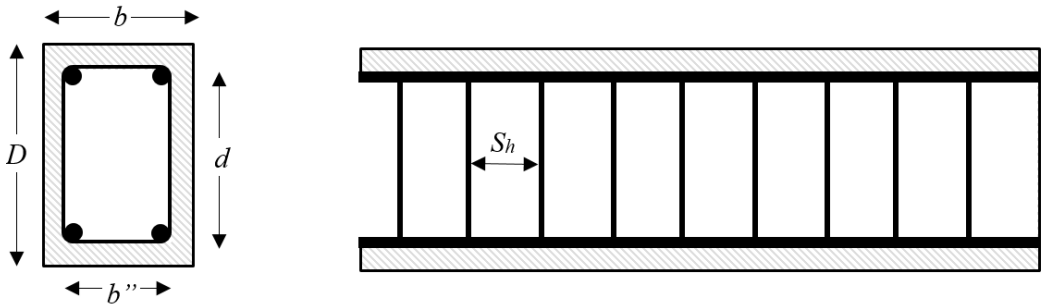


**Figure 2.8 :** Parameters used in the Kent and Park model shown in RC member

The region DC, which accounts for highly strained area on the stress-strain diagram, can be carried out as the following:

$$f_c = 0.2\, f'_c \tag{2.15}$$

### 2.2.7 Modified Kent stress-strain model

A modification was conducted on the Kent et al model later in 1982, by Park et al to elicit a better result of stress-strain model [10]. The coefficient $K$ has been defined to improve the strength of the concrete related the transverse confinement. Similar to Kent proposed model, this model consist of three branches, namely, AB, BC, and DC regions. The model schematically is shown in the figure below:

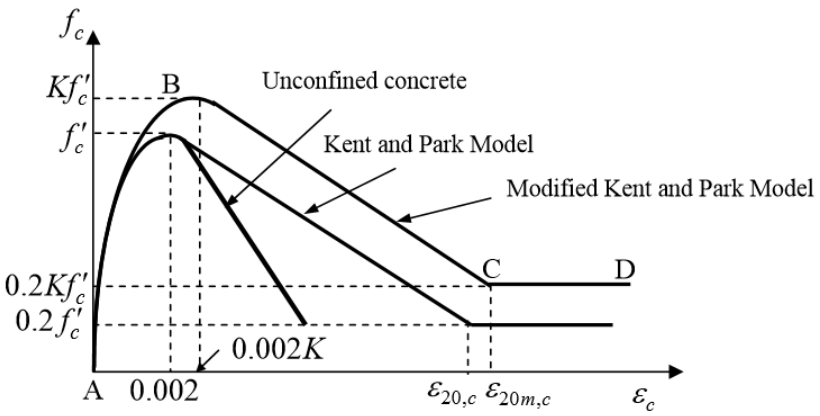


**Figure 2.9 :** Modified Kent stress-strain curve of concrete

$K$ coefficient is calculated as:

$$K = 1 + \frac{\rho_s\, f_{yh}}{f'_c} \tag{2.16}$$

where $f_{yh}$, is the yield strength of steel hoops.

The stress-strain relationship in the AB section can be calculated as the following

$0 < \varepsilon_c < 0.002K$

$$f_c = Kf'_c \left(\frac{2\varepsilon_c}{0.002} - \left(\frac{\varepsilon_c}{0.002}\right)^2\right) \quad (2.17)$$

BC branch in the diagram is carried out as:

$0.002K \leq \varepsilon_c \leq \varepsilon_{20,c}$

$$f_c = Kf'_c \left(1 - Z_m \left(\varepsilon_c - 0.002K\right)\right) \geq 0.2Kf'_c \quad (2.18)$$

where,

$$Z_m = \frac{0.5}{\frac{3 + 0.29f'_c}{145f'_c - 1000} + \frac{3}{4}\rho_s \left(\frac{\overline{b''}}{S_h}\right) - 0.002K} \quad (2.19)$$

$f'_c$ = Concrete $_{\text{cylinder}}$ strength in mega Pascal.

CD branch is given as:

$$f_c = 0.2\,Kf'_c \quad (2.20)$$

In order to carry out the Moment-Curvature diagram of the RC members in this particular research, the modified Kent model has been used to determine the equivalent concrete stress block. The rest of the proposed model will not be further discussed. In the following sections the modified Kent model has been explained to calculate the stress blocks in the concrete.

#### 2.2.7.1 Modified Kent model stress block parameters

An equivalent stress block can be used to represent the stress-strain curve of Kent modified model. The width of stress block is represented in term of the coefficient of concrete compression strength and denoted as *α*, and, its depth is the distance between the extreme compression fiber from the neutral axis, namely *kd*. The corresponding force of the stress block acts at the distance of *γkd* from the extreme

compression fiber. To calculate the α and γ parameters of modified Kent stress strain model based on proper $\varepsilon_{cm}$ value the following equations can be used:

For the region AB:

$\varepsilon_{cm} \leq 0.002K$

$$\alpha = \frac{\varepsilon_{cm}}{0.002K}\ 1 - \frac{\varepsilon_{cm}}{0.006K} \tag{2.21}$$

$$\gamma = 1 - \frac{\frac{2}{3} - \frac{\varepsilon_{cm}}{0.008K}}{1 - \frac{\varepsilon_{cm}}{0.006K}} \tag{2.22}$$

For the region BC:

$0.002K \leq \varepsilon_{cm} \leq \varepsilon_{20,c}$

$$\alpha = \frac{1}{\varepsilon_{cm}}\ \frac{0.004K}{3} + (\varepsilon_{cm} - 0.002K) - \frac{Z_m}{2}(\varepsilon_{cm} - 0.002K)^2 \tag{2.23}$$

$$\gamma = 1 - \frac{1}{\varepsilon_{cm}}\ \frac{\frac{{\varepsilon_{cm}}^2}{2} - \frac{(0.002K)^2}{12}\ - Z_m\ \frac{{\varepsilon_{cm}}^2}{3} - 0.001K{\varepsilon_{cm}}^2 + \frac{(0.002K)^3}{6}}{\varepsilon_{cm} - \frac{(0.002K)}{3}\ - Z_m\ \frac{{\varepsilon_{cm}}^2}{2} - 0.002K\varepsilon_{cm} + \frac{(0.002K)^2}{2}} \tag{2.24}$$

For the region CD:

$\varepsilon_{cm} > \varepsilon_{20,c}$

$$\alpha = \frac{1}{\varepsilon_{cm}}\ \frac{0.004K}{3} + \frac{0.32}{Z_m} + 0.2K\varepsilon_{cm} - 0.0004K \tag{2.25}$$

$$\gamma = 1 - \frac{1}{\varepsilon_{cm}}\ \frac{1.2667 \times 10^{-6} \times K^2 + \frac{0.00064K}{Z_m} + \frac{0.8^3}{6{Z_m}^2} + 0.1{\varepsilon_{cm}}^2}{\frac{0.004K}{3} - \frac{0.32}{Z_m} + 0.2K\varepsilon_{cm} - 0.0004K} \tag{2.26}$$

In this particular study the modified Kent model has been used to simulate the concrete stress block in any frame sections. Using the stress strain relationship for an RC section the moment-curvature can be calculated accordingly. All the Moment-curvature for column section has been calculated and explained in chapter 4.

After calculating the plastic length that is likely to take place on the RC frame, to simulate the bare frame, a multi-spring model has been implemented. The nonlinear plastic springs whose characteristic has been calculated, are assigned to the models at the locations where the plastic joints are likely to occur. Therefore, the base shear displacement backbone curve can be calculated for the RC bare frame.

To implement the effect of the Infill walls on the RC bare frame, pin jointed strut diagonally connected from the bare frame is used to increase the its rigidity accordingly. In this regard, in the following section, literature review to implement pin jointed strut models has been surveyed.

### 2.3 Infill Wall Equivalent Spring Rigidity; Literature Review

Although infill walls are considered non-structural elements, it is important to investigate its effect and in structural systems. Masonry wall consist of masonry brick or block unites and mortar to joint them together. Most widely used masonry units are burned clay brick and concrete block. The mortar of masonry wall can be lime or mixture of cement, lime, sand and water in the various proportions. Overall rigidity of the masonry infill wall depends on rigidity of masonry units and mortar and the bond between them. The compressive strength of masonry wall is very much higher from that its tensile strength and it is substantially less than masonry unit's tensile strength, due to presence of mortar. As it is mentioned by Mosalman K. et al. [11] the bond between the brick and the mortar due to either a chemical bond or friction. According to Mosalman the chemical bond between the brick and the mortar depends on the absorption rate of the brick unite. The higher the brick absorption is the lower the mortar strength will be. This is why during the construction of the masonry wall the brick unit is wetted. If the masonry wall is constructed the wrong way, it will significantly affect the masonry strength. Masonry walls with a weak mortar tensile strength are likely to fail due to sliding between brick units. An overall review of the publications reveals that the infill wall's failure can occur due to

inadequate shear strength or inadequate out-of-plane flexural strength (Dyngeland, 1998).

To study the lateral stiffness of the infill wall, and the failure mode of the infill frames, a numerous research has been conducted in the last four decades. Fiorato et al. [12] preformed monotonic an cyclic lateral loading on non-ductile reinforced concrete frame and they showed that horizontal sliding failure of masonry can introduce a mid-column failure in the frame. This failure occurs when the masonry infill wall has increased the rigidity of the frame, though its sliding effect has led to a mid-column failure mode.

Klinger and Bertero [13], and Brokken and Bertero [14] conducted tests of masonry infill with 1/3 of scale, on a thee story height reinforced concrete frame infilled with fully grouted hollow concrete masonry. The infill wall was reinforced with horizontal and vertical bendable bars. This experiment conducted under monotonic and cyclic loading of the specimen and revealed that the presence of the extra reinforcement can increase the seismic performance, its strength and ductility.

Kahn and Hanson [15] showed that by the gap generated between the infill wall and the column due to lateral loading of the frame, the shear transformation between beam and infill is increased, causing it behave in a significantly ductile manner. They also conducted their experiment on the reinforced infill. In addition, they observed that due to failure of the infill panel, a substantial load will be burdened by the columns, causing them to fail and lose the lateral stiffness immediately. To avoid columns shear failing, they suggested to use adequate shear confinement in them.

Mehrabi et al. [16] performed infill frame tests on ductile and non-ductile frames with in a single bay one story and a multiple bay one story frames with unreinforced infills. They observed that well designed and ductile concrete frames can prevent shear failure of columns, therefore, energy dissipation capability of infill walls could be taken into account in such frames. They also presented a novel analysis method to predict strength of the infilled frame as well as the failure mode of it. In their later study [17] they found out infills have a compression resistance forming a diagonal strut as a high lateral load level separates the infill from its boundaries.

Zovkic et al. [18] tested one bare frame and nine reinforced infill walls with scale of 1/2.5 of single bay reinforced concrete frame with various strength of masonry infill. They concluded that frames with infill has a higher ultimate stiffness, initial stiffness and dumping than those of the bare frame.

While modeling masonry infill elements in between any structural systems, the macro and micro models are addressed. The complexity of the micro models makes them practically unusable for multi-bay and multi-story structural systems. Therefore, it is demanding to simplify the rigidity of infill walls to implement easy-to-use and yet accurate methods.

An extensive number of researches have been carried out to model masonry infills in the RC or steel frames. In 1956, Polyakov et al. conducted number of experiments to model the effect of masonry infill in steel frames. They concluded that the existence of the infill increases the stiffness of a 14 story height by 10 to 20 percent [19]. Several researchers proposed the macro models to simplify the rigidity of infills [20], [21]. Despite of being a macro model, these models are still complicated and hard to implement. A very simplified and yet authentic method was proposed be Stafford Smith. A pin jointed diagonal strut was proposed according to this model, which the width of the strut depends on relative infill frame stiffness. He concluded that the load-deformation relationship of such models can be replaced by an equivalent strut diagonal strut element connecting the corners of the frame [22], [23], [24]. After Stafford, several researches tried to improved his analytical model. Mainstone obtained a new ratio for equivalent strut of infill which was applicable prior to the first infill crack [25]. Liauw and Kwan conducted tests of non-integral infills with rigid frames and obtained a new equivalent pin jointed strut rigidity [26]. Paulay and Priestley suggested that the width of the diagonal strut can be taken as one-fourth of infill's diagonal length for a force equal to one half of the ultimate load [27]. Flanagan and Bennet proposed an analytical procedure to model the masonry infill walls with the equivalent strut element. They conducted 21 experiments of steel frames with a clay tile infill walls [28]. A discrete element method were proposed by Mohebkhah et al. [29], in 2008, to simulate the nonlinear behavior of masonry infill steel frames. This study allowed to simulate the opening of cracks of masonry infill, sliding between blocks, and complete detachment of blocks while the model was exposed to large deformations.

While modeling masonry infill elements in between any structural systems, the macro and micro models are addressed. The complexity of the micro models makes them practically unusable for multi-bay and multi-story structural systems. Therefore, it is demanding to simplify the rigidity of infill walls to implement easy-to-use and yet accurate methods. Several researchers proposed the macro models to simplify the rigidity of infills [20], [21]. Despite of being a macro model, these models are still complicated and hard to implement. A very simplified and yet authentic method was proposed be Stafford Smith. A pin jointed diagonal strut was proposed according to this model, which the width of the strut depends on relative infill frame stiffness [22].

In this research pin jointed strut is used to simulate the effect and rigidity of the masonry infill walls in the reinforced concrete. The simulated results are compared against the experimental results in chapter 4.

# 3. STATEMENT OF THE EXPERIMENT

## 3.1 Geometry Properties of the Problem

Four sets of experiment have been carried out to assess the effect of infill wall in an RC frame exposed to a cyclic response. All of the specimen RC frames share the same shape and geometry characteristics, except for their infill properties. The RC frame specimen is 1.5 meters' height, with a single span bay with the length of 2.5 meters. The schematic view of the specimen is shown in the Figure 3.1. The two columns of the specimen have the rectangular frame section with dimension of 20 by 20 centimeters. The single beam of the RC frame connecting the top two columns has a tee frame section with the web dimension of 15 centimeters in width and 20 centimeters of depth and flange width dimension of 100 centimeters and 7 centimeters of thickness. The thickness of the infill element 10 centimeters. The section properties of such specimen is shown in the Figure 3.2.

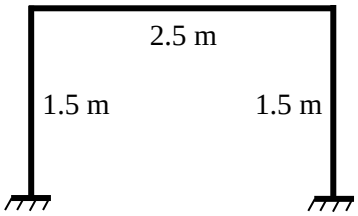


**Figure 3.1 :** Schematic shape of the RC frame of specimen

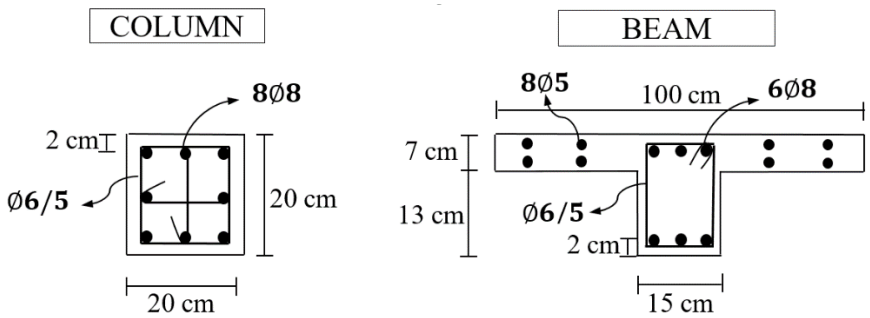


**Figure 3.2 :** The columns and the beam cross sectional detailing

An experiment has been carried out on an RC frame without any infill wall to obtain the isolated cyclic response of it. Then, the following sets of experiments focuses on the effect of infill on the RC bare frame. In this regard, three more experiment has been carried out on RC frame with an infill wall to study the effect of infill on the bare frame. Infill specimens contain an infill without reinforcement, step ties reinforcement (Figure 3.3), and continues ties reinforcement (Figure 3.4). These reinforced infill frame specimens represent different reinforcement configuration. So called continues ties and step ties are the types of reinforcement used in the infill walls. These two configurations are shown in the following figures.

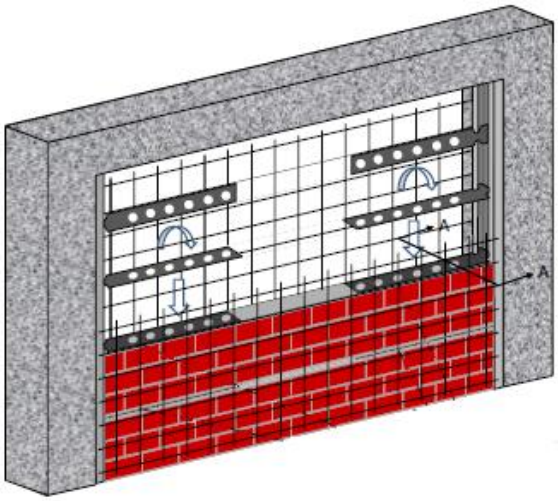


**Figure 3.3 :** Step ties reinforcement configuration

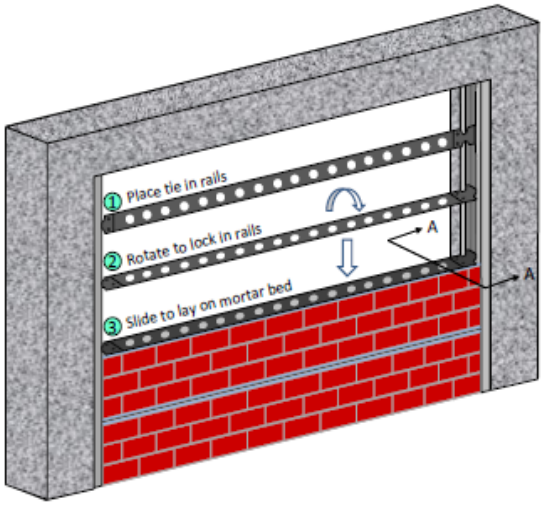


**Figure 3.4 :** Continues ties, reinforcement configuration of an RC frame

### 3.2 Material Properties

The materials required to build up an RC frame are concrete and longitudinal and transverse reinforcement bars. Each RC specimen has different concrete strength but the reinforcement bar characteristics are the same for all of them. The number of experiments has been carried out to assess the concrete specific strength for different RC frames. Table 3.1 shows the experimental results for the concrete specific strength test.

**Table 3.1.A :** Concrete specific strength for RC bare frame

| **Specimen** | **Date** | **Age of Specimen** |
|---|---|---|
| Bare Frame | 7/16/2014 | 92 days |
| **ID** | **$f_{ck}$ (MPa)** | **$f_{ctk}$ (MPa)** |
| N1 | 25.7 | 2.5 |
| N2 | 26.4 | 2.9 |
| N3 | 28.7 | 2.9 |
| N4 | 30.6 | |
| N5 | | |
| **Mean** | **27.85** | **2.76** |
| **St.Dev.** | **2.27** | **0.26** |

**Table 3.1.B :** Concrete specific strength for RC Infilled Frame

| **Specimen** | **Date** | **Age of Specimen** |
|---|---|---|
| Infilled Frame | 5/9/2014 | 23 days |
| **ID** | **$f_{ck}$(MPa)** | **$f_{ctk}$ (MPa)** |
| N1 | 25.5 | 2.4 |
| N2 | 19.4 | 2.8 |
| N3 | 22.0 | 2.9 |
| N4 | 21.9 | |
| N5 | 22.9 | |
| **Mean** | **22.34** | **2.70** |
| **St.Dev.** | **2.19** | **0.26** |

**Table 3.1.C :** Concrete specific strength for RC InfillTie – Continuous frame

| **Specimen** | **Date** | **Age of Specimen** |
|---|---|---|
| InfillTie - Continuous | 9/10/2014 | 40 days |
| **ID** | $f_{ck}$ **(MPa)** | $f_{ctk}$ **(MPa)** |
| N1 | 35.6 | 2.88 |
| N2 | 33.1 | 2.53 |
| N3 | 36.2 | 2.7 |
| N4 | 33.8 | 2.9 |
| N5 | 34.3 | |
| **Mean** | **34.59** | **2.75** |
| **St.Dev.** | **1.28** | **0.17** |

**Table 3.1.D :** Concrete specific strength for RC InfillTie - Step Frame

| **Specimen** | **Date** | **Age of Specimen** |
|---|---|---|
| InfillTie - Step | 29/12/2014 | 80 days |
| **ID** | $f_{ck}$ **(MPa)** | $f_{ctk}$ **(MPa)** |
| N1 | 32.3 | 3.193 |
| N2 | 31.6 | 2.895 |
| N3 | 32.8 | 2.453 |
| N4 | 34.6 | 2.95 |
| N5 | 34.9 | |
| **Mean** | **33.25** | **2.87** |
| **St.Dev.** | **1.47** | **0.31** |

To carry out the properties of the steel reinforcement bars the number of experiment has been conducted on longitudinal and transverse steel reinforcement to obtain the tensile yield and the ultimate stress and strain of them. All the frame specimens share the same type of longitudinal reinforcement, but the transverse reinforcement properties along frame specimen are different. Table 3.2 shows the experimental tensile strength test results for utilized bar reinforcement. Due to experimental inaccuracies in transverse reinforcement rebar for bare frame and infill frame, the parameters are assumed in the way that elasticity modules will be 200000 MPa.

**Table 3.2 :** Tensile strength of longitudinal reinforcement rebar used for all four frame specimen

| | **Reinforcement** | | **Diameter** | **Specimen** | |
|---|---|---|---|---|---|
| | Longitudinal | | 8 mm | All | |
| **ID** | $f_{yk}$ **(MPa)** | $f_{uk}$ **(MPa)** | $\varepsilon_y$ | $\varepsilon_u$ | $E_s$ **(MPa)** |
| N1 | 445.23 | 576.86 | 0.00210 | 0.22090 | 212014 |
| N2 | 423.00 | 545.24 | 0.00236 | 0.27660 | 179237 |
| N3 | 413.50 | 561.84 | 0.00217 | 0.25060 | 190202 |
| N4 | 396.00 | 549.16 | 0.00200 | 0.23200 | 198000 |
| N5 | 365.00 | 564.17 | 0.00280 | 0.20360 | 130357 |
| **Mean** | **408.55** | **559.45** | **0.00229** | **0.23674** | **181962** |
| **St.Dev.** | **30.14** | **12.64** | **0.00032** | **0.02807** | **31220** |

**Table 3.3 :** Tensile strength of transverse reinforcement rebar utilized for bare frame & Infill frame

| | **Reinforcement** | | **Diameter** | **Specimen** | |
|---|---|---|---|---|---|
| | Transverse | | 6 mm | Bare frame & Infill frame | |
| **ID** | $f_{yk}$ **(MPa)** | $f_{uk}$ **(MPa)** | $\varepsilon_y$ | $\varepsilon_u$ | $E_s$ **(MPa)** |
| N1 | 326.00 | 465 | 0.00163 | 0.16000 | 200000 |
| N2 | 330.00 | 469 | 0.00165 | 0.16000 | 200000 |
| N3 | 330.00 | 465 | 0.00165 | 0.16000 | 200000 |
| **Mean** | **328.67** | **466.33** | **0.00164** | **0.16000** | **200000** |
| **St.Dev.** | **2.31** | **2.31** | **0.00001** | **0.00000** | **0** |

**Table 3.4 :** Tensile strength of transverse reinforcement rebar utilized for step-tie & continues tie infill

| | **Reinforcement** | | **Diameter** | **Specimen** | |
|---|---|---|---|---|---|
| | Transverse | | 6 mm | Step-tie infill & continues tie infill | |
| **ID** | $f_{yk}$ **(MPa)** | $f_{uk}$ **(MPa)** | $\varepsilon_y$ | $\varepsilon_u$ | $E_s$ **(MPa)** |
| N1 | 455.64 | 512.94 | 0.00236 | 0.20370 | 193068 |
| N2 | 439.11 | 545.24 | 0.00228 | 0.27660 | 192592 |
| **Mean** | **447.38** | **529.09** | **0.00232** | **0.24015** | **192830** |
| **St.Dev.** | **11.69** | **22.84** | **0.00006** | **0.05155** | **336** |

### 3.3 Cyclic Lateral Loading and Gravity Loading Characteristics

To simulate the actual gravity loading of the upper columns on the columns of specimen, 185 KN vertical gravity load has been applied to two columns as axial loads. These axial loads have been applied to the frame via to two hydraulic jacks such that they apply the loading in the vertical direction but they do not resist the lateral direction while the lateral loading is applied (Figure 3.6). Such mechanism is shown in the Figure 3.6. This axil load acting on column will help us to study the P-Delta effect while applying lateral excitation.

The beam connecting two columns burdens 10.25 KN/m of distributed load. This distributed loads mimics the possible live and dead load acting on the beam.

To simulate the lateral loading to the RC frame and obtain its lateral response, a cyclic lateral displacement-controlled loading has been applied to the RC frame from the top of right column. The magnitude of the applied displacement load is increased and reversed to opposite direction in each cycle to assess the lateral response of the RC frame, with and without an infill wall. The lateral pattern of the displacement protocol is shown in the Figure 3.7.

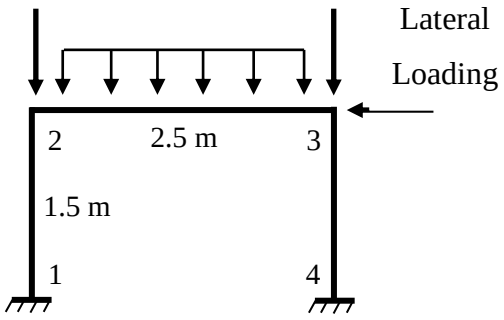


**Figure 3.5 :** Schematic representation of the loads acting of RC frame

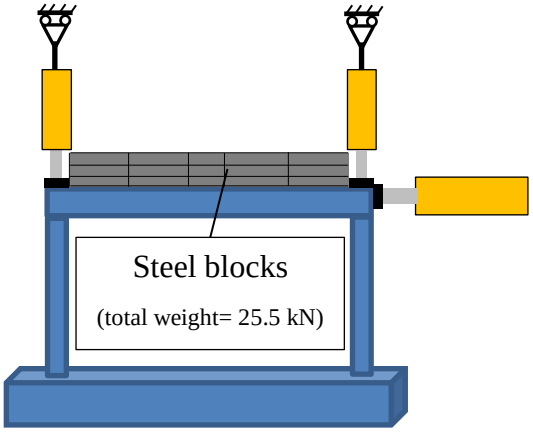


**Figure 3.6 :** Loading mechanisms

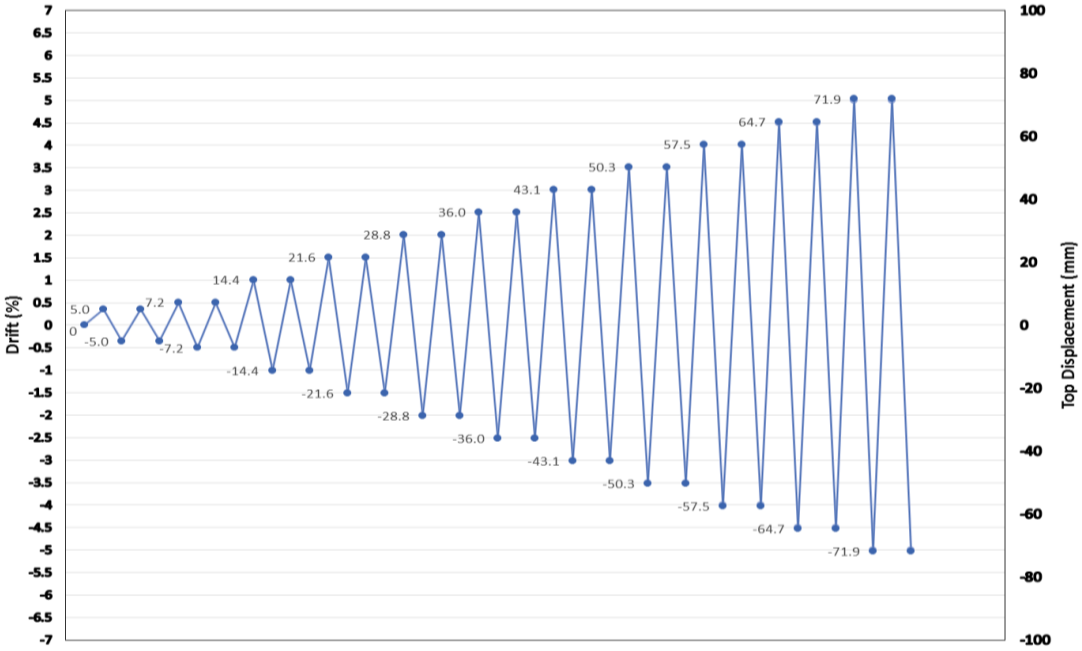


**Figure 3.7 :** The lateral loading protocol acting on the top right of the RC frame

### 3.4 Locations of the LVDTs

Data and displacement acquisition of the RC frame in different locations has been measured by Linear Variable Differential Transformers (or LVDTs in short) that was installed on the frame. LVDTs are devices used to measure the linear transformation (position) between two points. Figure 3.8 represents the locations and the configuration of the LVDTs on the RC test specimen.

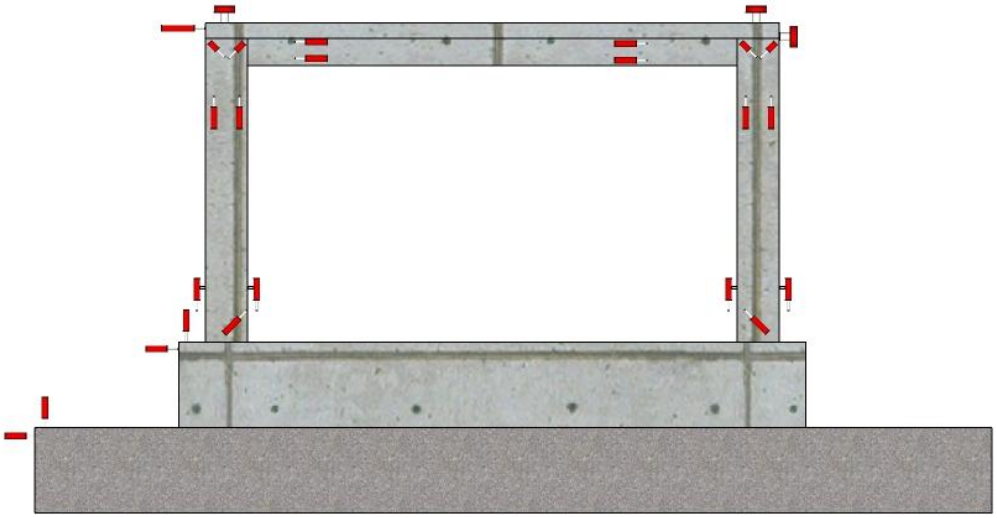

**Figure 3.8 :** Locations of LVDTs on the RC frame

### 3.5 An Acknowledgement for Conducting Experiments

All the experiments have been carried out in Middle East Technical University (METU) lab, and all of above information is obtained from the METU's experimental results. The current study focuses on the simulation strategies as oppose data acquisition methodologies. The METU has not technically collaborated with the author; therefore, simulation methodology has been fully carried out at Istanbul Technical University (ITU).

# 4. IMPLEMENTED METHODS BASED ON ANALYTICAL AND EXPERIMENTAL RESULTS

In this section the implemented models are presented. First, the models based on analytical results are obtained. Afterwards, reinforced concrete bare frame is modeled. Then, the effect of infill wall is added to the existing model using a pin jointed diagonal strut.

As the second implementation strategy, a novel method based on experimental results is presented. Genetic algorithm is used to calibrate the simulated results in a way that it fit the best to experimental results. Popular hysteresis models are introduced, and the most appropriate one that describes the data is assessed and is picked to represent the experimental results.

## 4.1 Implementing the Models Based On Analytical Results

In the following sections, simulation of RC bare frame has carried out based on the analytical results. First the moment curvature of the columns is calculated. Then a bare frame model is implemented based on rigid members and elastic springs. Elastic springs are assigned on the RC frame where plastic joints are likely to occur due to excessive lateral loadings. To model the rigidity of the masonry infill walls, the pin jointed strut model is used. The base shear versus displacement carried out from analytical results are compared against the experimental results.

### 4.1.1 Calculation of moment-curvature of the columns

While knowing strass-strain values at different levels in RC members, forces and moments acting on them based on any assumed strains levels can be calculated. In other words, by assuming an axial load condition acting in an RC member, the equilibrium for different strain levels could be checked to carry out the corresponding Moment-Curvature graph for any RC member. In this particular

research the following algorithm is used to determine the Moment-Curvature graph of RC column members based modified Kent model to simplify the stress-strain relationship of the concrete.

**Input:**
-Geometry information of RC member (Rectangular RC section dimension, longitudinal and transverse reinforcement configuration and their content),
-Material properties of steel and concrete
*-Axial Load acting on member*
**Output:** Moment-Curvature Graph

**1 for** $\varepsilon_{cm}$*= 0.0001* to *0.1*
**2 for** $kd$*=0.0001* to *depth of Rectangular section*
**3** **Append** stress block parameters to α and γ for the value of $\varepsilon_{cm}$. (using appropriate equation based on the region in which $\varepsilon_{cm}$ lies**)**
**4** **Append** total compressive force in concrete to $C_{con}$. (using α , γ and *kd*)
**5** **Append** strains at different levels of steel to $Strains_{n\times 1}$ (*n* being the number of layer of reinforcement)
**6** **Append** stresses in reinforcement bars using the stress-strain curve of steel $Stresses_{n\times 1}$.
**7** **Append** the summation of compressive and tensile forces in reinforcement bars to *P*. `
**8** **If** *Axial Load* equals to *P*
**9** **Append** the moment of resistance to *M*, and the corresponding curvature to $\varphi$.
**10** **else if** next index of *kd*
**11** **end if**
**12** **end for**
**13 end for**
**14 return** *M* and $\varphi$

**Figure 4.1 :** The flowchart of the used algorithm to carry out the Moment-Curvature graph

With geometry information of RC columns and the material properties, namely the compression strength of the concrete and the tensile strength for the longitudinal and transverse reinforcement in hand, its Moment-Curvature graph was calculated using the Algorithm mentioned in the previous section. For the different magnitude of axial loads the Moment-Curvature graph was plotted for RC columns, which their geometry information has been shown in Figure 3.2. It's been observed that for the increasing levels of axial load the moment carrying capacity of the RC column are increased. On the other hand, the ductility of the column is reduced. The ductility ratio of an RC member can be calculated from the division yield strain over the maximum strain capacity. The Figure below shows the Moment-Curvature diagram for the different levels of axil load acting on the columns in our case of study.

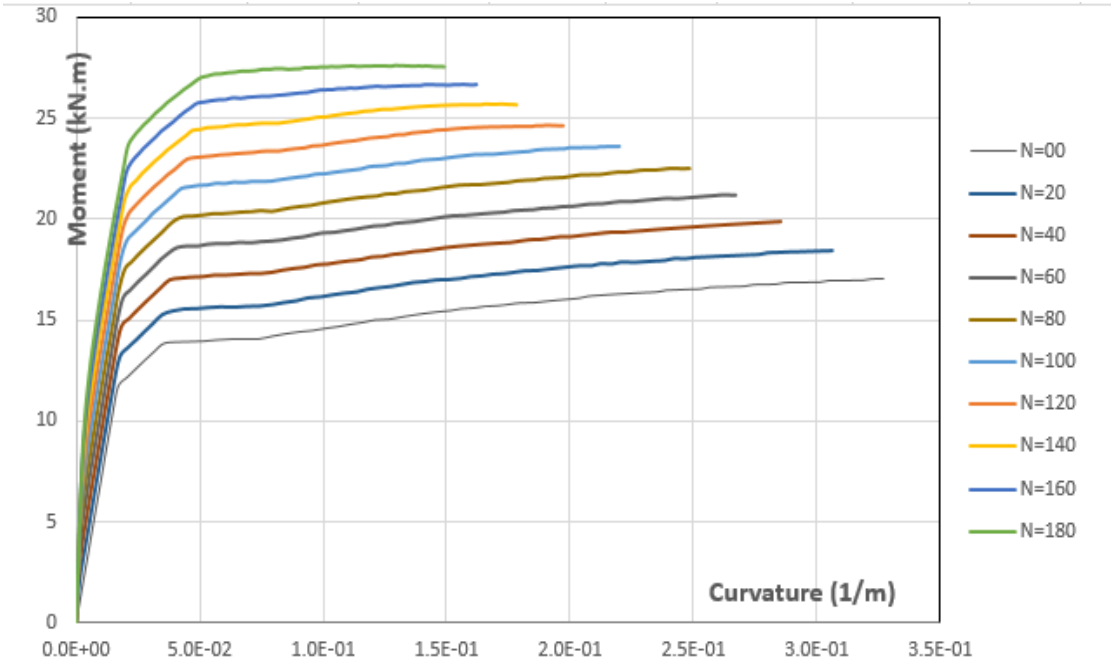


**Figure 4.2 :** Moment-Curvature diagram for different axial loading levels for bare frame's columns

To calculate the moment-rotation from the carried out moment-curvature relationship, the following equation can be used. Basically the rotation per length of the member is the curvature.

$$\Theta_{AB} = \int_{A}^{B} \Phi dx \qquad (4.1)$$

where:

$\Theta_{AB}$, is the rotation of the member between points A and B,

$\Phi$ , is the curvature of the member at the dx length of the member.

### 4.1.2 Implemented bare frame spring model case

The following Non-linear elastic spring configuration have been used to carry out the load-deformation relationship of the RC bare frame. The rigidity of the members has been assumed to be infinity. And the major rotations (plastic hinges) have been assumed to occur on the top of column members. The length of the plastic joint is calculated from Pauley-Priestley formula who recommend to use the half of the depth of the confined core as the plastic joint length [30]. Since the depth of confined

core in at columns are 16 centimeters, the plastic joint length can be calculated ad 8 centimeters. To easily calibrate the nonlinear elastic springs, and convert the analytical moment-curvature relationships to moment-rotation, the moment of inertia of the members are assumed to be infinity. Figure 3-12 schematically shows configuration of the bare simulation.

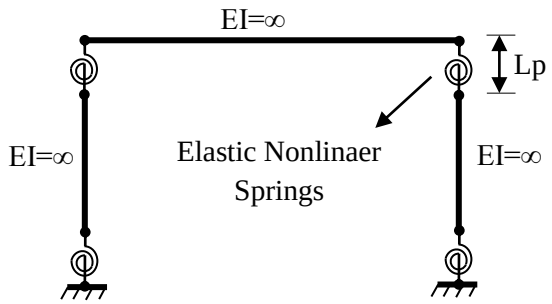


**Figure 4.3 :** Nonlinear elastic springs configurations

### 4.1.3 Comparison the load deformation analytical results with the Experimental results

The load-deformation relationship of the model, mentioned in the previous section, is shown against the experimental results. It can be concluded that the maximum shear peak capacity of the reinforced concrete bare frame, namely 75kN, is almost close to that value of the analytical results, which is 80kN. However, experimental data shows that the load-deformation curve of RC bare frame descends after a maximum shear value, which this descending branch is a straight line in simulated results. The other obvious thing that deviates the experimental and simulated results is the slope of load-deformation line around the origin. Analytical model suggests a high value of shear capacity for an assumed deformation around the origin. Figure below shows the analytical results versus the experiment load-deformation data. The experimental load-deformation data is idealized with a multilinear curve.

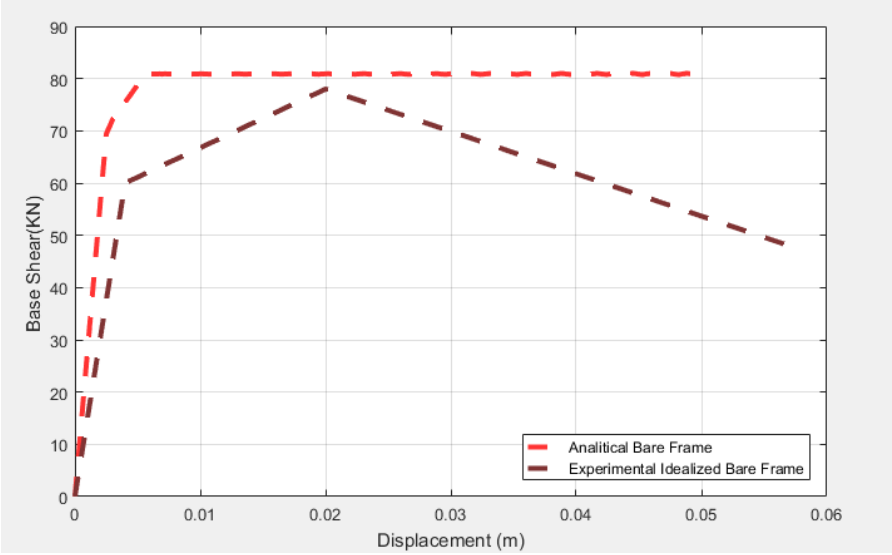


**Figure 4.4 :** Experimental versus analytical results of backbone load deformation curve of the bare frame

### 4.1.4. Implemented Pinned Jointed Strut Model:

Several researches has been conducted to model the rigidity of the infill masonry wall in an RC or steel frame using pin joined strut model. In these model the masonry infill element is replaced with a pin jointed diagonal spring connecting the corners of the frame. The idea behind this implementation method is to define an effective width of masonry wall that can transfer the lateral load diagonally to the other corner while the lateral loading has been applied to frame. This idea has been suggested by Holems in 1961 [31]. While replacing the masonry element with the strut, the thickness of the wall is assigned to replaced strut, in addition to the determined effective width. In the following section the effective width is calculated for masonry infill element with equation suggested by the famous researchers and then compared with each other.

### 4.1.5. Determination of the Equivalent Width of Strut Element:

A massive amount of research is presented to carry out the effective width of masonry wall in the literature from which the following equations drew most of attention from research community of their time. In 1961 Holems [31] suggested to use an equivalent strut with the width of one third of infill's diagonal length. This equation was independent from frame to infill's rigidity which is an important factor to carry out the equivalent rigidity of the strut. The equation can be shown as:

$$w = \frac{1}{3} d_{inf} \quad (4.2)$$

where $d_{inf}$ is the diagonal length of infill element.

Later Stafford Smith and Carter in 1969 stated the width of infill as the equation below [24]:

$$w = 0.58(\frac{1}{H})^{-0.445}.(\lambda_h H_{inf})^{0.335 d_{inf}} (\frac{1}{H})^{0.064} \quad (4.3)$$

where:

$$\lambda_h = \sqrt[4]{\frac{E_{inf} t \sin 2\theta}{4 E_c I_c H_{inf}}} \quad (4.4)$$

$t, H_{inf}$ and $E_{inf}$ are the thickness, height and modules of elastic of infill element respectively. $E_c$ and $I_c$ are modules and moment of inertia of the columns. The angle between the strut and the horizon is denoted as $\theta$. H is the height of frame. $\lambda_h$is a unite-less parameter which contributes the effect of frame's to infill's rigidity in the equation. $\lambda_h$ parameter has been widely used in research community to determine the width of the equivalent strut. In 1971 Mainstone conducted test of frames with brick infills and proposed to use the equation below to determine the width of the infill [25]:

$$\mathrm{w} = 0.16\, d_{inf} (\lambda_h H_{inf})^{-0.3} \quad (4.5)$$

Mainstone and week in 1972 stated a developed version of previous equation as the following to obtain the width of the equivalent strut [32]:

$$\mathrm{w} = 0.175\, d_{inf} (\lambda_h H_{inf})^{-0.4} \quad (4.6)$$

In 1984, the following equation was proposed by Liauw and Kwan regarding the width of the equivalent strut [26]:

$$w = \frac{0.95 H_{inf} \cos \theta}{\overline{\lambda_h H_{inf}}} \tag{4.7}$$

Paulay and Preistley in 1992 proposed the following conservative equation for width of equivalent strut. They suggested that a higher value for the width of equivalent strut will result in a substantially higher value for structural response. They proposed the width of the strut to be one fourth of infill's diagonal length as the following [30]:

$$w = 0.25\, d_{inf} \tag{4.8}$$

Durrani and Luo in 1994 studied the lateral response of reinforced concrete infilled frame with Milestone's equations and they proposed their own effective width of strut as the following [33]:

$$w = \gamma \ \overline{L^2 + H^2} \ \sin 2\theta \tag{4.9}$$

where:

$$\gamma = 0.32 \ \overline{\sin 2\theta} \ \left( \frac{H^4 E_{inf} t}{m E_c I_c H_{inf}} \right)^{-0.1} \tag{4.10}$$

$$m = 6 \ \left(1 + \frac{6 E_c I_b H}{\pi E_c I_c L}\right) \tag{4.11}$$

In 1998 Hendry contributed the contact length of column and beam in the effective length of equivalent strut as the following equation [34]:

$$w = 0.5 \ \overline{{\alpha_h}^2 + {\alpha_L}^2} \tag{4.12}$$

where:

$$\alpha_h = \frac{\pi}{2} \left( \frac{4 E_c I_c H_{inf}}{E_{inf} t \sin 2\theta} \right)^{\frac{1}{4}} \tag{4.13}$$

$$\alpha_L = \pi \left( \frac{4E_c I_b L_{inf}}{E_{inf} t \sin 2\Theta} \right)^{\frac{1}{4}} \quad (4.14)$$

In the following section the effective width of the equivalent strut has been calculated using all the aforementioned equations. Table 4.1 represent the material properties used to obtain the effective width of strut. Material properties are explained in chapter 3. The elasticity module of the infill element has been assumed as 12 GPa.

| *Parameters* | *Value* | *Unite* |
|---|---|---|
| $H$ | **1600** | mm |
| $L$ | **2500** | mm |
| $H_{inf}$ | **1300** | mm |
| $L_{inf}$ | **2300** | mm |
| $\Theta$ | **31** | degrees |
| $t$ | **100** | mm |
| $E_{inf}$ | **12** | GPa |
| $E_c$ | **22** | GPa |
| $A_c$ | **40000** | $mm^2$ |
| $I_b$ | **489000000** | $mm^4$ |
| $I_c$ | **133333333** | $mm^4$ |
| $d_{inf}$ | **2641** | mm |

**Table 4.1**: Geometrical parameters and material properties of frame members

The following Table illustrates the effective width of strut carried out with the aforementioned equations.

| *Researcher* | *Equation No.* | *Strut Width (m)* |
|---|---|---|
| **Holmes [31]** | (4.2) | **0.88** |
| **Stafford Smith and Carter [24]** | (4.3) | **2.76** |
| **Mainstone [25]** | (4.4) | **0.28** |
| **Mainstone and Weeks [32]** | (4.5) | **0.27** |
| **Liauw and Kwan [26]** | (4.6) | **0.54** |
| **Paulay and Preistley [30]** | (4.7) | **0.66** |
| **Durrani and Luo [33]** | (4.8) | **0.52** |
| **Hendry [34]** | (4.11) | **0.91** |

**Table 4.2**: Effective width of strut obtained from different researches

The non-linear stress-strain curves were obtained in an experimental study by Kaushik et al [35] in which three different mortar grades were used to construct masonry element. The average compressive strength of masonry wall obtained in his

study for the three grades of mortar was 4.1 MPa with COV of about 25% (1:0:6 mortar grade), 7.5 MPa with COV of about 20% (1:0:3 mortar grade), and 6.6 MPa with COV of about 20% (1:0.5:4.5 mortar grade) as shown in the figure below. In our study we have used the stress-strain relationship of the mortar with the grade (1:0:6) to represent the nonlinearity of masonry infill element.

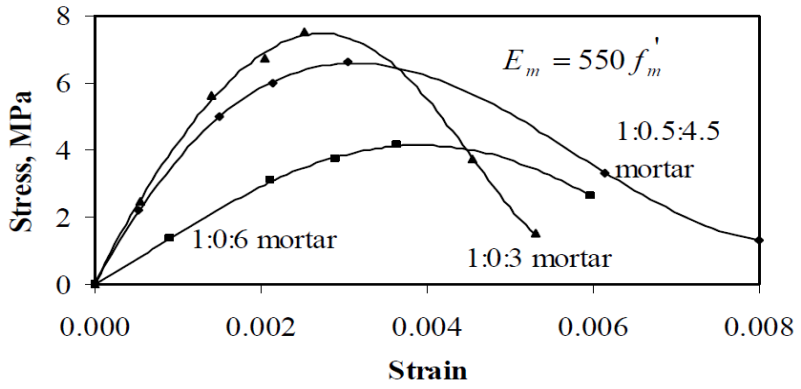


**Figure 4.5**: Stress-strain relationship for three grades of mortar

For different width of equivalent strut, mentioned in Table 4.2, to represent the infill element, numerous base shear-displacement relationships can be obtained considering the dimension of the infill. Figure 4.6 shows these relationships for different width of strut member.

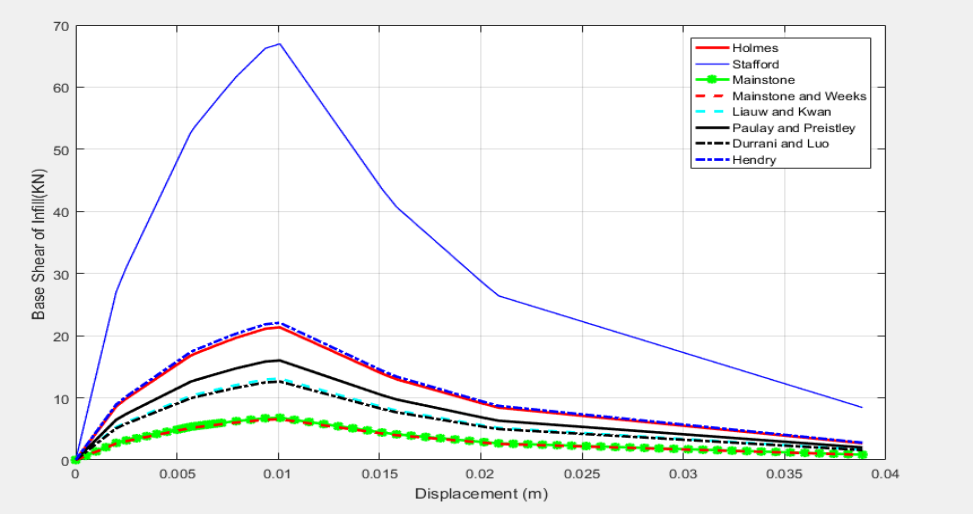


**Figure 4.6:** Base shear-displacement of infill element versus different width of strut

Numerous models have been implemented for different width of equivalent pin jointed strut to carry out specific base shear-displacement relationship which is

shown Figure 4.7. Base shear-displacement relationship of these models are then compared against with that of experimental results to pick the closest one. We concluded that Hendry width of equivalent strut best represents the infill behavior in the RC frame.

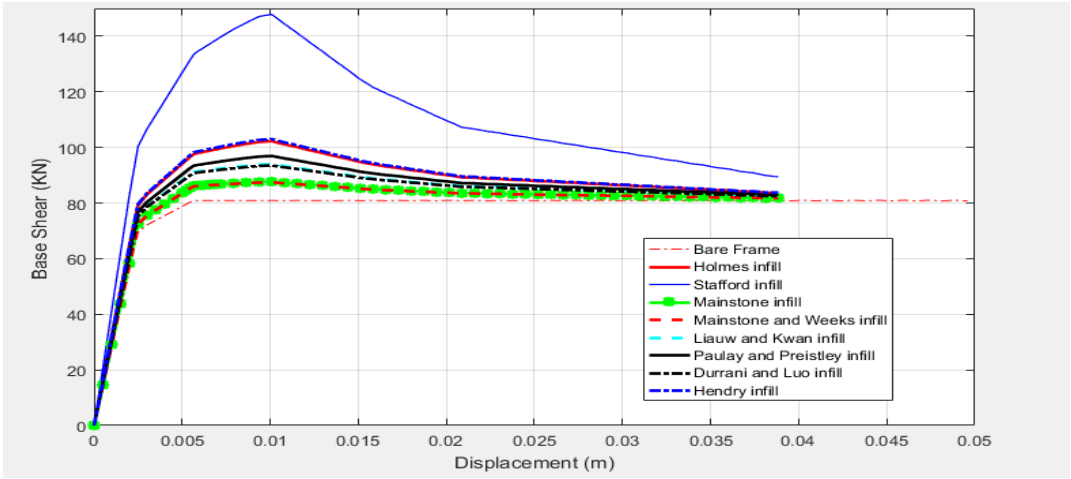


**Figure 4.7:** Base shear-displacement of infill frame versus different width of strut

Figure 4.8 shows the experimental and analytical results for both bare frame and infill frame case. Hendry width of strut is used in

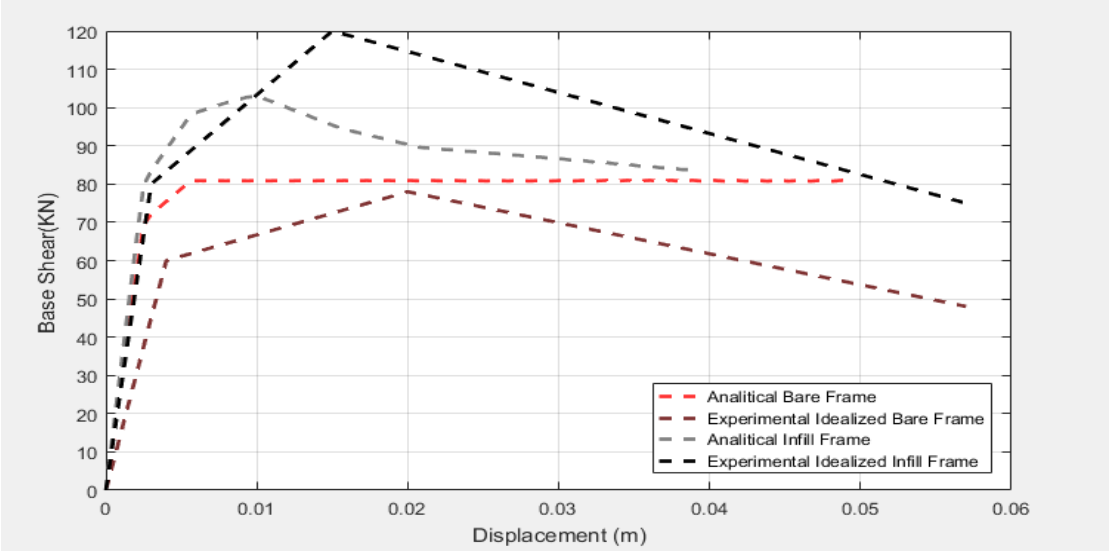


**Figure 4.8:** Analytical versus experimental base shear-displacement results for infill and base frame case

Despite obtaining precise analytical models, the complexity of implementation such models and variation between implementation strategies made us to further research to carry out the relationship between base shear and displacement of frames both infill and non-infill status. In regard, we leveraged experimental results and fit a hysteresis model with it which are explicitly detailed in the following sections.

## 4.2 Models Based on Experimental Results

In the following sections models based on experimental results are presented. After obtaining the backbone skeleton curve from the experimental results, the experimental results are resampled. This process is needed while conducting a curve fitting problem. Then, a genetic algorithm is introduced to fit the experimental to simulated results, while minimizing the deviation of two curves. The semi-automated platform is implemented to carry out all the calculations.

### 4.2.1. Obtaining idealized load-deformation backbone curve

Once that the experimental load-deformation cyclic data is recorded from any specimen, the backbone load-deformation relationship could be identified for it. The backbone curve represents the specimen inelastic non-linearity pattern for an excessive load or displacement setting. This loading pattern depicts the yielding and ultimate strength as well as the toughness of the specimen. Conventionally the load-deformation backbone relationship was extracted manually form the data, though, in this particular research this curve is extracted automatically from the experimental results.

To obtain the load-deformation relationship automatically from the experimental results the following steps are considered. First, the local maximums and minimums of load values for each cycle are extracted, and, each cycle is separated to be studied explicitly. Second, for each cycle, the maximum load value and its corresponding deformation value associated with each cycle is retrieved. After retrieving all load maximums of hysteresis data, to finalize calculation of the backbone curve, maximums points of each cycle are then sorted from their lowest to highest deformation value with an ascending rate. The following algorithm is developed to

obtain the load deformation curve automatically, from the experimental load-deformation cyclic results.

**Input:** Displacement LVDT recorded array: *(Displacement)*
Load LVDT recorded array: *(Load)*
**Output:** Backbone envelope curve's Displacement array**: (***EnvelopeDisplacement)*
Backbone envelope curve's Load array: *(EnvelopeLoad)*

(Obtaining the direction change in base-shear data record as the following)
**1 for** each consecutive member of **(***$Load_i$*, *$Load_{i+1}$*)
**2** *pp*← *$Load_i \times Load_{i+1}$*
**3 if** *pp<0*
**4** **Append** *i* index of the *Load* array to *DirectionChenge* array
**5** **end if**
**6 end for**
(Obtaining all of the local minima and maxima for *Load* array)
**7 for** each consecutive member of **(***$DirectionChenge_i$*, *$DirectionChenge_{i+1}$*)
**8** *Subset*← cut *$DirectionChenge_i$* to *$DirectionChenge_{i+1}$* members of *Load* array
**9** Set average of all *Subset* array members to *SubsetAve*
**10** **if** *SubsetAve > 0*
**11** **Append** maximum of *Subset* array to *LoadMaxima*
**12** *IndexVal*← Return index of *LoadMaxima in Load* array
**13** **Append** *IndexVal* to *LoadMaximaIndex*
**14** **else**
**15** **Append** minimum of *Subset* array to *LoadMinima*
**16** *IndexVal*← Return index of *LoadMinima in Load* array
**17** **Append** *IndexVal* to *LoadMinimaIndex*
**18** **end if**
**19 end for**
(Obtaining all corresponding maxima and minima for *Displacement* array)
**20 for** each member of **(***$LoadMaximaIndex_i$*)
**21** **Append** *LoadMaximaIndex'th* index of *Displacement* array to *DisplacementMaxima*
**22 end for**
**23 for** each member of **(***$LoadMinimaIndex_i$*)
**24** **Append** *LoadMinimaIndex'th* index of *Displacement* array to *DisplacementMinima*
**25 end for**
(Sort the resulting arrays)
**26 Append** *DisplacementMaxima* and *DisplacementMinima to EnvelopeDisplacement*
**27 Append** *LoadMaxima* and *LoadMinima* to *EnvelopeLoad*
**28 Sort** *EnvelopeDisplacement* and their corresponding *EnvelopeLoad* values with ascending rate
**29 Return** *EnvelopeDisplacement* and *EnvelopeLoad*

**Figure 4.9 :** Algorithm for obtaining backbone curve from cyclic data

The backbone curve is then idealized with seven points (three points at either positive and negative side, as well as one origin point). These three points at the positive and negative side of deformation axis are obtained as the following steps. First, to separate the elastic portion on the backbone curve on positive side, the origin is connected to lowest level of loading value, whose value exceeds the 65 percent of maximum loading value of the backbone curve in the positive deformation side. This will form the elastic portion of backbone, with two points. Second, on the positive side, the point whose loading value on the backbone curve is the maximum is taken

as the third idealization point, and, finally, the point whose deformation is the maximum is taken as the fourth point on the idealization curve. The similar rules are applied to carry out the idealize backbone at the negative deformation side.

This idealization methodology has retrieved promising results, while carrying out the idealization backbone curve. This method works with load-deformation backbone data whose loading capacity is degraded through higher deformation levels. This behavior is mostly observed in concrete and masonry specimens, concrete frames with or without infill masonry walls while they are exposed to in-plane excessive lateral excitations.

The following Figure represents the structure of the algorithm to idealize the backbone curve.

**Input:** Backbone envelope curve's Displacement array**: (***EnvelopeDisplacement)*
Backbone envelope curve's Load array: *(EnvelopeLoad)*
**Output:** Idealized backbone envelope curve's displacement array**: (***IdzEnvelopeDisplacement)*
Idealized backbone envelope curve's Load array: *(IdzEnvelopeLoad)*

**1** $IdzEnvelopeDisplacement_{7\times1} \leftarrow$ zero vector with size of 7×1
**2** $IdzEnvelopeLoad_{7\times1} \leftarrow$ zero vector with size of 7×1
(returning the ultimate displacement points of backbone curve)
**3** $IdzEnvelopeDisplacement_{7} \leftarrow$maximum**(***EnvelopeDisplacement)*
**4** $IdzEnvelopeLoad_{7} \leftarrow$ corresponding *EnvelopeLoad* of maximum *EnvelopeDisplacement*
**5** $IdzEnvelopeDisplacement_{1} \leftarrow$minimum**(***EnvelopeDisplacement)*
**6** $IdzEnvelopeLoad_{1} \leftarrow$ corresponding *EnvelopeLoad* of maximum *EnvelopeDisplacement*
(returning the ultimate load points of backbone curve*)*
**7** $IdzEnvelopeLoad_{6} \leftarrow$maximum**(***EnvelopeLoad)*
**8** $IdzEnvelopeDisplacement_{6} \leftarrow$ corresponding *EnvelopeDisplacement* of maximum *EnvelopeLoad*
**9** $IdzEnvelopeLoad_{2} \leftarrow$minimum**(***EnvelopeLoad)*
**10** $IdzEnvelopeDisplacement_{2} \leftarrow$ corresponding *EnvelopeDisplacement* of maximum *EnvelopeLoad*
(returning the yield points of backbone curve*)*
**11 for** all ascending positive consecutive member of ($EnvelopeLoad_i$)
**12 if** $EnvelopeLoad_i > 0.65 \times$ maximum*(EnvelopeLoad)*
**13** $IdzEnvelopeLoad_{5} \leftarrow EnvelopeLoad_i$
**14** $IdzEnvelopeDisplacement_{5} \leftarrow$ corresponding *EnvelopeDisplacement* of $EnvelopeLoad_i$
**15 end if**
**16 break**
**17 end for**
**18 for** all descending negative consecutive member of ($EnvelopeLoad_i$)
**19 if** $EnvelopeLoad_i < 0.65 \times$ minimum*(EnvelopeLoad)*
**20** $IdzEnvelopeLoad_{3} \leftarrow EnvelopeLoad_i$
**21** $IdzEnvelopeDisplacement_{3} \leftarrow$ corresponding *EnvelopeDisplacement* of $EnvelopeLoad_i$
**22 end if**
**20 break**
**21 end for**
**22 Return** *IdzEnvelopeLoad* and *IdzEnvelopeDisplacement*

**Figure 4.10:** Algorithm to carry out the idealization of the backbone curve

The backbone curve for two set of cyclic load-deformation data has been calculated automatically in the figure below, using the proposed method.

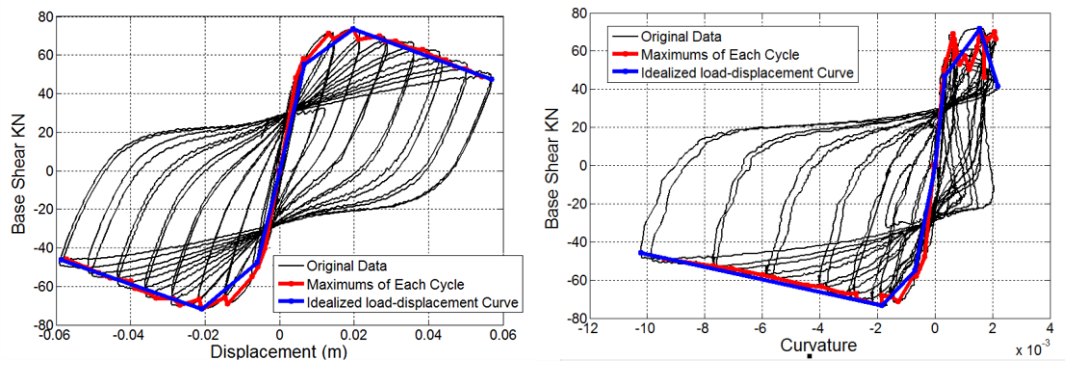


**Figure 4.11 :** Original LVDT load-deformation record versus calculated backbone curve

Cyclic data in left hand side is experimental base-shear versus displacement result of a reinforced concrete bare frame, which was exposed to a displacement controlled in-plane lateral excitation, and the data in the right, is base-shear versus curvature cyclic result of one of the same frame's plastic joints, recorded during experiment.

### 4.2.2 Resampling the data of the LVDTs

The raw data recorded from the LVDTs during the experiment period could have a very long dimension. This is because during the experiment period, the LVDTs are always active measuring and recording the data of the interest in the system, even though the change rate in the input parameters of the experiment are not tangible. For instance, this issue can take place when an examinee tries to record the displacements of the joints in a concrete frame subjected to a cyclic loading protocol. At each loading reversal the examinee crew will stop loading the frame, preparing for a reversal loading, while the LVDT instruments will keep restoring the steady measures in the system. Dealing and studying such a huge and abundant size of data is a very time-consuming and exhausting task. In this particular chapter the strategies to reduce the data size is introduced, the reduced data is compared against the smoothed raw recorded data and the errors are studied.

In the following sections the LVDT records of the base-shear versus the horizontal displacement will be processed as an example and the case of study. This data is shown in the Figure 4.12.

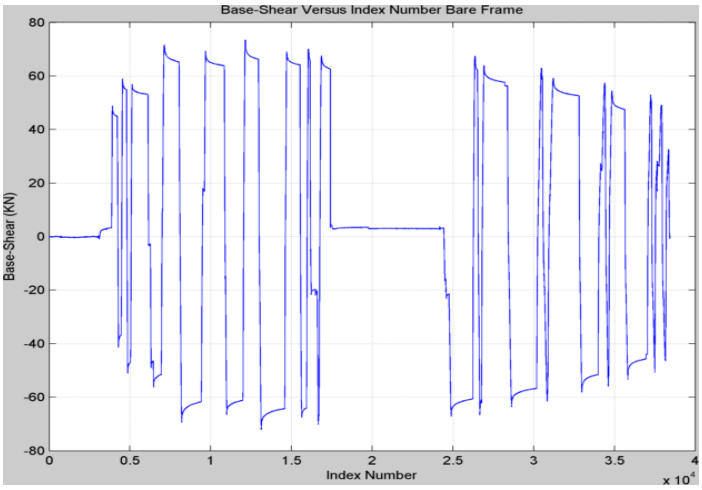


**a)** The base shear versus the index number in the recorded data.

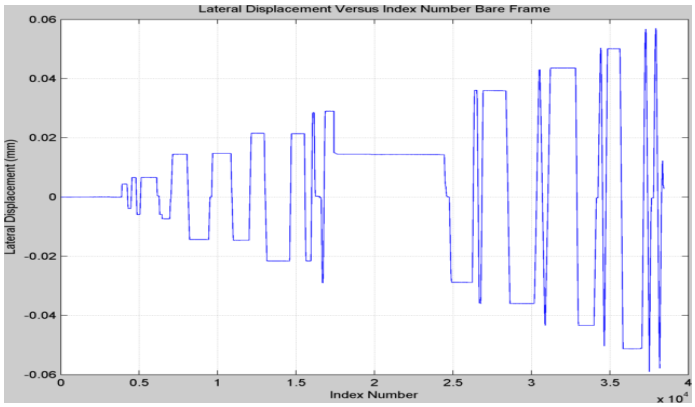


**(b)** The lateral displacement versus the index number in the recorded data

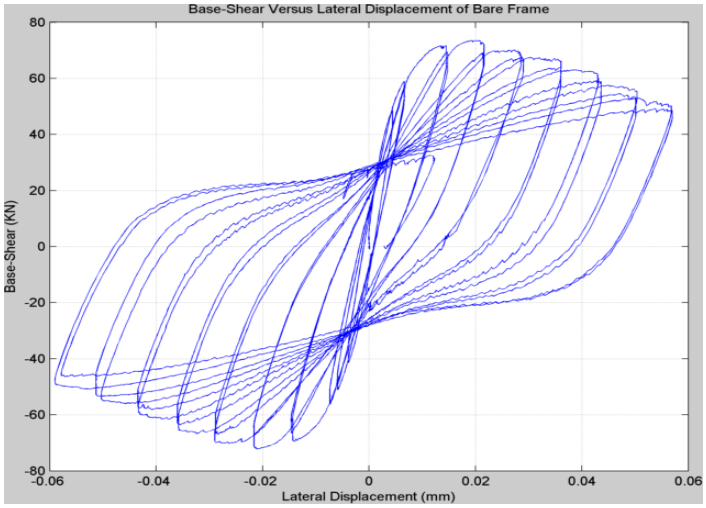


**(c)** The base-shear versus (in KN) lateral displacement (mm)

**Figure 4.12 :** Recorded LVDT cyclic data

#### 4.2.2.1 Smoothing the raw LVDT data

A noise in the data flow can be observed by a close look and inspection of the raw data recorded from LVTDs. This noise in the raw data is caused by the LVDT in measuring the displacement at each sequence of time. Dealing with such noise in the processing the data can be very challenging, and in some cases the elimination of the noise could be compulsory prior to utilizing the data.

#### 4.2.2.2 Shortening the data

The raw data coming from the LVTDs are very large in scale. During the experiment conduction, each LVDT recorded 38441 sequences of values to represent the deformation history of a particular location on the specimen frame. Obviously, all of the data with such dimension will not be used to in the analytical study of the parameters in the model. Therefore, the shortening the data and eliminating the steady record of LVDTs are compulsory. Figure 4.12.a, and Figure 4.12.b shows the steady record of the data.

Two main strategies are used to reduce the data size which can be described as:

1- Reduction of the data by based on regular resampling and elimination.
2- Reduction of the data to eliminate the steady record of the data.

**Reduction of the data based on regular resampling and elimination**

The number of members in recorded array could be resized to that of a smaller array without losing the data. This technique is called resampling of the data. A regular elimination and data removal have been implemented on the given array to reduce its size. The removal size is determined by the user with a trial and error approach. The overview of the algorithm is shown in Figure 4.13.

| |
|---|
| **Input:** Displacement LVDT record array with size of $n \times 1$: (*Dis)*<br>Load LVDT record array with size of $n \times 1$: (*Load*)<br>Reduction size: (*m)*<br>**Output:** Reduced size of displacement array (*RedDis*)<br>Reduced size of load array (*RedLoad*) |
| **1** *index* ←*1* to *n* with step size of *m*<br>**2 for** each member of *index* array, *j*<br>**3** **Append** *j*'th index of *Dis* array to *RedDis*<br>**4 end for**<br>**5 for** each member of *index* array, *j*<br>**6** **Append** *j*'th index of *Load* array to *RedLoad*<br>**7 end for**<br>**8 Return** *RedDis* and *RedLoad* |

**Figure 4.13:** The algorithm for regular data reduction

Figure below shows an example of regular resampling:

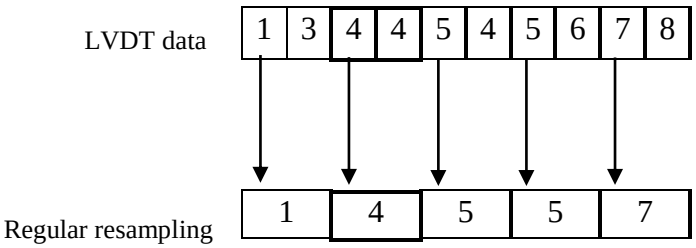


**Figure 4.14 :** Regular resampling the data

**Reduction of the data to eliminate the steady record of the data**

While recording the load and deformation data with LVDT devices, due to irregular and non-steady nature of excitation application on specimen, the measuring devices will always record a fairly large size of data with non-steady change rate of input excitation. To reduce the size of data, and, to stabilize excitation change rate, the irregular resampling will have to be conducted. The following figure explores example of irregular resampling on a reduced data. Figure 4.16 shows the structure of the algorithm to carry out the irregular resampling.

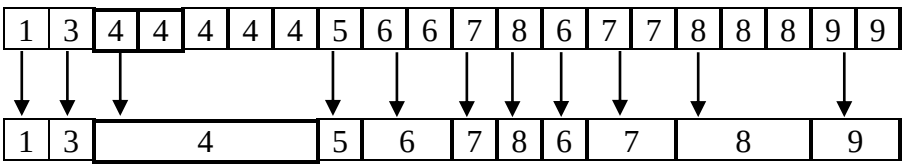


**Figure 4.15 :** Irregular resampling of data

**Input:** Regularly reduced displacement record array with size of $n1\times1$: (*RedDis)*
Regularly reduced loading array record with size of $n1\times1$: (*RedLoad*)
Reduction size which is always greater than ten: *ResamplingScale*
Indices of load direction change: *ChangeDir*
**Output:** Resampled load array: *LoadINT*, and resampled displacement array: *DispINT*

(Initialize the parameters)
**1 Append** the last value of *RedDis* to *ChangeDir* matrix
**2** *LoadINT* ← [ ]
**3** *DispINT* ← [ ]
**4** *FirstDispVal* ← **round***(*$RedDis_{(1)}$*)*
**5** *FirstDispIndex* ←1
(Algorithm main body)
**6** *RedDis* ← *RedDis*×*ResamplingScale*
**7** *RedLoad* ← *RedLoad*×*ResamplingScale*
**8 round** all members of toward negative infinity
**9 for** the second to the last member of $changeDir_i$
**10** **if** *FirstDispVal* < $ChangeDir_{(i)}$'th index of *RedDis*
**11** $LastDispIndex \leftarrow ChangeDir_{(i)}$
**12** $LastDispVal \leftarrow RedDis_{(LastDispIndex)}$
**13** *Disploop* ← create a set of integers from *(FirstDispVal+1)* to *(LastDispVal)* Value with ascending rate
**14** *DispFNC* ← create a set containing values of $RedDis_{(FirstDispIndex)}$ to $RedDis_{(LastCurvIndex)}$
**15** *DispFNC,Indices* ← **get** all the unique members of *DispFNC* and their indices (of first uniqueness)
**16** *DispFNC* ← **get** members of *RedDis* with following indices: [*Indices+FirstDispIndex-1*]
**17** *LoadFNC* ← **get** members of *RedLoad* with following indices: [*Indices+FirstDispIndex-1*]
**18** *LoadLoop* ← **get** linear interpolation of *DispFNC* over *LoadFNC* with query points of *Disploop*
**19** *FirstDispIndex* ← *LastDispIndex*
**20** *FirstDispVal* ← *LastDispVal*
**21** **Append** *Disploop* to *DispINT*
**22** **Append** *LoadLoop* to *LoadINT*
**23** **else if** *FirstDispVal* > $ChangeDir_{(i)}$'th index of *RedDis*
**24** $LastDispIndex \leftarrow ChangeDir_{(i)}$
**25** $LastDispVal \leftarrow RedDis_{(LastDispIndex)}$
**26** *Disploop* ← create a set of integers from *(FirstDispVal-1)* to *(LastDispVal)* Value with descending rate
**27** *DispFNC* ← create a set containing values of $RedDis_{(FirstDispIndex)}$ to $RedDis_{(LastCurvIndex)}$
**28** *DispFNC,Indices* ← **get** all the unique members of *DispFNC* and their indices (of first uniqueness)
**29** *DispFNC* ← **get** members of *RedDis* with following indices: [*Indices+FirstDispIndex-1*]
**30** *LoadFNC* ← **get** members of *RedLoad* with following indices: [*Indices+FirstDispIndex-1*]
**31** *LoadLoop* ← **get** linear interpolation of *DispFNC* over *LoadFNC* with query points of *Disploop*
**32** *FirstDispIndex* ← *LastDispIndex*
**33** *FirstDispVal* ← *LastDispVal*
**34** **Append** *Disploop* to *DispINT*
**35** **Append** *LoadLoop* to *LoadINT*
**36** **end if**
**37 end for**
**38** *LoadINT* ← *LoadINT/ ResamplingScale*
**39** *DispINT* ← *DispINT/ ResamplingScale*
**40 Return** *DispINT* and *LoadINT*

**Figure 4.16 :** Algorithm for irregular resampling

### 4.2.3 Hysteresis models

A hysteresis model is commonly used to simulate the load deformation respond of a specimen or a frame subjected to cyclic excitation. Hysteresis models always consist of two sets of parameters. One set of parameters describe the monotonic or the back bone curve of the cyclic loading, the other describe the degradation characteristic of

the specimen at loading reversals. There are so many proposed Hysteresis models to simulate a cyclic response. In this section, three commonly used methodologies as are introduced, their rules are reviewed and their parameters are described. These three models are the following:

1-Multilinear Kinematic Model

2-Multilinear Takeda Model

3-Multilinear Pivot Hysteretic Model

#### 4.2.3.1 Multi-linear Kinematic model

Kinematic hysteresis model that is based on kinematic hysteresis models commonly observed in metals and distributed hinge springs and truss elements, is described by a set of user-describe points. The first linear line on either side of the origin describes material's linear behavior. The following figures represent the shape of the Kinematic hysteresis model for two different loading criteria.

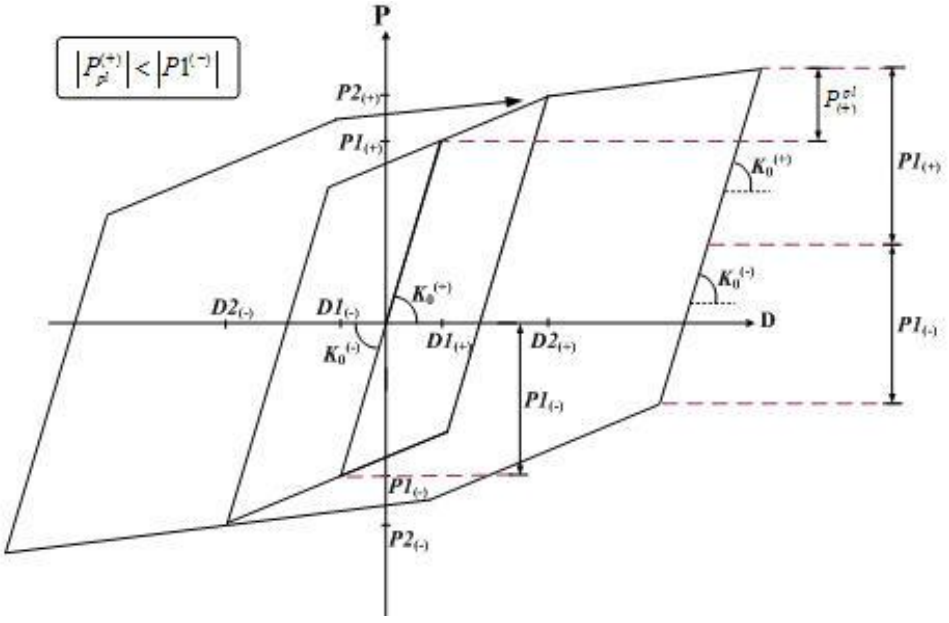


**Figure 4.17 :** Hysteresis Kinematic model while $|P_{pl}^{(+)}| < |Pl^{(-)}|$

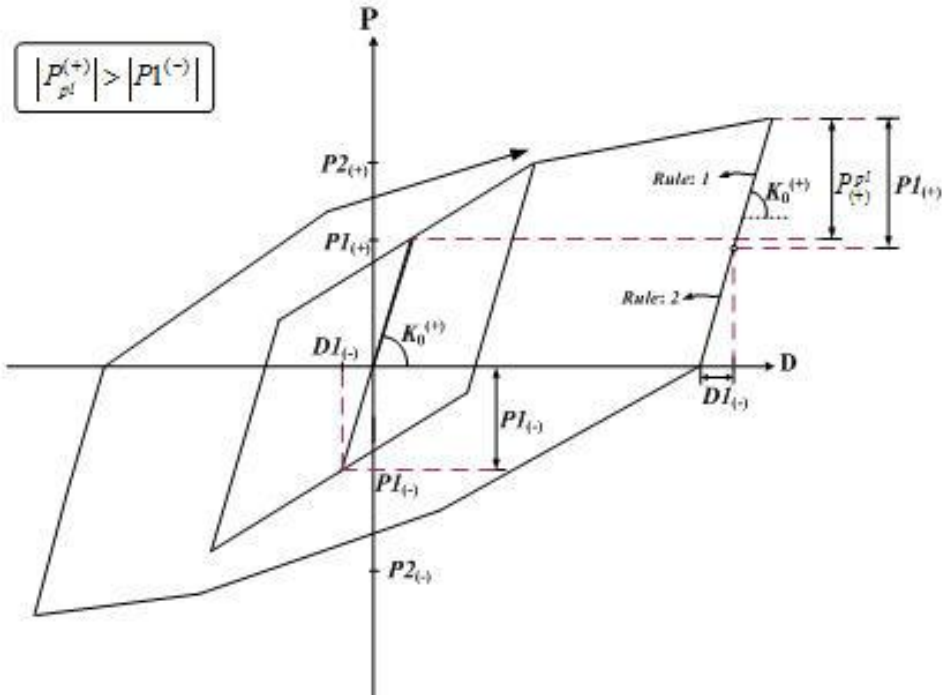


**Figure 4.18 :** Hysteresis Kinematic model while $|P_{pl}^{(+)}| > |PI^{(-)}|$

#### 4.2.3.2 Multi-linear Takeda model

One of the most popular hysteresis multi-linear models to simulate the stiffness degradation response in cyclic loading of an RC frame is Takeda model purposed by Takeda et al [36]. In this paper they compare their simulated result against the dynamic response test results disclosing a close match between them. This revolutionary paper showed the constantly changing stiffness of RC member in a cyclic loading leads to less energy dissipation that should be explicitly considered in the hysteresis rules to produce a demanding results close to real behavior of RC member.

Takeda curve can be symmetrically or unsymmetrically defined. The types of corresponding elements include lumped hinge, distributed hinge, spring and truss elements.

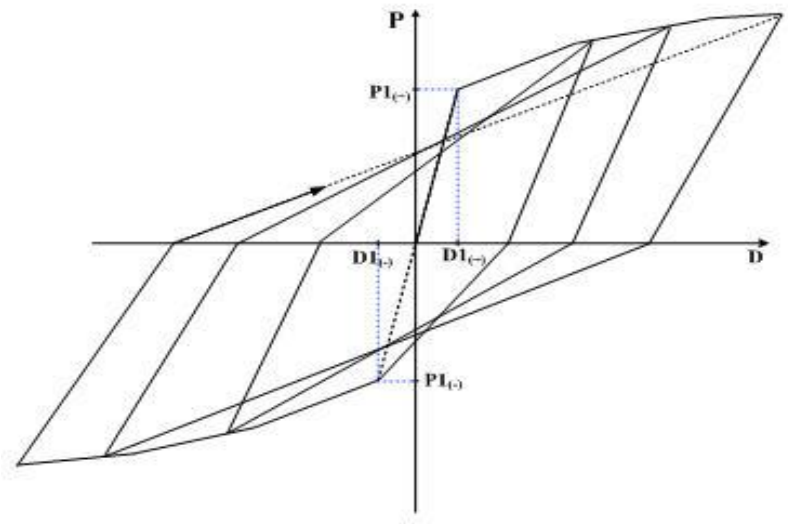


**Figure 4.19 :** Multi-Linear Plastic Takeda Hysteresis Model

#### 4.2.3.3 Multi-linear Pivot type hysteresis model

Multi-linear plastic pivot type hysteresis is a multi-linear stiffness degradation model proposed by Dowell et al [37]. Pivot Hysteresis uses multiple pivot points to control the nonlinear force-deformation relationship reinforced concrete members. Thus, this model can accurately depict the stiffness degradation and the pinching effect when unloading takes place.

The curve can be symmetrically or unsymmetrically defined. The types of corresponding elements include lumped hinge, distributed hinge, spring and truss elements.

**Primary pivot point**

The Primary Pivot Points, $P_1$ and $P_3$ represent the points towards which the unloading curves are oriented in the $Q_1$ and $Q_3$ zones. The Primary Pivot Points, $P_1$ and $P_3$ control the degradation of the unloading stiffness caused by the change in deformation or displacement. $P_1$ and $P_3$ are located along the extended lines of the initial stiffness on the positive and negative sides, which are defined by the yield strengths, $F_y^{(+)}$ and $F_y^{(-)}$ and Scale Factors, $\alpha_1$ and $\alpha_2$. $\alpha_1$ and $\alpha_2$ are always greater than one. ($\alpha_1, \alpha_2 \geq 1$)

The locations of the Primary Pivot Points, $P_1$ and $P_3$ move to $P_1$* and $P_3$* after yielding respectively, whenever the maximum displacement point is renewed by the

Initial Stiffness Softening Factor, η. However, when η=0, the locations of the Primary Pivot Points, $P_1$ and $P_3$ remain unchanged.

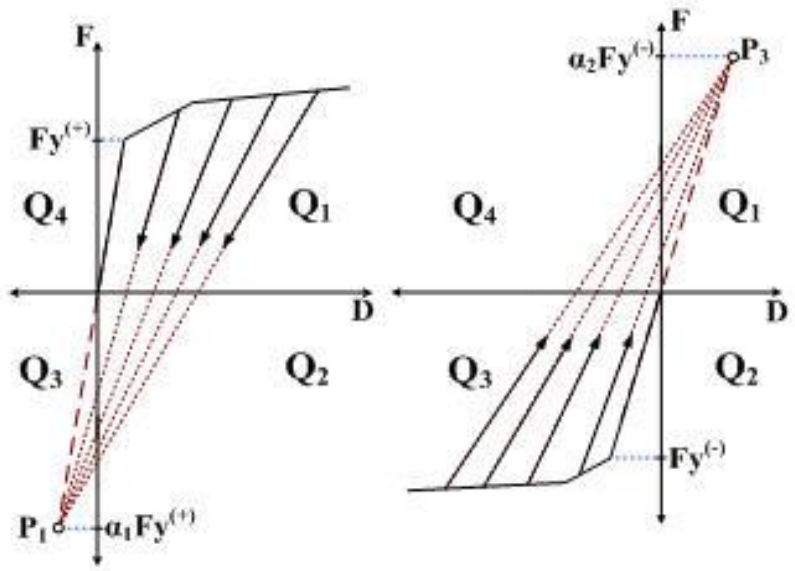


**Figure 4.20 :** Primary Pivot Point

**Pinching pivot point**

The Pinching Pivot Points, $PP_2$ and $PP_4$ represent the points towards which the unloading curves are oriented in the $Q_1$ and $Q_3$ zones after the restoring force exceeds zero. $PP_2$ and $PP_4$ are located on the skeleton curve in the elastic zone on the Positive and negative sides, which are defined by the yield strengths of the initial stiffness, $F_y^{(+)}$ and $F_y^{(-)}$ and Scale Factors, $\beta_1$ and $\beta_2$.

$\beta_1$: Scale Factor used to define the pivot point, $PP_2$ when loading on the $Q_2$ side. ($0< \beta_1 \leq 1$)

$\beta_2$: Scale Factor used to define the pivot point, $PP_4$ when loading on the $Q_4$ side. ($0< \beta_2 \leq 1$)

The locations of the Pinching Pivot Points, $PP_2$ and $PP_4$ after yielding will move to $PP_2$*and $PP_4$* respectively, whenever the maximum displacement point is renewed by the Initial Stiffness Softening Factor, η. However, when η =0, the Pinching Pivot Points, $PP_2$ and $PP_4$ remain unchanged.

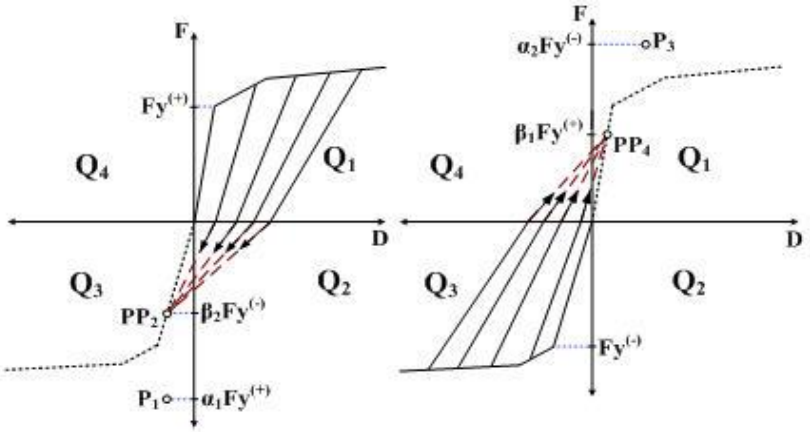


**Figure 4.21 :** Pinching Pivot Point

**Initial stiffness softening factor, η**

η is an initial stiffness softening factor used to control the initial stiffness degradation after yielding. After yielding, the Primary Pivot Points, $P_1$ and $P_3$ are relocated to $P_1^*$and $P_3^*$, which are located on the lines extended from the maximum displacement points on the positive and negative sides respectively. $P_1^*$and $P_3^*$ are defined by $F_y^{(+)}$ and $F_y^{(-)}$, Scale Factors, and , and the initial stiffness softening factor, η.

In addition, the Pinching Pivot Points, $PP_2$ and $PP_4$ move to $PP_2^*$ and $PP_4^*$ respectively. $PP_2^*$ (or $PP_4^*$) is defined by the intersection point of the straight line passing through $P_1^*$ and the origin (or $P_3^*$ and the origin) and the straight line connecting $PP_2$ (or $PP_4$) to the maximum displacement point on negative (or positive) side.

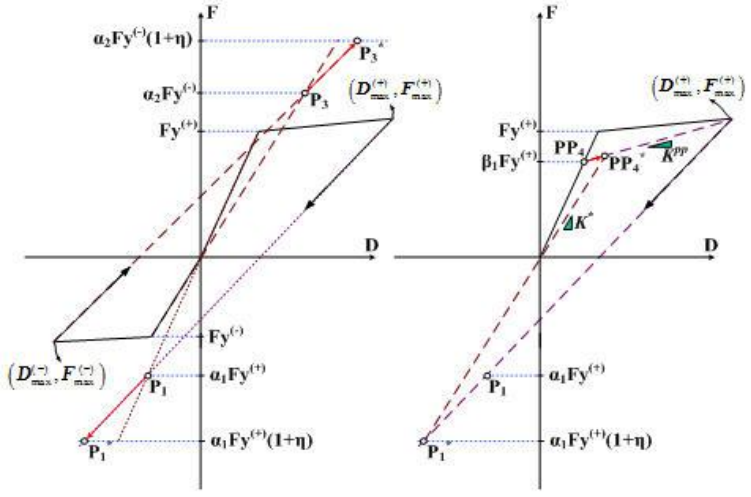


**Figure 4.22:** Initial Stiffness Softening Factor

**Update of scale factors, β1 and β2**

The Pinching Pivot Point Scale Factors, $\beta_1$ and $\beta_2$ are renewed after yielding under the conditions below.

$$\beta_i^* \begin{cases} = \beta_i & ; D_{max} \le D_{t1} \\ = \beta_i \cdot \dfrac{F_{max}}{F_{ti}} & ; D_{max} > D_{t1} \end{cases}$$

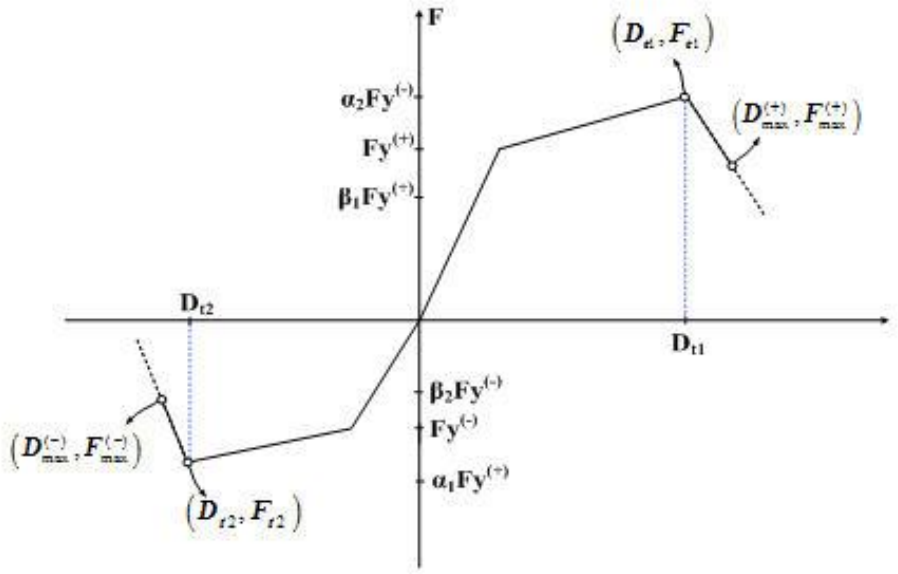


**Figure 4.23:** Skeleton (backbone) curve and Pivot hysteresis model parameters

To find the unknown parameters of Pivot hysteresis model Genetic Algorithm is used to fit the experimental and analytical data to each other through an optimization. Sections below detail the process.

## 4.3 An introduction to Genetic Algorithm

Genetic Algorithm (GA in short) is an optimization method based on heuristic search for the best solution that mimics the evolution of the creatures in nature. GA optimization model had been proposed by Joh Holland in the 1960s. It has been popular and widely been used in optimization problems. Its simple structure made it usable in different scientific fields such as aerospace engineering [38], financial marketing [39], geophysics [40], and material engineering [41].

In civil structural engineering great number of researches has been carried out to obtain the optimal design of two dimensional frames using genetic algorithm form which Lee and Ahn [42] and Camp et al [43] are the most popular ones. Optimal design of RC frames was carried out by Rajeev and Krishnamoorthy [44] using a Simple Genetic Algorithm (SGA). Optimum design of a continues beam using GA were introduced by Govindaraj and Ramasm [45, 46]. Optimization of T-shaped reinforced concrete using genetic algorithm were conducted by Ferrireira et al [47].

GA is a subcategory of evolutionary algorithms which are inspired by natural evolutions. At each iteration, each candidate solution is evaluated though the fitness function which assess the candidate's deviation with the fitness criteria. The best solution will be substitute with a candidate solution only if it has a better fit to the fitness function.

GA consists of individuals, who are the possible candidates at each step of iteration, and generations which are the populations that are evolving toward the optimal answer. The GA basically uses each individual as a parent to produce the population for the next generation. To converge to the optimal solution more quickly, GA produces the next generation population based on the mutation and crossover function which leads to a better diversity in population in the search for the most optimal answer. The main steps in each iteration of a GA optimization function can be described as the initialization of the first generation, evaluation toward the optimal answer, selection of the portion of the population in the generation that best fit the fitness function criterion, and crossover and mutation while breeding the offspring for the next generation.

An overview of structure of a classic Genetic Algorithm is shown in the Figure 4.24.

**Input:** Fitness function: *eval( )*
Number of variables in the problem: *nVar*
A set of Boundaries for variables: $[(a_1, b_1), (a_2, b_2), \ldots]_{1 \times nVar}$
Population size: *N*
Termination condition: total number of generations: *TotGen*, and stall iteration: *TotStall*
Crossover value
Mutation rate: *MutationRate*
**Output:** Optimized variables that maximized/minimized the fitness function

**INITIALIZE** population with random candidate solution
*CurrGen* ← *1*
*CurrStall* ← *0*
**for** *i = 1* to *N* **do**
**for j =** *1* to *nVar* **do**
*rand* ← a random number in between $a_j$ and $b_j$
**Append** all the *rand* values in *Individual*
**end for**
**Append** all the *Individual* values in *Population*
**end for**
**EVALUATE** each candidate solution
**for** *i = 1* to *N* **do**
**Append** *eval( Individual(i) )* to *Score*
**end for**
**while** *CurrGen* < *TotGen* and *CurrStall*< *TotStall* **do**
**SELECT** individuals to breed the next generation
**for** *i = 1* to *N* **do**
**Append** *nParents* number higher scores *Population* to *Parents*
**end for**
**REPRODUCTION** pairs of parents
**for** *i = 1* to *nParents* with step *2* **do**
**for** *j = 1* to *nVar* **do**
**if j <=** *CrossoverPoint*
**Append** variable *j* in *Parent ( i )* to variable *j* in *Offspring ( i )*
**Append** variable *j* in *Parent ( i +1 )* to variable *j* in *Offspring ( i + 1)*
**else**
**Append** variable *j* in *Parent ( i +1 )* to variable *j* in *Offspring ( i )*
**Append** variable *j* in *Parent ( i )* to variable *j* in *Offspring ( i + 1)*
**end if**
**end for**
**end**
**MUTATE** the resulting offspring
**for** *i = 1* to *N*
***if*** *random number < MutationRate*
**mutate*** *Offspring*
**end if**
**end for**
**EVALUATE** each *Offspring* through fitness function
**for** *i = 1* to *N* **do**
**Append** *eval(Offspring(i))* to *Score*
**end for**
*Population* ← *Offspring*
*CurrGenv* ← *CurrGenv + 1*
**If** highest *Offspring* score between two generations are the same
*CurrStall* ← *CurrStall + 1*
**else**
*CurrStall* ← *0*
**end if**
**end while**
**Return** highest *Offspring* score

**Figure 4.24 :** A classic Genetic Algorithm structure.

### 4.3.1 Initialization of GA parameters

The initial parameters to carry out the optimal solution the GA will generate the number of random solutions to obtain the population of the first generation. The random generated values in the first generation are likely to cover all the possible solution in the search space. The larger population sizes in GA will allow a better convergence rate by imposing a large number of possible solutions in the search space. On the other hand, very large population sizes will really slow the convergence rate of the GA, since the evaluation of the fitness values of all the individuals in a generation is certainly a time consuming task. The population size depends on the nature of the problem, but in general, it contains hundreds or thousands of possible solutions.

Beside the population size of a generation, the total number of the generations and the stall value are other key factors in initializing the GA parameters in the evaluation of the optimal solution. To terminate the iteration of the GA process a total number of generations is defined. The GA optimal solution seeding evaluation is terminated if one of the following criteria is satisfied:

1- If the number of generation exceeds a total number of the generations
2- If the best solution of GA does not vary for the number of generations in row and it exceeds the stall value, the algorithm is terminated. This is because the best answer is so close to the optimal solution of the problem or further proceeding of the GA evaluation will not converge to a better solution soon. Assignation of the larger numbers to the stall value will always guarantee the better solution in GA. The GA user will always have to set a proper stall value to get a desired solution.

The mutation and the crossover parameters are also initialized in this step. These parameters are described in the explicit details in the following sections.

#### 4.3.1.1 Selection

The successful portion of the population is selected to produce the next generation. The successive rate for each individual in a generation is measured and assessed through the fitness function. Due to larger population size, some of GA algorithms

may assess the fitness of the sample of individual in a generation since it might be a time-consuming task to assess fitness rate for all individuals.

#### 4.3.1.2 Reproduction

Diversity is a key factor in the evolution. If the next generation shares the same genetic code of the current generation, the evolution will never take place. To create the next generation using the same characteristics of the successful individuals of the current generation through a divertive process, it is crucial to combine and modify their characteristics.

The new population in the new generation is generated thanks to crossover and mutation functions to breed the successful parents of the previous generation into the new one. To combine two parents, crossover function generates a random portion rate value corresponding the two parents, and encodes the new individual by combing randomly generated portion length of two solutions (chromosomes of the parents) codes of the parents. In some of GA structures the crossover may have a constant value, in which the offspring share a specific rate of its parents' genes. The Figure below shows the parents' bit and the generated offspring through a 0.5 crossover rate.

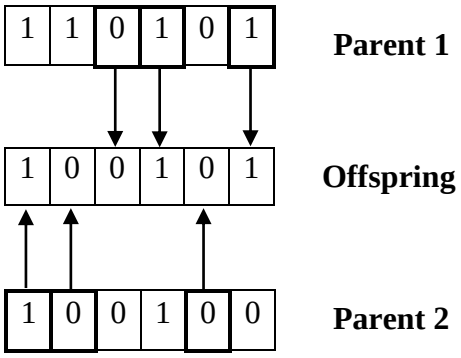


**Figure 4.25 :** Crossover function of 0.5 over two parent bit to generate an offspring

In the nature the crossover value is 0.5, meaning that a new offspring shares half of its parents' genes. In some GA structures the offspring may be generated with three or more parents. Different strategies may be considered to breed the new individuals with successful parents however explaining such methodologies is out of current research scope and might be considered trivial.

The mutation allows the algorithm to cover the solutions that is not in the actual search space and will increase the chance of obtaining offspring with better fit by modifying the genes of parents in each breeding process.

An iteration of the above steps will lead to obtain solutions that better fit to fitness function and will empower us to optimized the input parameters to get the demanding output results.

### 4.4 Minimizing the Disagreement Between the Simulated and Experimental Results of Hysteresis Data

To model the load-deformation response of a RC frame due to a lateral excitation using the existing hysteresis models, it is essential to carry out the parameters that best describe the load-deformation interaction. The better the simulated parameters fit to the characteristic of the experimental results, the less error and deviation will be obtained. However, the error and the deviation between the simulated and experimented data can be minimized through an optimization process. In other words, the deviation between the combinations of unknown parameters to define a desired solution can be assessed to carry out the best parameters that fit the desired condition. In this particular section, the application of the genetic algorithm is described to minimize the disagreement between the simulated and the experimental results to calculate the best parameters of a pivot model that describe the load-deformation curve for a bare RC frame. The parameters of GA including crossover and the mutation values as well as fitness function are described through the following sections.

### 4.5 Purposed Methodology and Decision Making to Decode Cyclic Experimental Results to Hysteresis Models:

In the previous chapters the recorded LVDT data were shortened thanks to the regular resampling and eliminating the steady record of the data. Also the hysteresis type model of Kinematic, Takeda and Pivot were explained in explicit details. Kinematic and Takeda models depend on their backbone curve represent the cyclic behavior of them, and since our idealized curve has six sets of load-deformation points (three sets on either side), each of these two models will require six sets of

load-deformation points to represent a specific cyclic behavior. On the other hand, Pivot hysteresis model depends on these six sets of load-deformation points to handle its monotonic backbone contour and five more additional parameters ($\alpha_1$, $\alpha_2$, $\beta_1$, $\beta_2$ and $\eta$) to represent its cyclic and degradation behavior. Since these five parameters are unknown to represent a load-deformation data using Pivot model, the genetic algorithm is used to optimize the deviation and achieve a satisfactory disparity or termination condition between simulated and experimental results. To perform such optimization, for given deformation cyclic record and a monotonic curve, five unknown parameters namely $\alpha_1$, $\alpha_2$, $\beta_1$, $\beta_2$ and $\eta$ will constantly change to obtain an optimum solution and basically, the cyclic loading record obtained from a particular combination of the unknown parameters will be compared against the loading record obtained from the experimental results. Once the optimized results do not significantly vary through iterations, the optimization process is terminated. The variation between the obtained Pivot, Takeda, and Kinematic model is compared against the experimental data and a specific score is associated to each of them (Figure 4.26.c). The model with the lowest score, namely lowest deviation, is selected to represent a cyclic hysteresis behavior. The following figures shows the flowchart for the algorithm used to pick the best model to represent the cyclic hysteresis behavior. The fitness function to assess the deviation between simulated and experimental results are explained in the following sections.

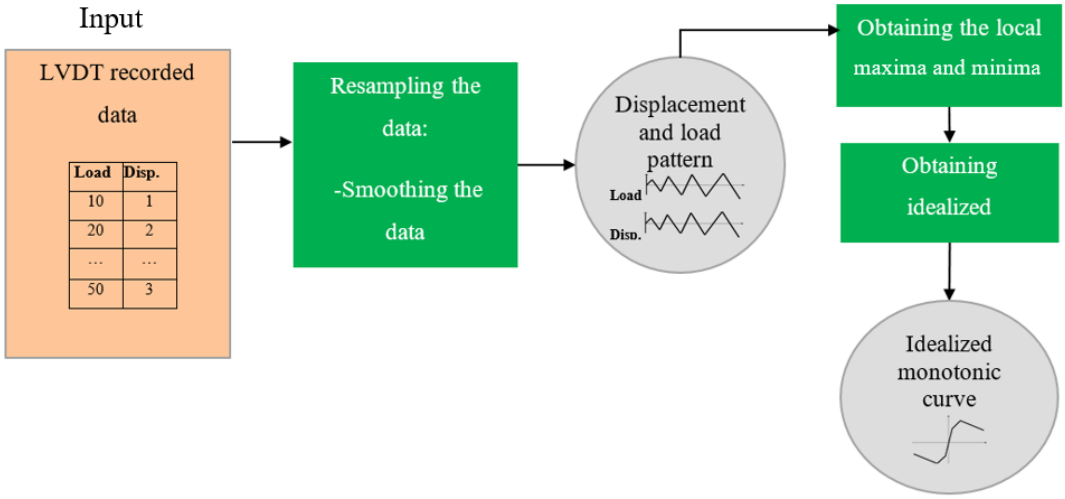


**Figure 4.26.a :** Obtaining the resampled data and idealized monotonic curve

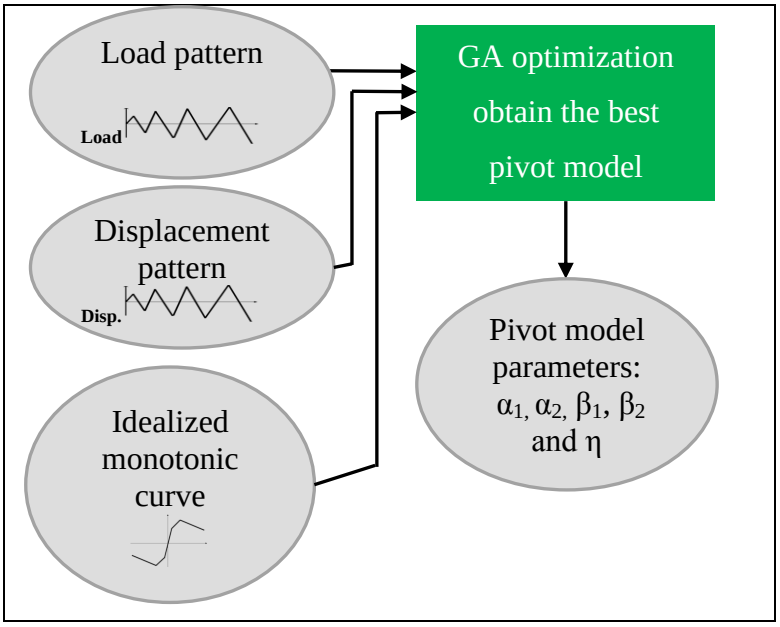


**Figure 4.26.b :** An over view of obtaining the best parameters of Pivot model while fitting the simulation to experimental results using Genetic Algorithm

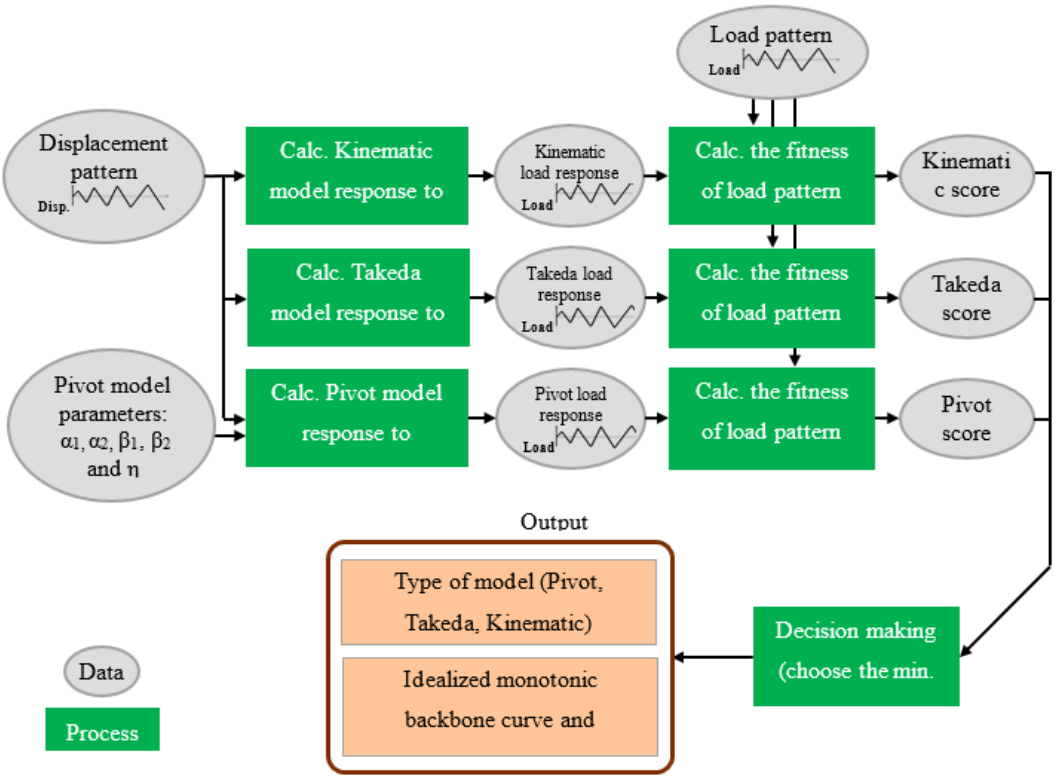


**Figure 4.26.c :** Obtaining Kinematic, Takeda and Pivot model response of displacement pattern to retrieve a unique load pattern associated with each model, and comparing that to resampled loading pattern, which leads to a decision making process of which of Kinematic, Takeda and Pivot model is appropriate to simulate the data

### 4.5.1 Genetic Algorithm parameters to obtain Pivot model's parameters

The concept of revolutionary algorithms is laid on individuals, namely unknown parameters, which evolve through generations to carry out and converge to the optimal solutions. The Genetic Algorithm is not an exception. Initially randomly generated parameters get better as the optimization proceed its process. Through the evolution process, new parameters are picked from the search domain, therefore, GA is allowed to seek for better parameter only in the search space. According to the previous sections and the definition of the Pivot hysteresis rules and its associated parameters, there are intervals are designated for each parameter to define a Pivot model, thus, to carry out the best solution, these intervals associated with each parameter will have to be taken into account in its search space. The designated interval based on Pivot model definition and GA interval for unknown parameters are shown in the table below:

**Table 4.3:** Eligible search space based on definition of the parameter vs modeled GA search space

| Definition intervals | GA intervals |
|---|---|
| $0 \leq \alpha_1 \leq 1$ | $0 \leq \alpha_1 \leq 1$ |
| $0 \leq \alpha_2 \leq 1$ | $0 \leq \alpha_2 \leq 1$ |
| $1 \leq \beta_1$ | $1 \leq \beta_1 \leq 100$ |
| $1 \leq \beta_2$ | $1 \leq \beta_2 \leq 100$ |
| $0 \leq \eta$ | $0 \leq \eta \leq 1000$ |

To converge to meaningful answers sooner, the search space for Beta and Eta parameters are tightened and limited between one to a hundred and one to a thousand respectively. This is also assumed that the optimal solution will be confirmed to be somewhere away from the defined interval boundaries so that the reduced interval makes scenes.

The number of possible candidates in each generation is known as population size. For the greater number of population in each generation, there is a higher probability of the better solutions to be in that generation, thus the algorithm may converge toward the optimal solution quickly. However, assigning a higher value to population size may slow the convergence rate, since, it consumes more time to evaluate the fitness value for each individuals in the generation with a higher population. For this

particular research population size of twenty has been considered in the GA processes.

The termination condition may be considered to quench GA process. In this research a hundred number of iterations are considered as the total number of generations. It is assumed that if the best mean in last generation does not show an extreme change, otherwise the user will have to increase the total number of generations to converge to a satisfactory optimal solution. To end the GA processes while the best solution is identical between generations, the Stall value may be considered as the termination condition. For non-convex convergence problems, the lower Stall value may cause the GA to stop in a local minimum as oppose a global minimum or the optimal solution. In the search for optimal parameters in this research, twenty iterations with the same best solution is considered as Stall value.

### 4.5.2 The fitness function to assess the deviation between simulated and experimental results and decision making:

For a given idealized load-deformation curve and a displacement cyclic record, a load hysteresis response can be obtained using rules for each of Kinematic, Takeda and Pivot models. The obtained hysteresis response of each model can be compared against the experimental results. However, to assess the deviation between the simulated and experimental data easily, the size of array containing simulated and experimental results will have to be the same. This is why before processing on data they were shortened and resampled. The following equation is used to assess the deviation between load response of a model and the experimental results;

$$Model\ Score = \sum_{i=1}^{n} (LoadResp_i - LoadExp_i)^2 \qquad (4.15)$$

where $LoadResp$ is load response record of a model calculated based on its hysteresis rules with size of $n \times 1$, and $LoadResp_i$, being the $i$th member in $LoadResp$ array. $LoadExp$, is an array containing resampled experimental loading response with size of $n \times 1$, and $LoadExp_i$, is the $i$th member in $LoadExp$ array.

The above equation has been used in twice in the process of algorithm which is explained in the following:

- The unknown parameters to obtain the Pivot model in GA optimization are constantly changed to converge to an optimum solution. To assess and to carry out its similarity with experimental data, each sets of parameters in any population is scored through fitness function. Individuals, namely set of unknown parameters, with lowest score (lowest deviation with experimental results) are selected breed and form the next generation Figure 4.26.b.

- The fitness function is used to score the model of different kind. After obtaining the optimal parameters to represent the Pivot model, the disparity the experimental results and each of three model is assess through fitness function. The model with the lowest is score is the most proper way to represent the cyclic excitation behavior Figure 4.26.c.

## 4.6 The Use of Application Programming Interface (API) to Integrate the Software Packages and to Automate the Parametric Studies:

Without a need to program a large number of codes to study and analyze the data corresponding to a given input, nowadays already written software packages can act like an engine under the hood, allowing the user to integrate them with a programming platform to request the inputs and yield the outputs through the Application Programming Interface (APIs). In other words, the sophisticated functionality of software packages can be manipulated thanks to APIs to study large number of inputs while doing iterations, optimizations and parametric studies. This empowers the programmers and software developers to take advantage of the-state-of-the-art technologies and implement their codes and implementations upon them to introduce a better software platform. With the power of the API in mind, it is no wonder that the Apple founder, Steve Jobs, builds his 3D map software upon Google Maps, though an API, to deliver a better software experience.

In this particular research SAP2000 has been integrated with MATLAB through an API to perform optimizations. None of the hysteresis rules were defined or coded but it was requested from Sap2000 from MATLAB to study different model's load responses of a given displacement input. Similar studies have been carried out by

using SAP200 API and MATAB integration [48], [49], [50], [51], [52]. Figure below shows the schematic structure of MATLAB and Sap2000 data request and retrieve.

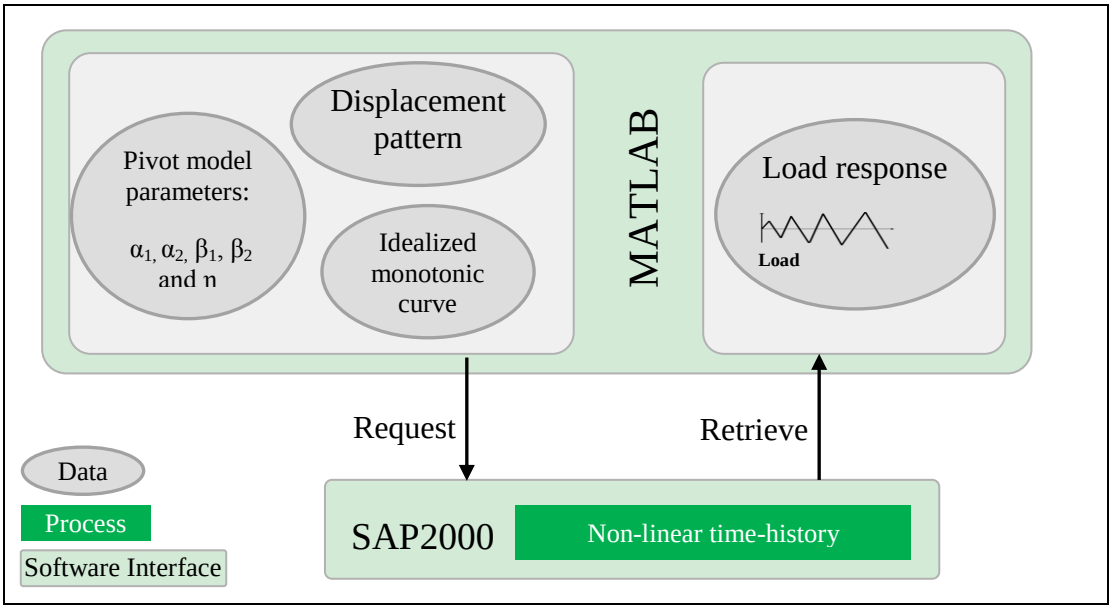


**Figure 4.27 :** Schematic used structure of MATLAB and SAP2000 API

### 4.7 Discussion of the Results; Analytical Modeling Versus Modeling Based on Experimental Results:

Even though modeling based on experimental results yields a very accurate results, it is hard to perform since it relies on numerous specimen to conduct experiments on and obtain the required experimental results to train a prediction model. In this strategy, more experimental results can lead to more precise predictions, and since obtaining experimental results are expensive, this method has not been commonly used by research community to predict the output results.

On the other hand, analytical modeling provides the outputs based on characteristics of each and every components of the specimen. Therefore, by capturing the characteristics of components of specimen, finite element strategy can be utilized to predict the characteristics of the specimen. However, finite element strategy may not necessarily reflect the behavior of specimen well. The precision of the simulation correlates with the number of elements in the finite element model. The specimen nonlinearity should also be reflected in finite element model.

In this research macro finite element model strategy has been used to simulate the behavior of bare frame and infill wall. It was observed that the backbone load-deformation curve coming from macro finite element strategy was close to the backbone obtained from experimental results. The issue with the implemented finite element macro model is that it simulated the behavior of the frames while applying a lateral monotonic loading and it did not work well while applying a cyclic lateral loading to the frame. Therefore, to represent the cyclic load-deformation relationship of the frame we used pivot hysteresis model. The backbone curve of this hysteresis model was obtained from our analytical result discussed in section 4.1 and parameters associated with the pivot hysteresis model was carried out from GA optimization which is discussed in the section 4.4. The only difference of this implementation with the model discussed in the section 4.4 is that the backbone curve is extracted from the finite element analytical results. Since currently there is no equation to obtain backbone curve of infill-tie frames, these specimens cannot be simulated. Figure below shows the behavior bare frame and infill frame versus the experimental results.

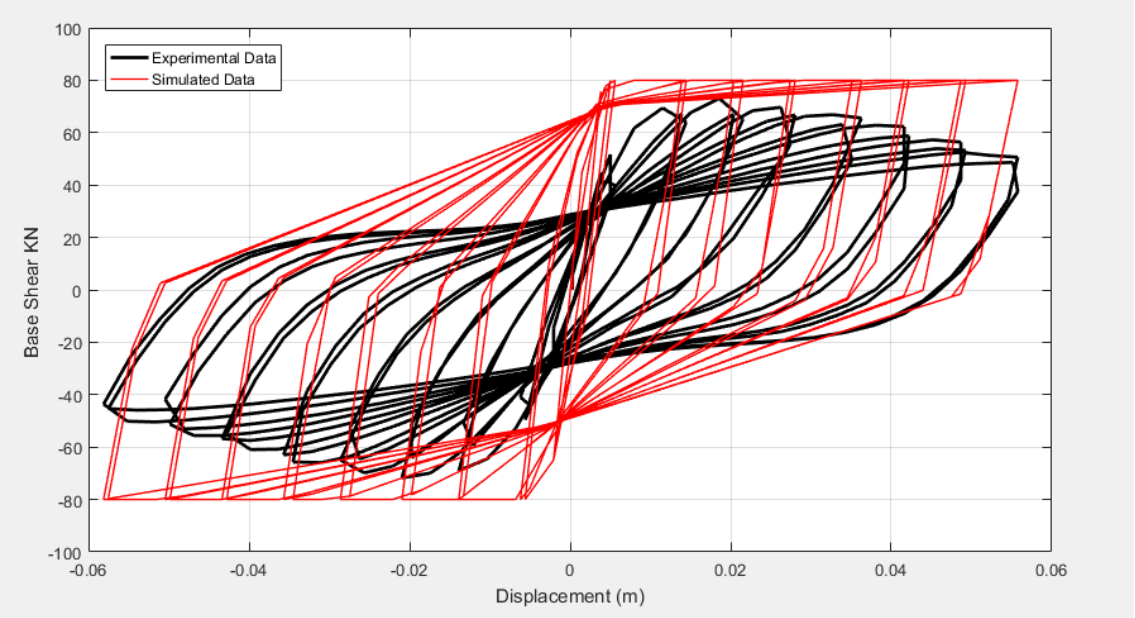


**Figure 4.28 :** Cyclic experimental result versus simulated results for bare frame; backbone was obtained analytically and pivot hysteresis parameters was obtained from experimental results

Pivot hysteresis parameters, which was captured from experimental results through GA optimization, is assigned as Alpha1=19.82, Alpha2=16.11, Beta1=0.73,

Beta2=0.80, Eta=147.4. These parameters can also be found in Appendix D, Figure D.3.

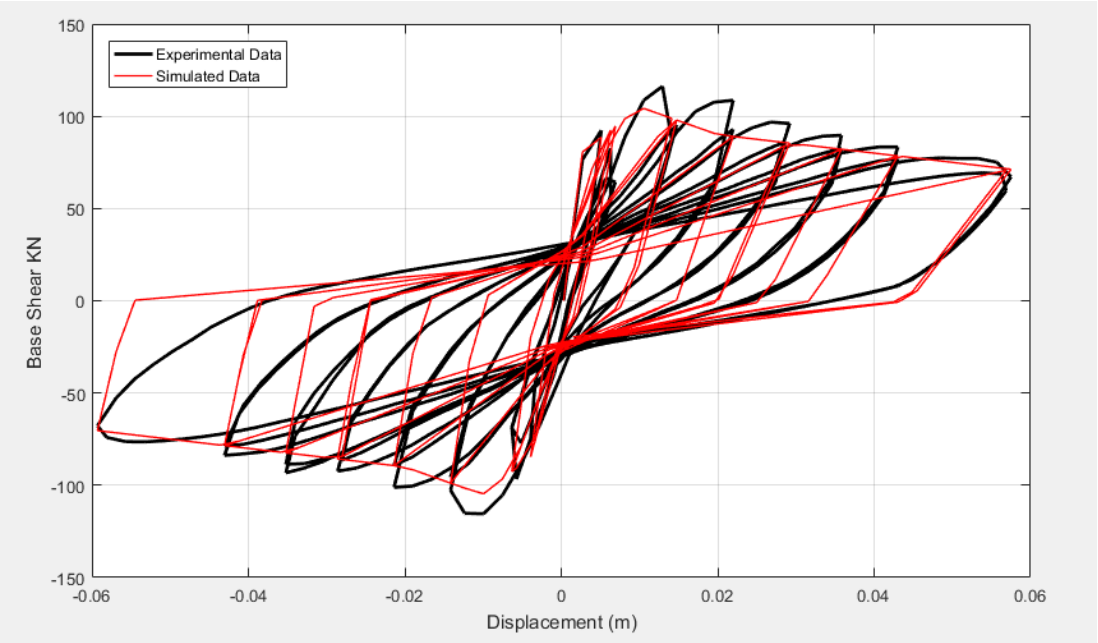


**Figure 4.29 :** Cyclic experimental result versus simulated results for infill frame; backbone was obtained analytically and pivot hysteresis parameters was obtained from experimental results

For infill frame pivot hysteresis model parameters are assigned as Alpha1=3.69, Alpha2=28.31, Beta1=0.34, Beta2=0.38, Eta=273.7. These parameters are found in Appendix E, Figure E.3.

By analytically obtaining the backbone load deformation curve, material and geometry characteristics of the specimen is considered. It can also be assumed that pivot hysteresis model parameters are not highly varied while geometry and material characteristics of the frame are changed. Therefore, pivot hysteresis parameters that have been captured from cyclic excitation behavior of a frame can be taken for almost any frames that have approximately the same geometry and material characteristics to that frame. It can be observed that since our analytical backbone curve for the bare frame does not match quite well with the experimental results, the pivot hysteresis representation the bare frame does match with experimental results too. On the other hand, simulated results for infill frame match quite well with the experimental results due to close-to-reality characteristic of the backbone curve.

# 5. CONCLUSION

The increase the in-plane rigidity of infill wall a reinforcement technic of infill wall is proposed, thus, four sets of experiments are conducted to carry out the load deformation relationship of bare frame, infill wall frame, infill frame with stepped-tie reinforcement, and infill frame with continues-tie reinforcement. An analytical model and a model based on experimental results has been implemented. The analytical simulation, which is based on taking the material and geometry information characteristics into account, has been carried out to model a bare frame. A spring model has been implemented on the locations where plastic joints are likely to occur, namely the top and the bottom of the columns. To do so, a literature corresponding to modeling load-deformation relationship has been reviewed to calibrate nonlinear springs with the appropriate length at the top and the bottom of the columns. To carry out the rigidity corresponding the infill masonry walls, simulation strategies has been reviewed. A macro equivalent pin-jointed truss model has been implemented. Base shear versus displacement of the analytical infill model has been compared against the experimental results.

The raw data coming from the LVDT recorded results were resampled to be further processed. Rules associated with popular hysteresis models used in most of commercially available software packages have been reviewed and Kinematic, Takeda, and Pivot models has been explained in explicit details. A semi-automated platform to study the parameters of hysteresis models have been developed. It has been concluded that without resampling the LVDT recorded data, it is impossible to use the curve fitting technics to carry out the demoing parameters associated to a cyclic data. The Genetic Algorithm is used to seek for the best parameters of Pivot hysteresis model that best describe the experimental results. A score has been assign to each of Kinematic, Takeda, and Pivot hysteresis models to assess the disagreement between the experimental data and simulated model. The Hysteresis model with the lowest score is selected to represent the cyclic recorded data. It has been concluded

that between Kinematic, Takeda and Pivot hysteresis models, always Pivot model can fit to experimental results much more accurately. Despite the fact that Pivot model is the most accurate from the rest, to calculate the parameters associated with it, a time-consuming operation is conducted, therefore, representation of cyclic data in terms of Pivot model is computationally expensive. The computational time for to carry out Pivot model parameters using the Genetic Algorithm is about 2 hours. On the other side, to represent the cyclic data in terms of Takeda and Kinematic model the computational time is less than a minute.

According to the decision tables, which represent the disagreement between simulated and the experimental results and are shown in the appendix, despite having a negligible computational time, Takeda model is a good fit to the experimental data. The average of four Takeda model scores over Pivot model score was about 1.7, while the average of four Kinematic score over Pivot model score was about 17.1. This can disclose the fact that Takeda models are far better than Kinematic models to represent the load deformation cyclic response of RC frames with and without masonry walls.

# REFERENCES


[1] **Townsend, W.H.and Hanson, R.** (1973) Hysteresis loops for reinforced concrete beam-column connections, Proceedings of 5th world conference on earthquake engineering, pp. 1131-4.

[2] **Anderson, J.C.and Townsend,** W.H. (1977). Models for RC frames with degrading stiffness, Journal of the Structural Division, 103, 2361-2376.

[3] **Soleimani, D., Popov, E.P.and Bertero V.V.** (1979) Hysteretic behavior of reinforced concrete beam-column subassemblages, Journal Proceedings, pp. 1179-1196.

[4] **Chan, W.** (1955). The ultimate strength and deformation of plastic hinges in reinforced concrete frameworks, Magazine of Concrete Research, 7, 121-132.

[5] **Baker, A.and Amarakone, A., N.** (1964) Inelastic hyperstatic frames analysis, Proceedings of the International Symposium on the Flexural Mechanics of Reinforced Concrete, pp. 85-142.

[6] **Roy, H.and Sozen, M.A.** (1965). Ductility of concrete, Special Publication, 12, 213-235.

[7] **Soliman, M.and Yu, C.** (1967). The flexural stress-strain relationship of concrete confined by rectangular transverse reinforcement, Magazine of Concrete Research, 19, 223-238.

[8] **Sargin, M., Ghosh, S.and Handa, V.** (1971). Effects of lateral reinforcement upon the strength and deformation properties of concrete, Magazine of Concrete Research, 23, 99-110.

[9] **Kent, D.C.and Park, R.** (1971). Flexural members with confined concrete, Journal of the Structural Division, 97, 1969-1990.

[10] **Park, R., Priestley, M.and Gill, W.D.** (1982). Ductility of square-confined concrete columns, Journal of the Structural Division, 108, 929-950.

[11] **Mosalam, K., Glascoe, L.and Bernier, J.** (2009). Mechanical properties of unreinforced brick masonry section-1, Documented to US Department of Energy by Lawrence Livermore National Laboratory.

[12] **Fiorato, A.E., Sozen, M.A.and Gamble, W.L**. (1970) An Investigation of the Interaction of Reinforced Concrete Frames with Masonry Filler Walls, DTIC Document,

[13] **Klingner, R.and Bertero, V.V.** (1976). Infilled frames in earthquake-resistant construction.

[14] **Brokken, S.and Bertero, V.V.** (1981). Studies on effects of infills in seismic resistant R/C construction, NASA STI/Recon Technical Report N, 82, 31576.

[15] **Kahn, L.F.and Hanson, R.D.** (1979). Infilled walls for earthquake strengthening, Journal of the Structural Division, 105, 283-296.

[16] **Mehrabi, A.B., Benson Shing, P., Schuller, M.P.and Noland, J.L.** (1996). Experimental evaluation of masonry-infilled RC frames, Journal of structural engineering, 122, 228-237.

[17] **Shing, P.B.and Mehrabi, A.B.** (2002). Behaviour and analysis of masonry-infilled frames, Progress in Structural Engineering and Materials, 4, 320-331.

[18] **Zovkic, J., Sigmund, V.and Guljas, I.** (2013). Cyclic testing of a single bay reinforced concrete frames with various types of masonry infill, Earthquake engineering & structural dynamics, 42, 1131-1149.

[19] **Polyakov, S.and Cairns, G.** (1956) Masonry in framed buildings, Gosudarstvennoe izdatel'stvo Literatury postroitel'stvu i arkhitekture

[20] **Chrysostomou, C., Gergely, P.and Abel, J.** (2002). A six-strut model for nonlinear dynamic analysis of steel infilled frames, International Journal of Structural Stability and Dynamics, 2, 335-353.

[21] **Kadysiewski, S.and Mosalam, K.** (2008). Modeling of unreinforced masonry infill walls considering in-plane and out-of-plane interaction, PEER 2008/102, University of California, Berkeley.

[22] **Smith, B.S.** (1966). Behavior of square infilled frames, Journal of the Structural Division, 92, 381-404.

[23] **Smith, B.S.** (1962). Lateral stiffness of infilled frames, Journal of the Structural Division, 88, 183-226.

[24] **Stafford Smith, B.and Carter, C.** (1969). A method of analysis for infilled frames, Proceedings of the Institution of Civil Engineers, 44, 31-48.

[25] **Mainstone, R.J.** (1971). SUMMARY OF PAPER 7360. ON THE STIFFNESS AND STRENGTHS OF INFILLED FRAMES, Proceedings of the Institution of Civil Engineers, 49, 230.

[26] **Te-Chang, L.and Kwok-Hung, K.** (1984). Nonlinear behaviour of non-integral infilled frames, Computers & structures, 18, 551-560.

[27] **Priestley, M.and Paulay, T.** (1992). Seismic design of reinforced concrete and masonry buildings, New York: John Wiley & Sons, Inc.

[28] **Flanagan, R.D.and Bennett, R.M.** (1999). In-plane behavior of structural clay tile infilled frames, Journal of structural engineering, 125, 590-599.

[29] **Mohebkhah, A., Tasnimi, A.and Moghadam, H.** (2008). Nonlinear analysis of masonry-infilled steel frames with openings using discrete element method, Journal of Constructional Steel Research, 64, 1463-1472.

[30] **Thomas, P.and Priestley, M.** (1992) Seismic design of reinforced concrete and masonry buildings, New York Wiley-Interscience, America.

[31] **Holmes, M.** (1961). Steel frames with brickwork and concrete infilling, Proceedings of the Institution of Civil Engineers, 19, 473-478.

[32] **Mainstone, R.J.and Weeks, G.** (1972) The influence of a bounding frame on the racking stiffness and strengths of brick walls, Building Research Station.

[33] **Durrani, A.J.and Luo, Y.**, (1994) Seismic retrofit of flat-slab buildings with masonry infills, Technical Report, National Center for Earthquake Engineering Research1994, pp. 1-8.

[34] **Hendry, A.W., Sinha, B.P.and Davies, S.**, Design of masonry structures, CRC Press2003.

[35] **Kaushik, H.B., Rai, D.C.and Jain, S.K.** (2007). Stress-strain characteristics of clay brick masonry under uniaxial compression, Journal of materials in Civil Engineering, 19, 728-739.

[36] **Takeda, T., Sozen, M.A.and Nielsen, N.N.** (1970). Reinforced concrete response to simulated earthquakes, Journal of the Structural Division, 96, 2557-2573.

[37] **Dowell, R.K., Seible, F.and Wilson, E.L.** (1998). Pivot hysteresis model for reinforced concrete members, Structural Journal, 95, 607-617.

[38] **Obayashi, S., Sasaki, D., Takeguchi, Y.and Hirose, N.** (2000). Multiobjective evolutionary computation for supersonic wing-shape optimization, Evolutionary Computation, IEEE Transactions on, 4, 182-187.

[39] **Mahfoud, S.and Mani, G.** (1996). Financial forecasting using genetic algorithms, Applied Artificial Intelligence, 10, 543-566.

[40] **Sambridge, M.and Gallagher, K.** (1993). Earthquake hypocenter location using genetic algorithms, Bulletin of the Seismological Society of America, 83, 1467-1491.

[41] **Giro, R., Cyrillo, M.and Galvão, D.** (2002). Designing conducting polymers using genetic algorithms, Chemical Physics Letters, 366, 170-175.

[42] **Lee, C.and Ahn, J.** (2003). Flexural design of reinforced concrete frames by genetic algorithm, Journal of structural engineering, 129, 762-774.

[43] **Camp, C.V., Pezeshk, S.and Hansson, H.** (2003). Flexural design of reinforced concrete frames using a genetic algorithm, Journal of structural engineering, 129, 105-115.

[44] **Rajeev, S.and Krishnamoorthy, C.** (1998). Genetic algorithm–based methodology for design optimization of reinforced concrete frames, Computer-Aided Civil and Infrastructure Engineering, 13, 63-74.

[45] **Govindaraj, V.and Ramasamy, J.** (2005). Optimum detailed design of reinforced concrete continuous beams using genetic algorithms, Computers & structures, 84, 34-48.

[46] **Govindaraj, V.and Ramasamy, J.** (2007). Optimum detailed design of reinforced concrete frames using genetic algorithms, Engineering Optimization, 39, 471-494.

[47] **Ferreira, C., Barros, M.and Barros, A.** (2003). Optimal design of reinforced concrete T-sections in bending, Engineering Structures, 25, 951-964.

[48] **ESER, C.** (2014) Optimum Design of Steel Structures Via Atrificial Bee Coloney (ABC) Algorithm and SAP2000, Middle East Technical University.

[49] **Gomez, D., Silva, C.E., Dyke, S.J.and Thomson, P.**, (2015) Interactive Platform to Include Human-Structure Interaction Effects in the Analysis of Footbridges, Dynamics of Civil Structures, Volume 2, Springer2015, pp. 59-65.

[50] **Goo, Z.J.,** (2013) Topology optimization of building bracing schemes, Massachusetts Institute of Technology.

[51] **Jones, G.P.** (2013) Interoperable software for parametric structural analysis and optimization, Massachusetts Institute of Technology.

[52] **Papadrakakis, M., Fragiadakis, M.and Plevris, V.** Using the New SAP2000 Open Application Programming Interface to Develop an Interactive Front-end for the Modal Pushover Analysis of Bridges

# APPENDICES

**APPENDIX A:** Backbone envelope results of bare-frame, infill frame, infill stepped frame, infill continues frame

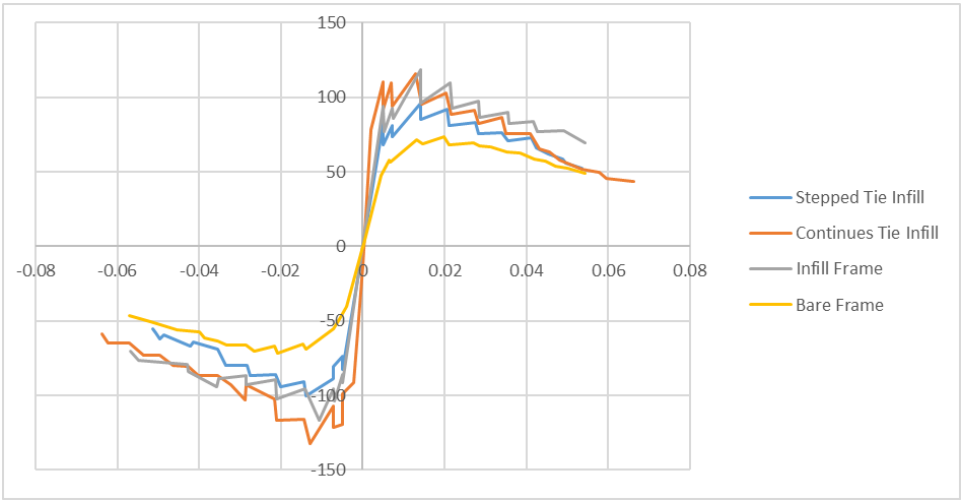


**Figure A.1 :** Experimental load-deformation envelope results

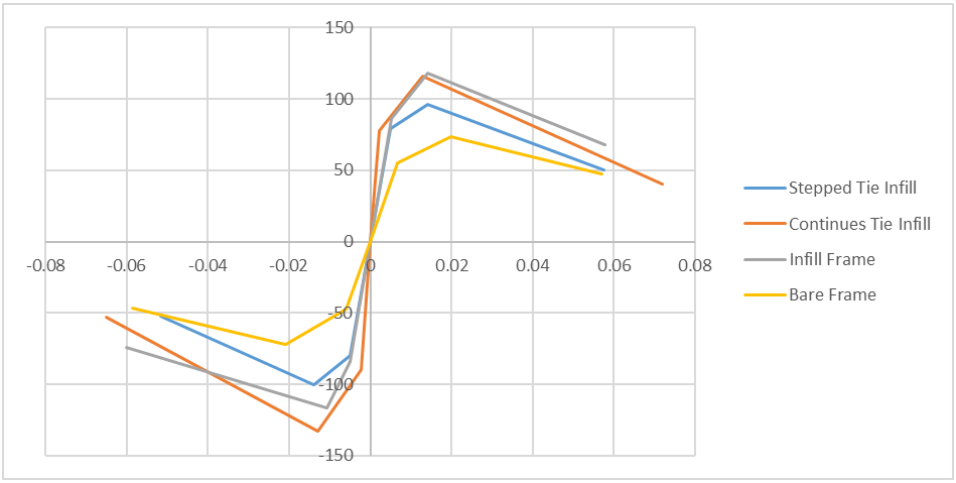


**Figure A.2 :** Idealized experimental load-deformation envelope results

**APPENDIX B**: Resampling the LVDT recorded data

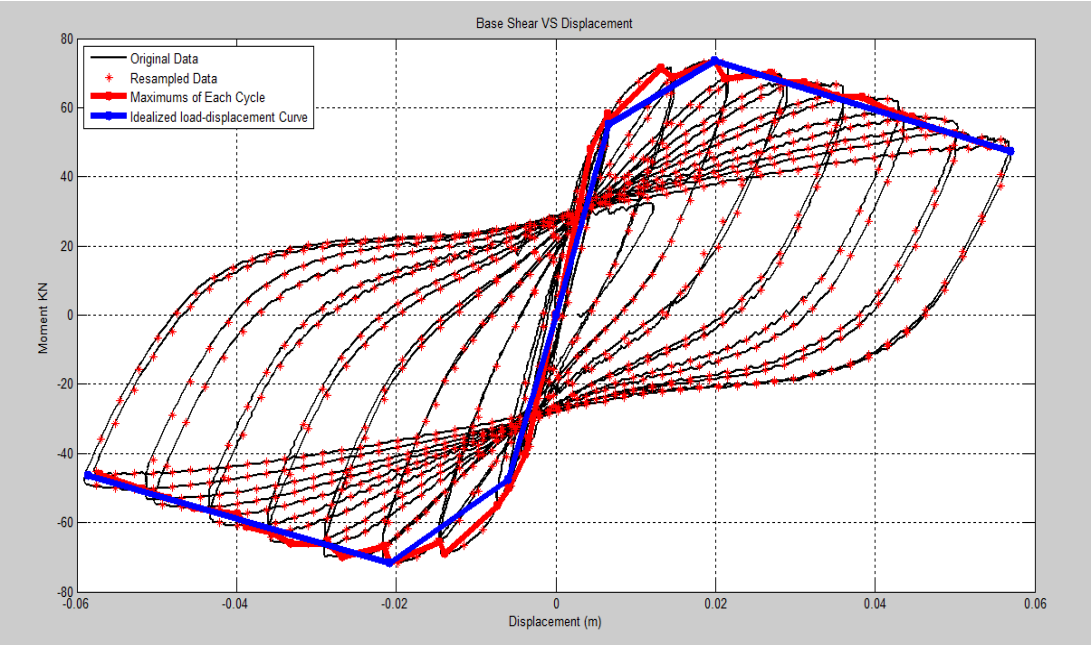


**Figure B.1.a :** Base shear versus displacement in bare frame

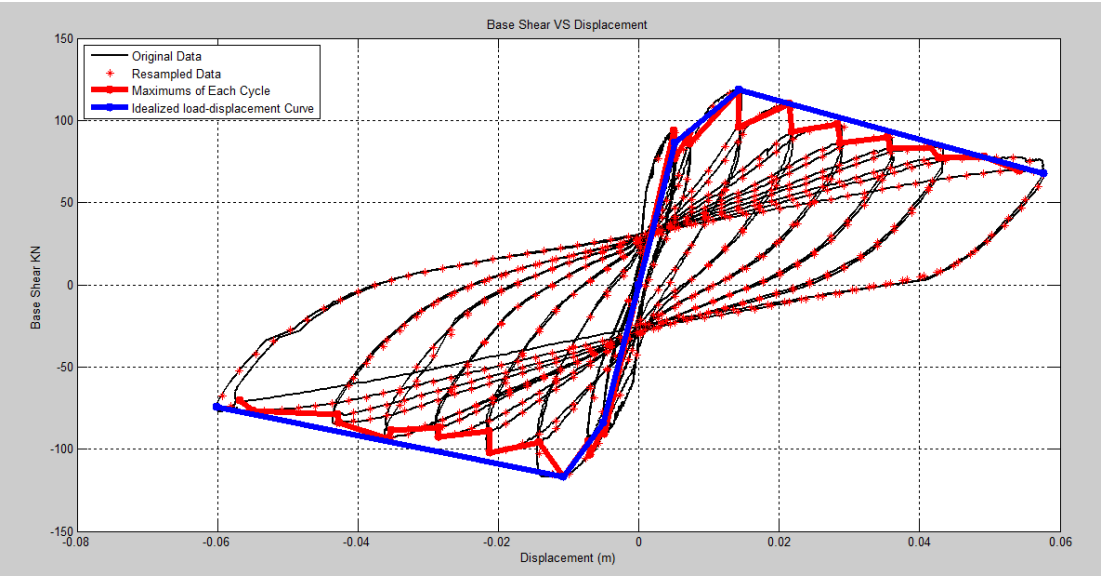


**Figure B.1.b :** Base shear versus displacement in infill frame

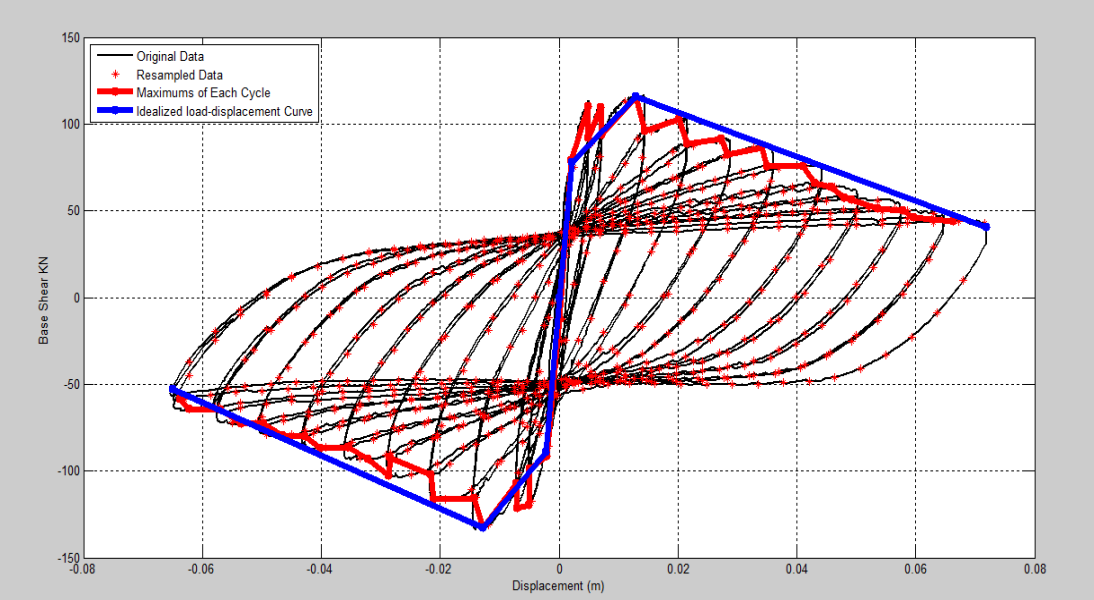


**Figure B.1.c :** Base shear versus displacement in infill continues tie frame

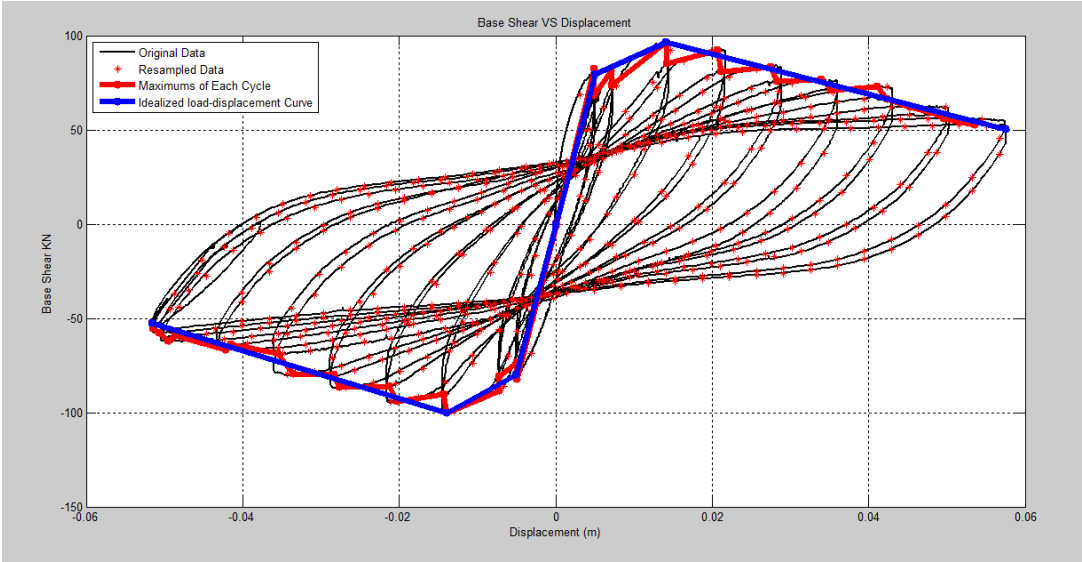


**Figure B.1.d :** Base shear versus displacement in infill stepped tie frame

Original LVDT data is shown in black. The resampled data is shown with red star dots. The local maximum of each cycle is show in red line (monotonic backbone curve). The idealized monotonic backbone curve is shown in blue

**APPENDIX C**: Genetic Algorithm process to fit the simulated model to experimental results.

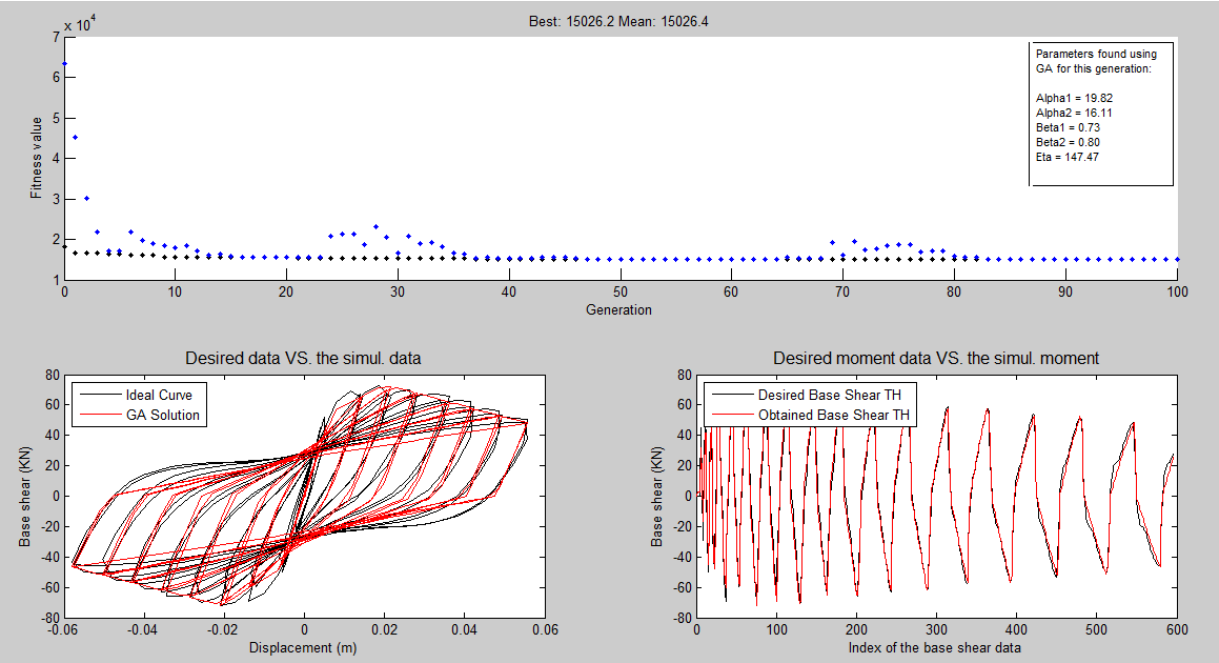


**Figure C.1 :** A snapshot of GA optimization process over bare frame's base shear-displacement cyclic response. Computational time: 2 hours 20 minutes

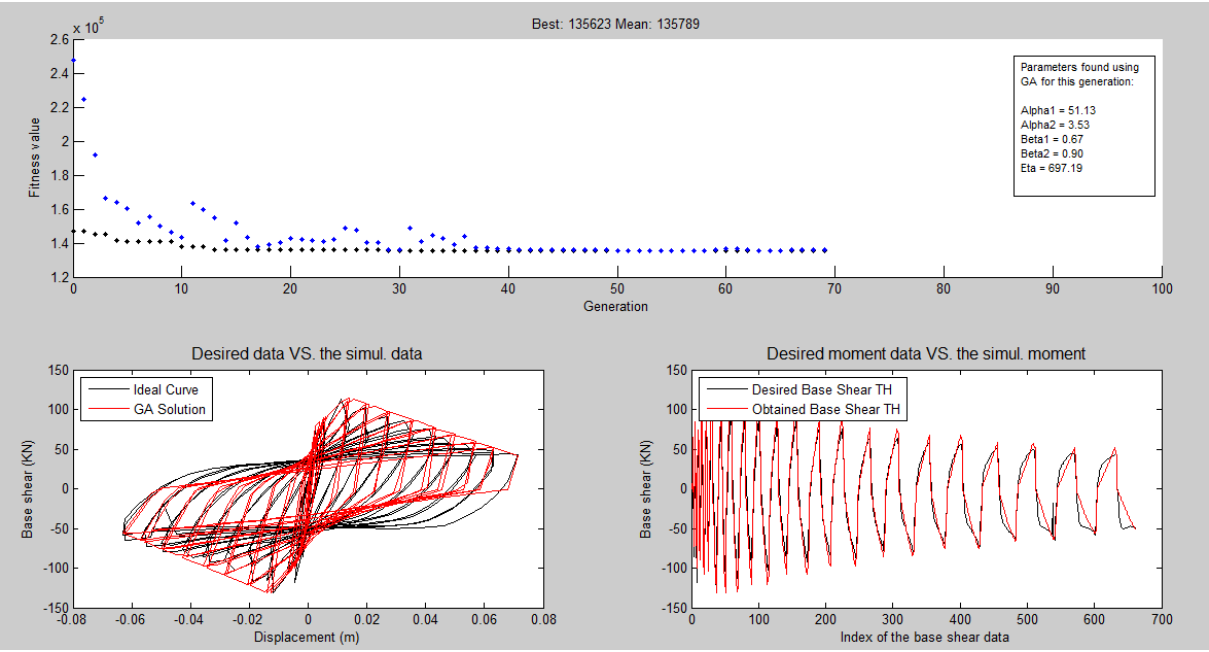


**Figure C.2 :** A snapshot of GA optimization process over Infill Continues Tie frame's base shear-displacement cyclic response. Computational time: 1 hour 50 minutes

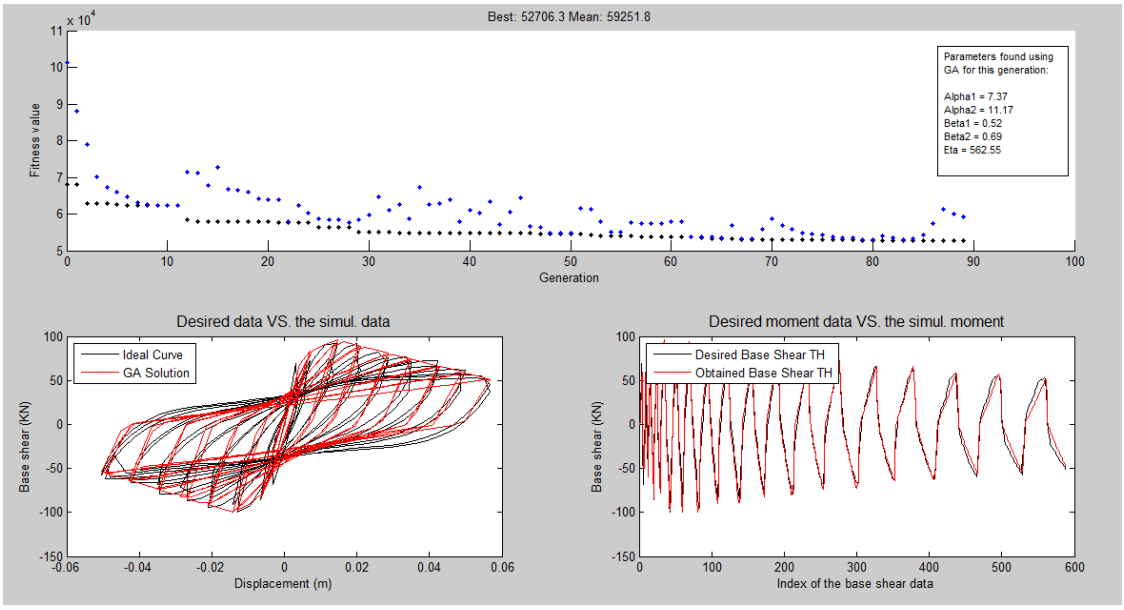


**Figure C.3 :** A snapshot of GA optimization process over Infill Step Tie frame's base shear-displacement cyclic response. Computational time: 2 hours

The top figure illustrates the GA optimization process to minimize the disagreement between simulated and experimental results. The best fitness value (disagreement between simulated and experiment data) of each generation is shown in black dots, and the mean fitness value of the population of each generation is shown with blue dots. Bottom left figure shows the resampled LVDT data (in black), against the simulated results (in red). Resampled base shear record is shown in black against the simulated base shear in red. The optimization parameters are shown in top right corner.

**APPENDIX D**: Experimental versus the simulated results for bare frame:

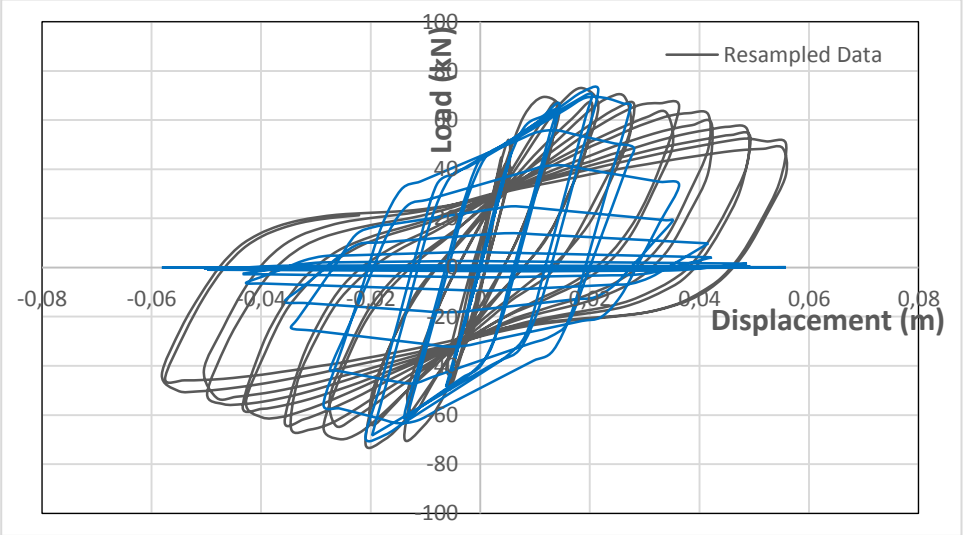


**Figure D.1 :** Kinematic model response versus resampled experimental data of bare frame.

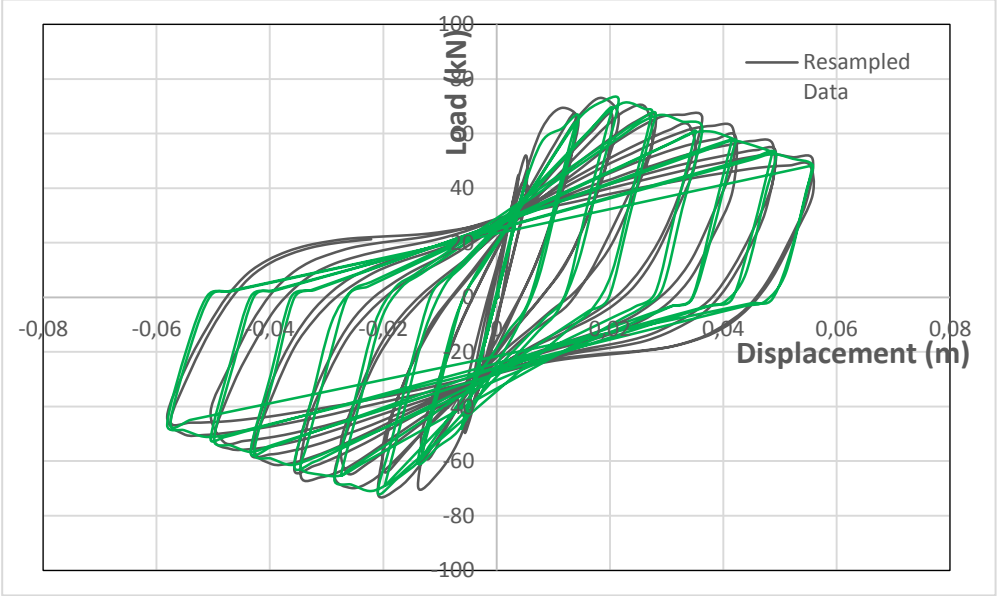


**Figure D.2 :** Takeda model response versus resampled experimental data of bare frame.

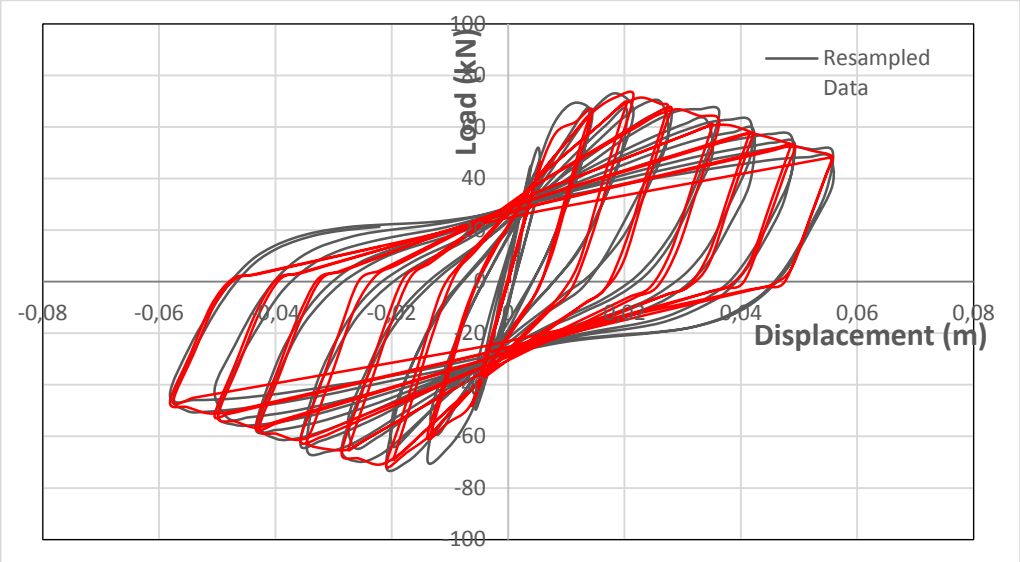


**Figure D.3 :** Pivot model response versus resampled experimental data of bare frame. The unknown parameters required to represent the pivot model were calculated as:
**Alpha1=19.82, Alpha2=16.11, Beta1=0.73, Beta2=0.80, Eta=147.4**

**Table D.1 :** The score for Pivot, Takeda and Kinematic model responses for Infill-Stepped-Tie frame. The model that best fits the experimental results has the lowest score

| | |
|---|---|
| **Pivot Score:** | **15026.44** |
| **Takeda Score:** | **20165.01** |
| **Kinematic Score:** | **456823.2** |

**APPENDIX E:** Experimental versus the simulated results for infill frame:

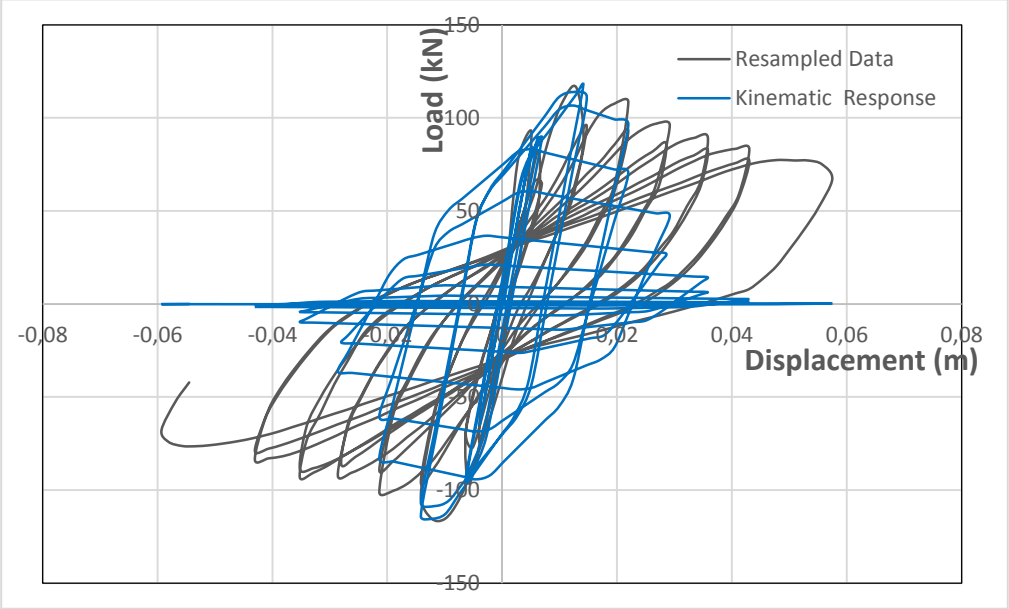


**Figure E.1 :** Kinematic model response versus resampled experimental data of infill frame.

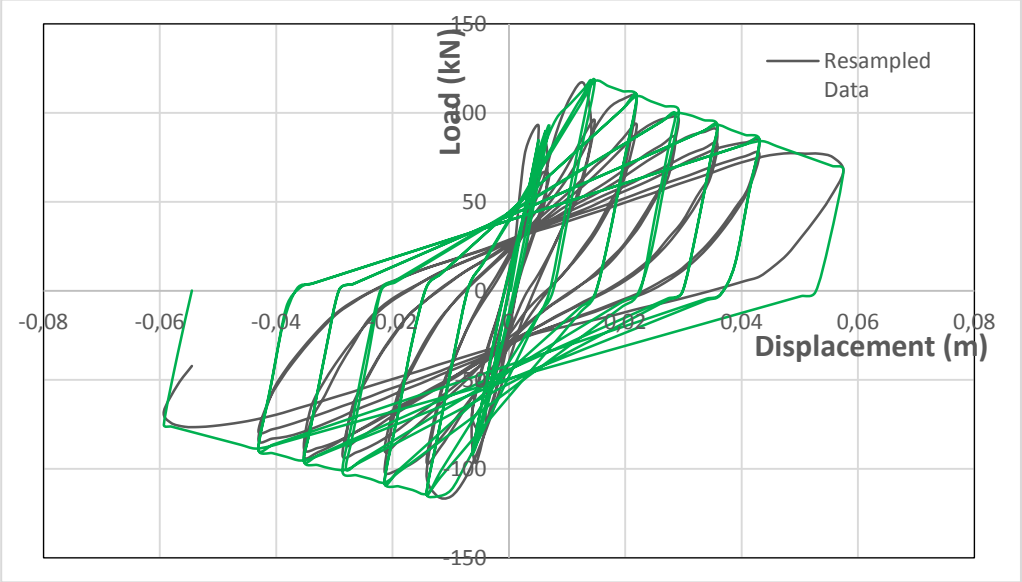


**Figure E.2 :** Takeda model response versus resampled experimental data of infill frame.

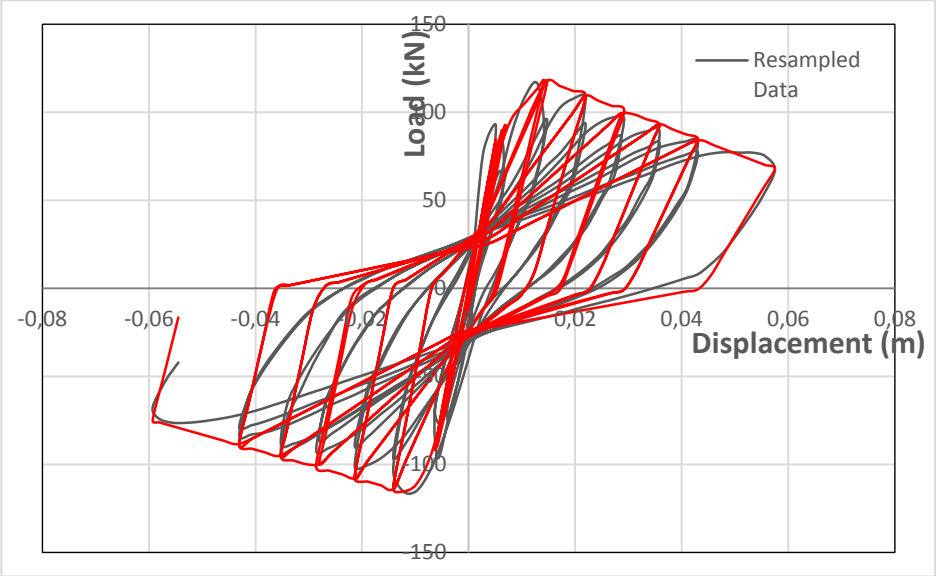


**Figure E.3 :** Pivot model response versus resampled experimental data of infill frame. The unknown parameters required to represent the pivot model were calculated as:
**Alpha1=3.69, Alpha2=28.31, Beta1=0.34, Beta2=0.38, Eta=273.7**

**Table E.1 :** The score for Pivot, Takeda and Kinematic model responses for Infill-Stepped-Tie frame. The model that best fits the experimental results has the lowest score

| | |
|---|---|
| **Pivot Score:** | **76879.84** |
| **Takeda Score:** | **214391.2** |
| **Kinematic Score:** | **1062500** |

**APPENDIX F:** Experimental versus the simulated results for Infill-Continues-Tie frame:

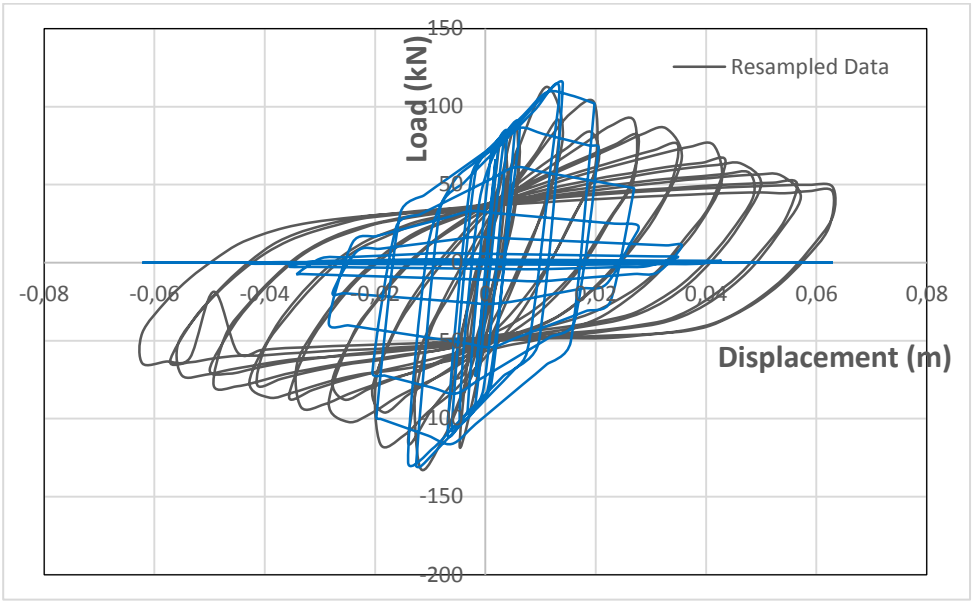


**Figure F.1 :** Kinematic model response versus resampled experimental data of Infill-Continues-Tie frame.

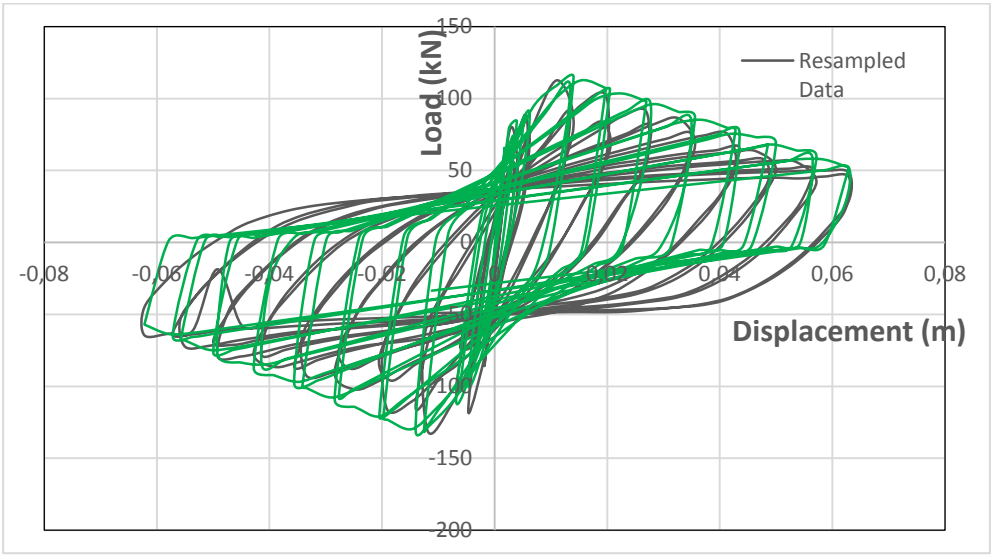


**Figure F.2 :** Takeda model response versus resampled experimental data of Infill-Continues-Tie frame.

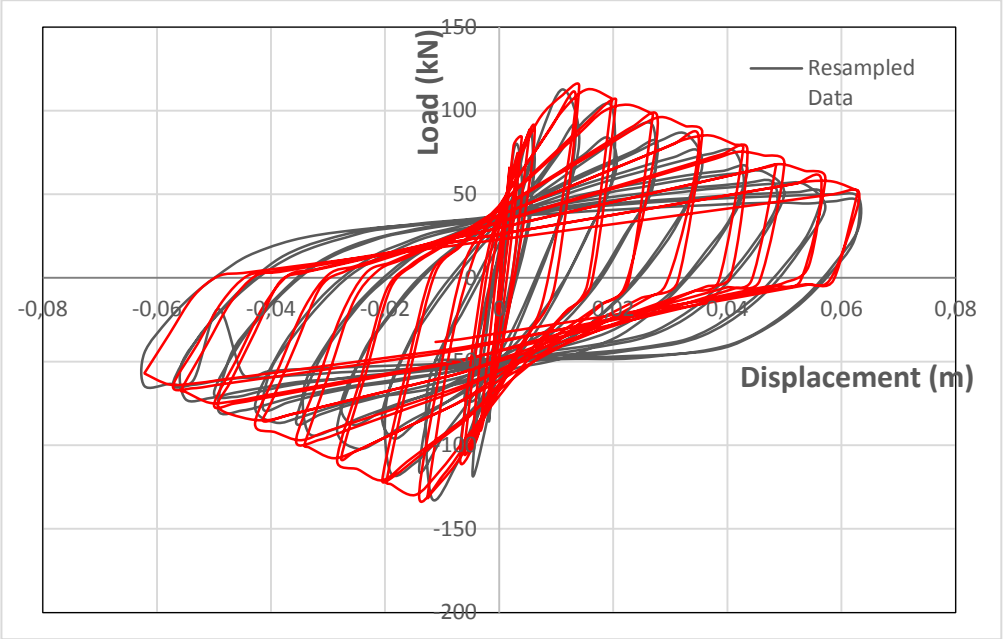


**Figure F.3 :** Pivot model response versus resampled experimental data of Infill-Continues-Tie frame.

The unknown parameters required to represent the pivot model were calculated as:
**Alpha1=51.14, Alpha2=3.54, Beta1=0.66, Beta2=0.89, Eta=697.2**

**Table F.1** : The score for Pivot, Takeda and Kinematic model responses for Infill-Stepped-Tie frame. The model that best fits the experimental results has the lowest score

| | |
|---|---|
| **Pivot Score:** | **135624.4323** |
| **Takeda Score:** | **179684.3096** |
| **Kinematic Score:** | **1291377.456** |

**APPENDIX G:** Experimental versus the simulated results for Infill-Stepped-Tie frame:

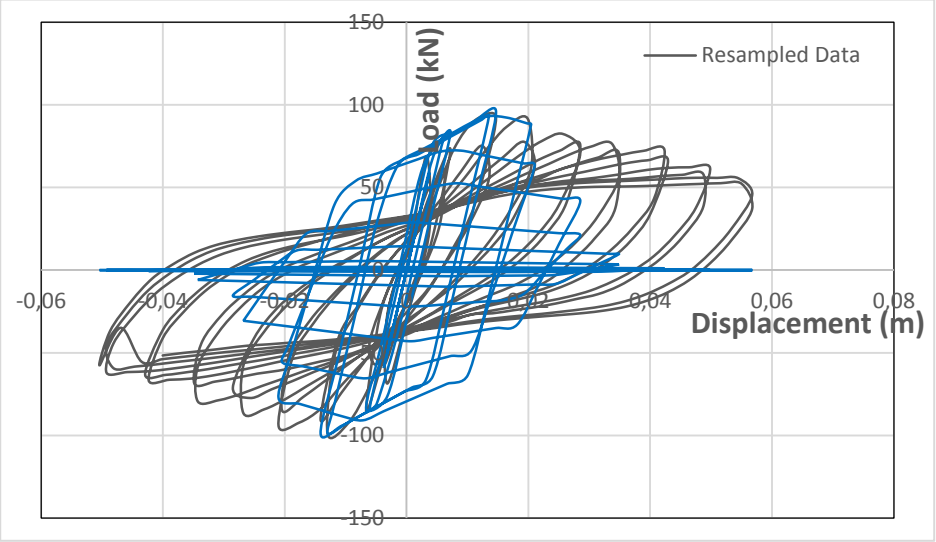


**Figure G.1 :** Kinematic model response versus resampled experimental data of infill stepped tie frame.

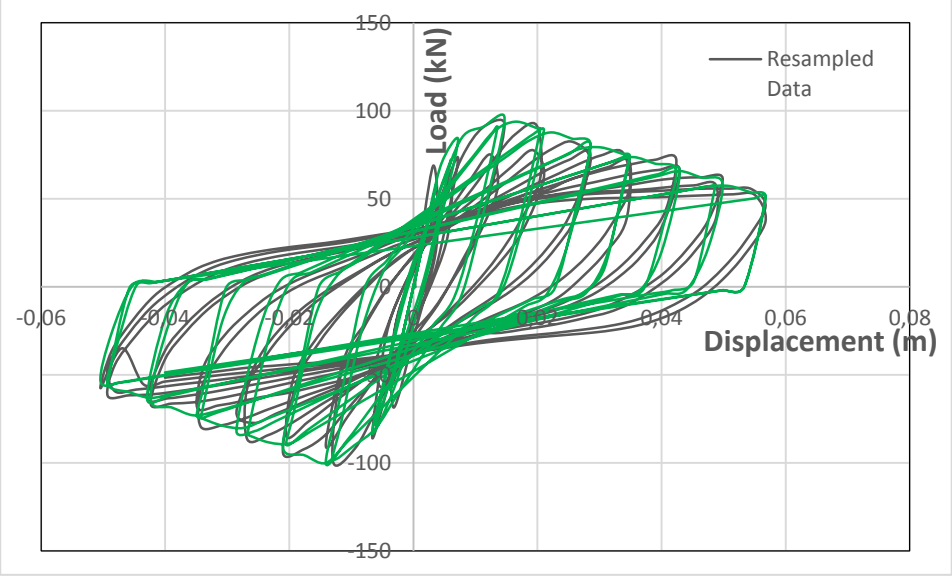


**Figure G.2 :** Takeda model response versus resampled experimental data of infill stepped tie frame.

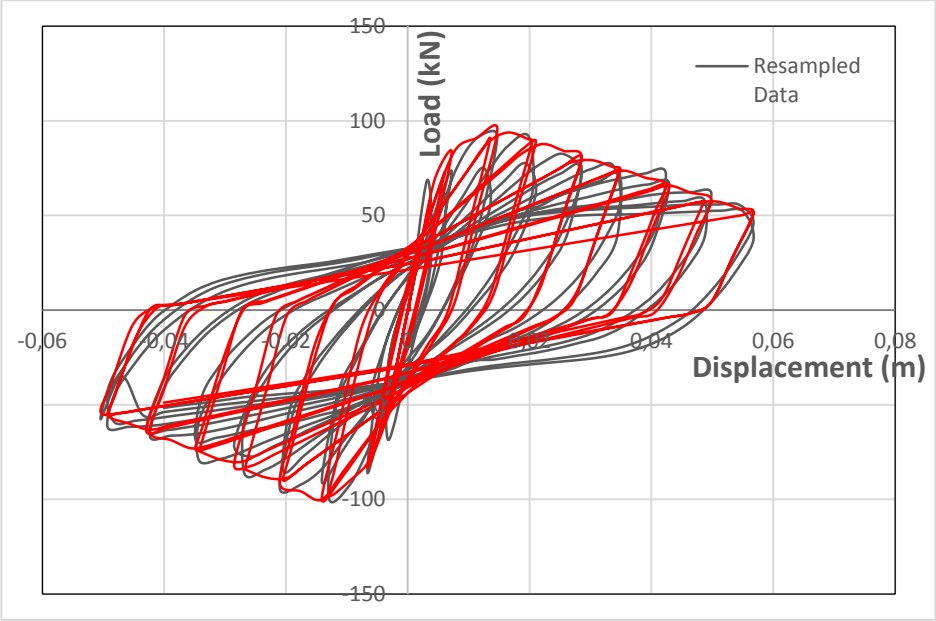


**Figure G.3 :** Pivot model response versus resampled experimental data of Infill-Stepped-Tie frame.
The unknown parameters required to represent the pivot model were calculated as: Alpha1=7.37, Alpha2=11.16, Beta1=0.52, Beta2=0.69, Eta=562.5

**Table G.1 :** The score for Pivot, Takeda and Kinematic model responses for Infill-Stepped-Tie frame. The model that best fits the experimental results has the lowest score

| | |
|---|---|
| **Pivot Score:** | **52706.29047** |
| **Takeda Score:** | **69251.16368** |
| **Kinematic Score:** | **817009.0686** |

## **APPENDIX H:** The Algorithm.

As the programming platform, MATLAB is used to analyze the data. Sap2000 has been integrated with MATLAB through application programming interface (API). The following functions have been used in this research. The following functions has BDS license and can be found in Mathworks exchange dataset. The user is encouraged to use the following content for the sake of research as long as they cite our work. Please note that any commercial use is prohibited.

### 1-Main.m

```
close all;
clear;
clc;
%% Set preferences file for Sap 2000
PreferencesFile=strcat(' ~~~~~ \JointModelNewVersion.sdb');

%% Feed the cyclic data
CurvatureTH= xlsread('PD for the Bare Frame','O:O');% curvature is
the displacement
MomentTH= xlsread('PD for the Bare Frame','M:M');
PostReduction=12;
ID='Base Shear VS Displacement';

    %% Calibre the data (Plot the dat for the calibration purposes)
% CurvatureTH=CurvatureTH+1.43;
figure;
plot(CurvatureTH,MomentTH);grid on;title(ID)
%% Save the Moment-Curvature curve

%% Filter & Shorten the data
[CurvatureTH_SM_SH] = FilterShorten(10,1,CurvatureTH,0);
[MomentTH_SM_SH] = FilterShorten(10,1,MomentTH,0);
%% Obtaining the PD Curve
[PD_Maximums,PD_Pushed,PD_Final,ChangeSign]
=P_DObtainer(CurvatureTH_SM_SH,MomentTH_SM_SH,2);% The las parameter
is the PD kind==> PD =1, PD_Pushed = 2
%% Ignore the speed the loading

ResamplingScale=200/max(abs(min(CurvatureTH)),max(CurvatureTH)); %
the more the scale is, the richer the data will be, The value is
calculated with some experiments
MaximumsIndeces= sortrows(PD_Pushed(:,3));
[CurveINT,MomentINT]=IgnoreSpeed(CurvatureTH_SM_SH,MomentTH_SM_SH,Ma
ximumsIndeces,ResamplingScale,1,ID);

%% shorthen the data
CurveINT=CurveINT([1:PostReduction:length(CurveINT)]);
MomentINT=MomentINT([1:PostReduction:length(MomentINT)]);


%% Display the results
```

```
figure('units','normalized','outerposition',[0 0 1 1]); % open
figure in screen size
title('')
plot(CurvatureTH,MomentTH,'k','LineWidth',2)
hold on;
plot(CurveINT,MomentINT,'*r');
hold on;
plot(PD_Maximums(:,1),PD_Maximums(:,2),'-*r','LineWidth',5);
hold on;
plot(PD_Final(:,1),PD_Final(:,2),'-*b','LineWidth',5);
legend('Original Data','Resampled Data', 'Maximums of Each Cycle',
'Idealized load-displacement Curve','Location','northwest');

        xlabel('Displacement (m)');
        ylabel('Base Shear KN ');
grid on;
hold off;title(strcat('',ID));


PD_Final
 end

CurvaturePD=PD_Final(:,1);
MomentPD=PD_Final(:,2);
CurvatureTH=CurveINT;
MomentTH=MomentINT;

%MomentINT% Start Sap2000
[SapObject,SapModel]=SapStart( PreferencesFile );
%% Set the Time History loading parameters to Sap2000
ret =
SapModel.LoadCases.DirHistNonlinear.SetTimeStep('RotaionLoading',
length(CurvatureTH)-1, 1);
%% pass the curve to Sap2000
% Set the P-D curve
ret = SapModel.SetPresentUnits('KN_m_C');
ret = SapModel.PropLink.SetMultiLinearPoints('LIN1', 6,
max(size(CurvaturePD)), MomentPD, CurvaturePD);

% set the TH curve (curvature) to get the base shear
NumberItems = length(CurvatureTH);
Value=CurvatureTH;
MyTime=[0:length(Value)-1]';
ret = SapModel.Func.FuncTH.SetUser('TH-1', NumberItems, MyTime,
Value);
%% Hide Sap object
% ret = SapObject.Hide
%% Set Initial Parameters to the Pivot model
Alpha1=5;
Alpha2=5;
Beta1=0.5;
Beta2=0.5;
Eta=0.5;

%% GA setting
PlotHandle=@(a1,a2,a3)PlotCust(a1,a2,a3, Alpha1, Alpha2, Beta1,
Beta2, Eta, MomentTH, SapObject,SapModel, MomentPD, CurvaturePD,
CurvatureTH ,ID);
lb=[1 1 0.02 0.02 1];
```

```
ub=[100 100 1 1 1000];
%IntCon=1:5;
options=gaoptimset('CrossoverFrac', .5,'PopulationSize',15 ...
    ,'StallGen', 100, 'Generation',100,'PlotFcns',
@gaplotbestf,PlotHandle},'Display','iter');
% [xopt, Fval]=ga(@(Fitness)RetFitness( Alpha1, Alpha2, Beta1,
Beta2, Eta, MomentTH, SapObject,SapModel, MomentPD,
CurvaturePD),5,[],[],[],[],lb,ub,[],IntCon,options)
[xopt, Fval]=ga(@(x)ObjectiveFuc(x, MomentTH, SapObject,SapModel,
MomentPD, CurvaturePD),5,...
    [],[],[],[],lb,ub,[],options)

%% Calc. the Pivot response
ret = SapModel.SetModelIsLocked(false);% unlock model
% swich to Pivot
ret = SapModel.SetPresentUnits('KN_m_C');
ret = SapModel.PropLink.SetMultiLinearPoints('LIN1', 6,
max(size(CurvaturePD)), MomentPD, CurvaturePD, 3);

% set pivot parameters
Alpha1= xopt(1)
Alpha2= xopt(2)
Beta1= xopt(3)
Beta2= xopt(4)
Eta= xopt(5)



ret = SapModel.PropLink.SetMultiLinearPoints('LIN1', 6,
max(size(CurvaturePD)), MomentPD, CurvaturePD,3,Alpha1, Alpha2,
Beta1, Beta2, Eta);

% Pivot score
ret = SapModel.Analyze.RunAnalysis();
        Name ='1';
        Element = 0;
        NumberResults = 0;
        Obj = cellstr(' ');
        ObjSta = zeros(1,1,'double');
        Elm = cellstr(' ');
        ElmSta = zeros(1,1,'double');
        LoadCase = cellstr(' ');
        StepType= cellstr(' ');
        StepNum = zeros(1,1,'double');
        P = zeros(1,1,'double');
        V2 = zeros(1,1,'double');
        V3 = zeros(1,1,'double');
        T = zeros(1,1,'double');
        M2 = zeros(1,1,'double');
        M3 = zeros(1,1,'double');
        ret =
SapModel.Results.Setup.DeselectAllCasesAndCombosForOutput;
        ret =
SapModel.Results.Setup.SetCaseSelectedForOutput('RotaionLoading');
%         ret = SapModel.Results.Setup.SetOptionNLStatic(2);
        ret = SapModel.Results.Setup.SetOptionDirectHist(2);
        [ret, NumberResults, Obj, ObjSta, Elm, ElmSta, LoadCase,
StepType, StepNum, P, V2, V3, T, M2, M3] =
SapObject.SapModel.Results.FrameForce(Name, Element, NumberResults,
```

```
Obj, ObjSta, Elm, ElmSta, LoadCase, StepType, StepNum, P, V2, V3, T,
M2, M3);

        % unlock the model
        ret = SapModel.SetModelIsLocked(false);
        M=[];
for i=2:2:length(M3)
    M(i/2)=M3(i);
end
OOMPivot=-M';
[ OOFitnessPivot ] = FitnessCalc( OOMPivot,MomentTH );


%% Calc. the takeda response
ret = SapModel.SetModelIsLocked(false);% unlock model
% swich to takeda
ret = SapModel.SetPresentUnits('KN_m_C');
ret = SapModel.PropLink.SetMultiLinearPoints('LIN1', 6,
max(size(CurvaturePD)), MomentPD, CurvaturePD, 2);
% takeda score
ret = SapModel.Analyze.RunAnalysis();
        Name ='1';
        Element = 0;
        NumberResults = 0;
        Obj = cellstr(' ');
        ObjSta = zeros(1,1,'double');
        Elm = cellstr(' ');
        ElmSta = zeros(1,1,'double');
        LoadCase = cellstr(' ');
        StepType= cellstr(' ');
        StepNum = zeros(1,1,'double');
        P = zeros(1,1,'double');
        V2 = zeros(1,1,'double');
        V3 = zeros(1,1,'double');
        T = zeros(1,1,'double');
        M2 = zeros(1,1,'double');
        M3 = zeros(1,1,'double');
        ret =
SapModel.Results.Setup.DeselectAllCasesAndCombosForOutput;
        ret =
SapModel.Results.Setup.SetCaseSelectedForOutput('RotaionLoading');
%         ret = SapModel.Results.Setup.SetOptionNLStatic(2);
        ret = SapModel.Results.Setup.SetOptionDirectHist(2);
        [ret, NumberResults, Obj, ObjSta, Elm, ElmSta, LoadCase,
StepType, StepNum, P, V2, V3, T, M2, M3] =
SapObject.SapModel.Results.FrameForce(Name, Element, NumberResults,
Obj, ObjSta, Elm, ElmSta, LoadCase, StepType, StepNum, P, V2, V3, T,
M2, M3);

        % unlock the model
        ret = SapModel.SetModelIsLocked(false);
        M=[];
for i=2:2:length(M3)
    M(i/2)=M3(i);
end
OOMTakeda=-M';
[ OOFitnessTakeda ] = FitnessCalc( OOMTakeda,MomentTH );


%% Calc. the kinematic response
ret = SapModel.SetModelIsLocked(false);% unlock model
```

```
% swich to Kinematic
ret = SapModel.SetPresentUnits('KN_m_C');
ret = SapModel.PropLink.SetMultiLinearPoints('LIN1', 6,
max(size(CurvaturePD)), MomentPD, CurvaturePD, 1);
% Kinematic score
ret = SapModel.Analyze.RunAnalysis();
        Name ='1';
        Element = 0;
        NumberResults = 0;
        Obj = cellstr(' ');
        ObjSta = zeros(1,1,'double');
        Elm = cellstr(' ');
        ElmSta = zeros(1,1,'double');
        LoadCase = cellstr(' ');
        StepType= cellstr(' ');
        StepNum = zeros(1,1,'double');
        P = zeros(1,1,'double');
        V2 = zeros(1,1,'double');
        V3 = zeros(1,1,'double');
        T = zeros(1,1,'double');
        M2 = zeros(1,1,'double');
        M3 = zeros(1,1,'double');
        ret =
SapModel.Results.Setup.DeselectAllCasesAndCombosForOutput;
        ret =
SapModel.Results.Setup.SetCaseSelectedForOutput('RotaionLoading');
%         ret = SapModel.Results.Setup.SetOptionNLStatic(2);
        ret = SapModel.Results.Setup.SetOptionDirectHist(2);
        [ret, NumberResults, Obj, ObjSta, Elm, ElmSta, LoadCase,
StepType, StepNum, P, V2, V3, T, M2, M3] =
SapObject.SapModel.Results.FrameForce(Name, Element, NumberResults,
Obj, ObjSta, Elm, ElmSta, LoadCase, StepType, StepNum, P, V2, V3, T,
M2, M3);

        % unlock the model
        ret = SapModel.SetModelIsLocked(false);
        M=[];
for i=2:2:length(M3)
    M(i/2)=M3(i);
end
OOMKinematic=-M';
[ OOFitnessKinematic ] = FitnessCalc( OOMKinematic,MomentTH );
```

**2-FilterShorten.m**

```
function [ VectorTH_SM_SH ] = FilterShorten(
FilteringSize,ShorteningSize, VectorTH, ShowResults )
%% Filter the data
VectorTH_SM=fastsmooth(VectorTH,FilteringSize,1,1);
%% Shorten the data
VectorTH_SM_SH=zeros(1,1,'double');
for j=1:ShorteningSize:max(size(VectorTH_SM))
VectorTH_SM_SH((j-1)/ShorteningSize+1,1)=VectorTH_SM(j,1);
end
%% Show the results
if ShowResults == 1
    figure
    plot([1:max(size(VectorTH))]',VectorTH,'b')
    hold on;

plot([1:max(size(VectorTH_SM))]',VectorTH_SM+2/100*max(VectorTH_SM),
'r')
    plot([0:max(size(VectorTH_SM_SH))-
1]'*ShorteningSize,VectorTH_SM_SH+4/100*max(VectorTH_SM_SH),'k');
    hold off;
end

end

%% Template
function SmoothY=fastsmooth(Y,w,type,ends)
if nargin==2, ends=0; type=1; end
if nargin==3, ends=0; end
  switch type
    case 1
       SmoothY=sa(Y,w,ends);
    case 2
       SmoothY=sa(sa(Y,w,ends),w,ends);
    case 3
       SmoothY=sa(sa(sa(Y,w,ends),w,ends),w,ends);
  end
end
function SmoothY=sa(Y,smoothwidth,ends)
w=round(smoothwidth);
SumPoints=sum(Y(1:w));
s=zeros(size(Y));
halfw=round(w/2);
L=length(Y);
for k=1:L-w,
   s(k+halfw-1)=SumPoints;
   SumPoints=SumPoints-Y(k);
   SumPoints=SumPoints+Y(k+w);
end
s(k+halfw)=sum(Y(L-w+1:L));
SmoothY=s./w;
% Taper the ends of the signal if ends=1.
  if ends==1,
  startpoint=(smoothwidth + 1)/2;
  SmoothY(1)=(Y(1)+Y(2))./2;
  for k=2:startpoint,
```

```
      SmoothY(k)=mean(Y(1:(2*k-1)));
      SmoothY(L-k+1)=mean(Y(L-2*k+2:L));
  end
  SmoothY(L)=(Y(L)+Y(L-1))./2;
  end
```

---

### 3-FittnessCalc.m

```
function [ Fitness ] = FitnessCalc( M,MomentTH )
%FITNESSFNC Summary of this function goes here
%   Detailed explanation goes here
Fitness=0;
if length(M)==length(MomentTH)
    for i=1:length(M)
        Fitness=Fitness+(M(i)-MomentTH(i))^2;
    end
end
```

---

### 4-ObjectiveFuc.m

```
function G = ObjectiveFuc( x, MomentTH, SapObject,SapModel,
MomentPD, CurvaturePD)

Alpha1=x(1);
Alpha2=x(2);
Beta1=x(3);
Beta2=x(4);
Eta=x(5);
%% Display the results
display('Random variables for the current loop is the following:');
display(strcat('Alpha1=',num2str(Alpha1)));
display(strcat('Alpha2=',num2str(Alpha2)));
display(strcat('Beta1=',num2str(Beta1)));
display(strcat('Beta2=',num2str(Beta2)));
display(strcat('Eta=',num2str(Eta)));
%% Calc. the fitness
G=RetFitness( Alpha1, Alpha2, Beta1, Beta2, Eta, MomentTH,
SapObject,SapModel, MomentPD, CurvaturePD);
%% Display the fitness value
% display(strcat('Fitness for this loop is:',num2str(G)));

end
```

**5-IgnoreSpeed.m**

```
%% Input the data
function
[CurveINT,MomentINT]=IgnoreSpeed(CurvatureTH,MomentTH,ChangeDir,Resa
mplingScale, ShowResults,ID)

%% Resampling Scale
% resampling scale will control the size of the output function. The
% higher of this value will make the output data richer.

% saling up the input data, We will scale it down at the end.
CurvatureTH=CurvatureTH*ResamplingScale;
MomentTH=MomentTH*ResamplingScale;


% Shift maximums to the


%% Redim the values
ChangeDir=[ChangeDir;length(CurvatureTH)];% set the end value of
CuvTH
FirstCurvVal=round(CurvatureTH(1));
MomentINT=[];
CurveINT=[];
%% Del all the direction change less than the following
ChangeDirNew=[];
for i=2:length(ChangeDir)
    if ChangeDir(i)-ChangeDir(i-1)>2
        ChangeDirNew=[ChangeDirNew;ChangeDir(i)];
    end
end
%% floor the results of the Curvature
CurvatureTH=floor(CurvatureTH)+1;
%% Redim the values
YFuncNew=[];XFuncNew=[0];MomentINT=[];FirstCurvIndex=1;
for i=2:length(ChangeDirNew)
    if FirstCurvVal<CurvatureTH(ChangeDirNew(i)) % for the values of
the positive increaments
        LastCuvIndex=ChangeDirNew(i);
        LastCurvVal=CurvatureTH(LastCuvIndex);
        Curveloop=FirstCurvVal+1:LastCurvVal;

        CurveFNC=CurvatureTH(FirstCurvIndex:LastCuvIndex);
        [CurveFNC,Indeces] =
unique(CurveFNC,'first');CurveFNC=CurveFNC';
        CurveFNC=CurvatureTH([Indeces+FirstCurvIndex-1]);
        MoomentFNC=MomentTH([Indeces+FirstCurvIndex-1]);

% save the results
        CurveINT=[CurveINT,Curveloop];% Save the values to the final
dimanded curve
        MomentINT =
[MomentINT,interp1(CurveFNC,MoomentFNC,Curveloop)];% save values to
the Final dimanded moment
```

```
        FirstCurvIndex=LastCuvIndex;
        FirstCurvVal=LastCurvVal;

    elseif FirstCurvVal>CurvatureTH(ChangeDirNew(i))  % for the
values of the negative increaments
        LastCuvIndex=ChangeDirNew(i);
        LastCurvVal=CurvatureTH(LastCuvIndex);
        Curveloop=FirstCurvVal-1:-1:LastCurvVal;

        CurveFNC=CurvatureTH(FirstCurvIndex:LastCuvIndex);
        [CurveFNC,Indeces] =
unique(CurveFNC,'first');CurveFNC=CurveFNC';CurveFNC=fliplr(CurveFNC
);Indeces=flipud(Indeces);
        CurveFNC=CurvatureTH([Indeces+FirstCurvIndex-1]);
        MoomentFNC=MomentTH([Indeces+FirstCurvIndex-1]);
% save the results
        CurveINT=[CurveINT,Curveloop];% Save the values of the
Curvature
        MomentINT =
[MomentINT,interp1(CurveFNC,MoomentFNC,Curveloop)];

        FirstCurvIndex=LastCuvIndex;
        FirstCurvVal=LastCurvVal;

    end

end

%% Coverage the end of the curve
% for i=1:length(CurveINT)
% end
%% sacale the data down
CurveINT=CurveINT/ResamplingScale;
MomentINT=MomentINT/ResamplingScale;
CurvatureTH=CurvatureTH/ResamplingScale;
MomentTH=MomentTH/ResamplingScale;
%% Plot the results
if ShowResults==1
figure('units','normalized','outerposition',[0 0 1 1]); % open
figure in screen size
x=CurvatureTH;
v=MomentTH;
xq=CurveINT;
vq1=MomentINT;
plot(x,v,'-r',xq,vq1,':.');
        xlabel('Rotation (Rad)');
        ylabel('Base Shear (KN) ');
        legend('Smoothed Data','Resampled','Location','northwest');
        title(strcat('Smoothed Data VS. Remapled Data-',ID))
        % save the figure
        figname=(strcat(ID,'Resampling','.png'));
        saveas(gcf,figname);
end
CurveINT=CurveINT';MomentINT=MomentINT';
end
```

**6-P_DObtainer.m**

```
%% Description
%The maximum & minimums are selected with respect
%to each step's Y value and then are sorted with X column
%increment.
%%
function [PD,PD_Pushed,PD_Final,ChangeSignY]
=P_DObtainer(x,y,P_DKind)%PD=[SortedXvalues, Yvalue, Indecis] ]
ChangeSignY=0;
for i=1:length(x)-1
    n1=y(i);n2=y(i+1);
    if n1*n2<0
        ChangeSignY=[ChangeSignY;i];
    end
end
ChangeSignY
%% find the maximums & minimums at each cycle
PD=[];
for i=1:length(ChangeSignY)-1
    Func=y(ChangeSignY(i)+1:ChangeSignY(i+1));
    if y(ChangeSignY(i)+1)>0
    [M,I] = max(Func(:));
    PD=[PD;0,M,ChangeSignY(i)+I];
    else
    [M,I] = min(Func(:));
    PD=[PD;0,M,ChangeSignY(i)+I];
    end
end

% obtaining X value
for i=1:length(PD)
    PD(i,1)=x(PD(i,3));
end

%% Calculation of the change sign data for Y

ChangeSignX=0;
for i=1:length(y)-1
    n1=x(i);n2=x(i+1);
    if n1*n2<0
        ChangeSignX=[ChangeSignX;i];
    end
end
ChangeSignX
%% find the PUSHED maximums & minimums at each cycle
PD_Pushed=[];
for i=1:length(ChangeSignX)-1
    Func=x(ChangeSignX(i)+1:ChangeSignX(i+1));
    if x(ChangeSignX(i)+1)>0
    [M,I] = max(Func(:));
    PD_Pushed=[PD_Pushed;M,0,ChangeSignX(i)+I];
    else
    [M,I] = min(Func(:));
    PD_Pushed=[PD_Pushed;M,0,ChangeSignX(i)+I];
    end
end
```

```
% obtaining Y value
for i=1:length(PD_Pushed)
    PD_Pushed(i,2)=y(PD_Pushed(i,3));
end
%% Sort the data with X column increment
PD=sortrows(PD,1);
display(PD);
%% Sort the data with X column increment
PD_Pushed=sortrows(PD_Pushed,1);
display(PD_Pushed);
%% Del results less than 10 percent of up and down the Y value
% ymax=max(y);
% ymin=min(y);
% PD_Deleted=PD;
% for i=1:length(PD)
%     if PD(i,2)<ymax*.1 && PD(i,2)>ymin*.1;%investigate less than
10 percent
%         %del raw
%         PD_Deleted(i,:)=[];
%     end
% end
%% display the results
% plot(PD(:,1),PD(:,2),'k')
% display(PD_Deleted);

%% Determine the final data
if P_DKind==1
    PD_temp=PD;
end
if P_DKind==2
   PD_temp=PD_Pushed;
end

PD_Final=[];
slopemaxp=0;slopemaxn=0;
PD_ymax=max(PD(:,2));
PD_ymin=min(PD(:,2));
PD_xmax=max(PD_temp(:,1));
PD_xmin=min(PD_temp(:,1));


for i=1:length(PD)% determination of the points 2 and 6
    if PD_ymax==PD(i,2)% for points 2 and 6 it is always to get the
maximum Y value, So PD is perefered as oppouse PD_temp
        PD_Final(6,1)=PD(i,1);
        PD_Final(6,2)=PD(i,2);
        PD_Final(6,3)=PD(i,3);
    end
    if PD_ymin==PD(i,2)% for points 2 and 6 it is always to get the
maximum Y value
        PD_Final(2,1)=PD(i,1);
        PD_Final(2,2)=PD(i,2);
        PD_Final(2,3)=PD(i,3);
    end
end
for i=1:length(PD_temp)% ditermination of the points 1 and 7
    if PD_xmax==PD_temp(i,1)
        PD_Final(7,1)=PD_temp(i,1);
        PD_Final(7,2)=PD_temp(i,2);
        PD_Final(7,3)=PD_temp(i,3);
    end
```

```
    if PD_xmin==PD_temp(i,1)
        PD_Final(1,1)=PD_temp(i,1);
        PD_Final(1,2)=PD_temp(i,2);
        PD_Final(1,3)=PD_temp(i,3);
    end
    %% determination of the yielding point
if PD_temp(i,2)>0.65*PD_ymax
    slope=PD_temp(i,2)/PD_temp(i,1);
    if slope > slopemaxp
        PD_Final(5,1)=PD_temp(i,1);
        PD_Final(5,2)=PD_temp(i,2);
        PD_Final(5,3)=PD_temp(i,3);
        slopemaxp=slope;
    end
end

if PD_temp(i,2)<0.65*PD_ymin
    slope=PD_temp(i,2)/PD_temp(i,1);
    if slope > slopemaxn
        PD_Final(3,1)=PD_temp(i,1);
        PD_Final(3,2)=PD_temp(i,2);
        PD_Final(3,3)=PD_temp(i,3);
        slopemaxn=slope;
    end
end
end
PD_Final(4,1)=0;PD_Final(4,2)=0;PD_Final(4,3)=0;
display(PD_Final)
```

---

### 7- ReadMoment.m

```
function [ MomentTH ] =
ReadMoment(CurvatureTH,MomentCurvatureRelation )
MomentTH=[];
for i=1:length(CurvatureTH)


Moment=interp1(MomentCurvatureRelation(1,:),MomentCurvatureRelation(
2,:),CurvatureTH(i));
    MomentTH=[MomentTH,Moment];

end
end
```

## 8- PlotCust.m

```
function  [state,options,optchanged]=PlotCust( options,state,flag,
Alpha1, Alpha2, Beta1, Beta2, Eta, MomentTH, SapObject,SapModel,
MomentPD, CurvaturePD, CurvatureTH, ID )
%PLOTF Summary of this function goes here
%   Detailed explanation goes here
optchanged = false;
        grid on;
        hold on;
        subplot(2,2,3);
        plot(CurvatureTH,MomentTH,'k');
        xlabel('Displacement (m)');
        ylabel('Base shear (KN)');
        title('Desired data VS. the simul. data','FontSize',12);
[~,loc] = min(state.Score); % Find location of best
Paramters=state.Population(loc,:);
Alpha1=Paramters(1);
Alpha2=Paramters(2);
Beta1=Paramters(3);
Beta2=Paramters(4);
Eta=Paramters(5);

        s{1} = sprintf('Parameters found using GA for this
generation: \n');
        s{Deseilligny,  #5} = sprintf('Alpha1 = %.2f ', Alpha1);
        s{Deseilligny,  #5} = sprintf('Alpha2 = %.2f ', Alpha2);
        s{4} = sprintf('Beta1 = %.2f ', Beta1);
        s{5} = sprintf('Beta2 = %.2f', Beta2);
        s{6} = sprintf('Eta = %.2f ', Eta);
        annotation(gcf, 'textbox', [0.8 0.7 0.1 .2], 'String', s,...
            'BackGroundColor','w','FontSize',8);




[ Fitness,M ] = RetFitness(Alpha1, Alpha2, Beta1, Beta2, Eta,
MomentTH, SapObject,SapModel, MomentPD, CurvaturePD);
        hold on;
        plot(CurvatureTH,M,'r');
        legend('Ideal Curve','GA Solution','Location','northwest');
        drawnow;
        hold off;

        subplot(2,2,4);
        plot(1:length(MomentTH),MomentTH,'k');
        hold on;
        plot(1:length(M),M,'r');
        xlabel('Index of the base shear data');
        ylabel('Base shear (KN)');
        title('Desired moment data VS. the simul.
moment','FontSize',12);
        legend('Desired Base Shear TH','Obtained Base Shear
TH','Location','northwest');

        end
```

### 9- RetFitness.m

```
function [ Fitness ,M] = RetFitness(  Alpha1, Alpha2, Beta1, Beta2,
Eta, MomentTH, SapObject,SapModel, MomentPD, CurvaturePD )
%RETALPHABETA Summary of this function goes here
%   Detailed explanation goes here

ret = SapModel.PropLink.SetMultiLinearPoints('LIN1', 6,
max(size(CurvaturePD)), MomentPD, CurvaturePD,3,Alpha1, Alpha2,
Beta1, Beta2, Eta);
%% Run alalysis
ret = SapModel.Analyze.RunAnalysis();
%% Get the Base-Shear/Curvature value for the joint
% Get the shear base for steps 1 to 100
        Name ='1';
        Element = 0;
        NumberResults = 0;
        Obj = cellstr(' ');
        ObjSta = zeros(1,1,'double');
        Elm = cellstr(' ');
        ElmSta = zeros(1,1,'double');
        LoadCase = cellstr(' ');
        StepType= cellstr(' ');
        StepNum = zeros(1,1,'double');
        P = zeros(1,1,'double');
        V2 = zeros(1,1,'double');
        V3 = zeros(1,1,'double');
        T = zeros(1,1,'double');
        M2 = zeros(1,1,'double');
        M3 = zeros(1,1,'double');
        ret =
SapModel.Results.Setup.DeselectAllCasesAndCombosForOutput;
        ret =
SapModel.Results.Setup.SetCaseSelectedForOutput('RotaionLoading');
%         ret = SapModel.Results.Setup.SetOptionNLStatic(2);
        ret = SapModel.Results.Setup.SetOptionDirectHist(2);
        [ret, NumberResults, Obj, ObjSta, Elm, ElmSta, LoadCase,
StepType, StepNum, P, V2, V3, T, M2, M3] =
SapObject.SapModel.Results.FrameForce(Name, Element, NumberResults,
Obj, ObjSta, Elm, ElmSta, LoadCase, StepType, StepNum, P, V2, V3, T,
M2, M3);

        % unlock the model
        ret = SapModel.SetModelIsLocked(false);
        M=[];
for i=2:2:length(M3)
    M(i/2)=M3(i);
end
M=-M';
[ Fitness ] = FitnessCalc( M,MomentTH );

End
```

### 10- SapStart.m

```
function  [SapObject,SapModel]=SapStart( PreferencesFile )
%% Create Sap2000 object
```

```
feature('COM_SafeArraySingleDim', 1);
feature('COM_PassSafeArrayByRef', 1);
SapObject = actxserver('SAP2000v16.SapObject');
%start Sap2000 application
%   (This command will start sap2000)
SapObject.ApplicationStart;

%create SapModel object:
%   (For every model to be analyzed and designed 'SapModel =
SapObject.SapModel' command creates list of
%    API function in which SapModel handes names of all functions
using struct class.)

SapModel = SapObject.SapModel;
ret = SapModel.InitializeNewModel;
ret = SapModel.File.NewBlank;
% Set units to Kgf_cm_C
ret = SapModel.SetPresentUnits('Kgf_cm_C');
ret = SapModel.File.OpenFile(PreferencesFile);
ret = SapModel.SetModelIsLocked(0);
% ret = SapObject.Hide;

end
```

# CURRICULUM VITAE

Name: **MirSalar Kamari**
Birth Date: Jun. 18, 1991
E-mail: kamari@itu.edu.tr/salar.kamari@gmail.com
Cellphone No: (+90)5312424223
Province of resident: Istanbul, Turkey

## Educational Background

**- B.Sc. in Civil Engineering**, Sept. 2009-Jun. 2013

*Department of Civil Engineering, University of Shahid Madani, Tabriz, Iran*; GPA: **14.60**/20

**- M.Sc. in Civil Engineering**, Sept. 2013 until now
*Department of Civil Engineering, Istanbul Technical University, Istanbul Turkey,*
*GPA:* **3.69/4**

## Transcript of Master of Science

| | |
|---|---|
| **-Composite Materials** | BA |
| **-Engineering Mathematics** | AA |
| **-Matrix Methods in Structural Analysis** | BA |
| **-Finite Element Methods** | BA |
| **-Advanced Structural Analysis** | BB |
| **-Pre-Stressed Reinforced Concrete Structures** | AA |
| **-Ductile Design of Steel Structures** | AA |
| **-Design of Prefabricated Structures** | AA |

## Skills

### 1-Software experience

- Image Processing though MATLAB
- MATLAB & SAP2000 API (Controlling SAP2000's functions using MATLAB)
- SAP2000

- Autodesk Maya (Advanced 3D modeling, Texturing, Rendering, Rigging, and Animating)
- AutoCAD (Generating DXF drawings using MATLAB)
- Visual Basic (Being able to publish software related to civil engineering)
- ETABS
- SAFE
- Geo studio 2004
- KeyShot photo realistic 3D image renderer
- Mental-Ray photo realistic 3D image renderer
- Adobe After Effects

## 2-Programming and 3D Experience

-Segmentation and Analysis of a Hand Sketched Truss Frame Using Morphological Image Processing Techniques and Sap2000 API

Quick Snapshot on YouTube:

https://www.youtube.com/watch?v=-q9B8ItKyeE

-Modeling the P-Delta curve of a reinforced concrete frame using MATLAB & Sap2000 API through Genetic Algorithm

https://www.youtube.com/watch?v=RYv9A6v3ba8

-Automated design of structure using MATLAB & Sap2000 API.

Quick Snapshot on YouTube:

https://www.youtube.com/watch?v=7MRw_wCpvzU

-Analyzing Kinematic, Takeda and pivot bars using MATLAB & Sap2000 API.
https://www.youtube.com/watch?v=dgSZCC0W_mA

-Image processing about OCR (Optical Character Recognition) for Latin fonts revised and conducted with MATLAB.

-Interaction between Sap2000 and AutoCAD to automate the drawing procedures to generate DXF file of concrete reinforcement.

-Axial Load and Moment Relationship for Reinforced Concrete Columns program (published by me)
https://www.youtube.com/watch?v=ItIjv0rJ5F4
For instruction about the program please visit the link below
https://www.dropbox.com/s/gje7ihh1z70uxp0/Reinforced%20Concrete%20Column%20P-M%20Interaction.pdf?dl=0

-3D modeling and rendering of the buildings (some are shown in the link below), *(Modeling Autodesk Maya/ Rendering Keyshot)*

https://www.dropbox.com/sh/m2gwsv2wtik5mp6/AAD2OaEVvpI-omQnXwLsPJkra?dl=0

-3D workshop presenter at the Shahid Madani University, Tabriz, Iran. A video capture from one of my classes can be found in the link below:

https://www.youtube.com/watch?v=OKQ_rw3DYwQ

-My brief 3D portfolio can be found in the link below:
https://www.dropbox.com/s/u2q5pncxushdm3i/3d%20Portfolio%20Mirsalar%20kamari.pdf?dl=0

## Research Interests

- Building Information Modeling (BIM)
- Augmented Reality in construction
- Virtual Reality in construction
- Geo Tagging
- Construction management (through leveraging point clouds to BIM)
- Building safety assessment
- Simplifying design of structures
- Automation of the analysis of the structures and buildings
- Perform building analysis based on 3D scanning of them
- Image Processing and machine learning
- Earthquake engineering

## Research Experience

- **Masonry walls and infill ties rigidity in the reinforced concrete frames**. Research Assistant, *Funded by TÜBİTAK***,** Jun. 2014 (Advisor: Ph.D. Oğuz Güneş, Assistant professor, Istanbul Technical university)

- **Segmentation and Analysis of a Hand Sketched Truss Frame Using Morphological Image Processing Techniques and Sap2000 API.** Research Assistant, Jun. 2015 till now (Advisor: Ph.D. Oğuz Güneş, Assistant professor, Istanbul Technical university)

- **Design of integrated concrete formworks**, Jun. 2013 (Advisor: Ph.D. Mirheyder Hashemi, Assistant professor)

- **Determination of optimal concrete column dimension based on computer programming,** Jun. 2012 (Advisor: Ph.D. Alireza Entezari, Assistant Professor)

- **Evaluation of seepage conditions in dams,** *Student project,* Dec. 2012(Advisor: Ph.D. Farshbaf, Assistant Professor)

## Language Skills

| Language | Writing | | | | Reading | | | | Speaking | | | |
|---|---|---|---|---|---|---|---|---|---|---|---|---|
| | Native | Good | Fair | Poor | Native | Good | Fair | Poor | Native | Good | Fair | Poor |
| English | | x | | | | x | | | | x | | |
| Turkish | | x | | | | x | | | | x | | |
| Persian | x | | | | x | | | | x | | | |
| Azeri | | x | | | | x | | | x | | | |

## GRE Quantitative

Score: 170/170